Technical Assistance for the Deployment of Airborne Limbsounders during ESSenCe			
ESA Contract No: PFL-PSO/FF/fk/11.456	SUBJECT: **Final Report**		CONTRACTOR: Research Centre Jülich, IEK
	Volume / Total Volumes: 1 / 1	VERSION: v2.3 (final version)	DATE: 10 June 2013

ABSTRACT:

The ESa Sounder Campaign 2011 addresses field measurements utilizing the high-altitude research aircraft Geophysica to quantify processes that control the composition and structure of the mid to upper troposphere and lower stratosphere. This activity supports the demonstration of the capabilities of the Earth Explorer Core mission candidate PREMIER.

This document includes the following deliverables of the ESSenCe project:

DOC-D9 Final Report

Prepared by:

Martin Kaufmann, J. Blank, F. Friedl-Vallon, D. Gerber, T. Guggenmoser, M. Hoepfner, A. Kleinert, M. K. Sha, H. Oelhaf, M. Riese, O. Suminska-Ebersoldt, W. Woiwode, R. Siddans, B. Kerridge, B. Moyna, S. Rea, M. Oldfield

Change log:

- 29.08.2012 draft version 1.0
- 05.10.2012 version 2.0
  - added comments according to the action items identified in the final presentation
  - updated GLORIA dynamics mode data
- 20.12.2012 version 2.1
  - revised MARSCHALS chapter
  - added a plot related to the cold offset retrieval
  - added a table about O_2 spectral parameter updates according to latest HITRAN database
  - added table for bad channel listing
- 11.01.2013 version 2.2
  - added MIPAS-STR data inventory descritption
- 10.06.2013 version 2.3
  - modified MARSCHALS chapter according to the AI of the telecon of 12th March 2013
  - **final version**

Contents

1. Introduction

1.1. Background

The ESA Sounder Campaign 2011 conducted field measurements utilizing the high-altitude research aircraft Geophysica to quantify processes that control the composition and structure of the mid to upper troposphere and lower stratosphere (UTLS). This campaign supported the in-flight testing of an imaging infra-red limb-sounder (GLORIA) and millimeter-wave limb-sounder (MARSCHALS) to contribute to the demonstration of capabilities of ESA's Earth Explorer 7 candidate PREMIER.

The PREMIER mission aims to quantify processes that control the composition and structure of the mid to upper troposphere and lower stratosphere. This region of the atmosphere is particularly important for climate studies because it is where the atmosphere cools to space and where it is most sensitive to changes in the distribution of atmospheric constituents. The key innovation of the PREMIER mission is the provision of three-dimensional atmospheric temperatures and constituent fields with unprecedented spatial resolution. This is achieved by employing the new limb-imaging technique (using 2D detector arrays) that provides an across-track (across line-of-sight) measuring capability to fill the observational gap between synoptic-scale structures resolved by current satellite instruments and small-scale features resolved by airborne in-situ instruments. Furthermore, PREMIER employs the complementary attributes of infra-red and millimeter-wave limb-sounding.

1.2. Campaign Summary

1.2.1. Activities

To achieve the objectives of the ESSenCe campaign, Arena Arctica in Kiruna / northern Sweden, located 145 kilometers north of the Arctic Circle, was chosen as the base of operation. Airplane carrier for the instruments was the Russian M55-Geophysica airplane with a ceiling altitude of up to 21 km. The M55 has demonstrated the ability to fly under most conditions in numerous campaigns in the frame of EU research projects (EuPLEx, TROCCINOX, SCOUT-O3, AMMA, RECONCILE) as well as within ESA funded ENVISAT validation campaigns.

The campaign has covered ground based measurements inside and outside of Arena Arctica to assure the interaction of all subsystems of the GLORIA instrument after transport and final integration. Two so called "Test Flights" are conducted to test the functionality and performance of GLORIA under all major conditions. This included particularly EMC considerations (under flight conditions), the thermal behavior of the sensor and the gimbaled frame, the detector and instrument optics cooling system, the pointing system, the interferometer control system and the SATCOM (up/downlink). All critical subsystems have been checked under typical flight conditions (ascent, descent, linear flight at fixed pressure level) and applying major viewing geometries (fixed limb view, limb view with changing azimuth, and blackbody measurements).

Two flights were conducted during ESSenCe; the first one on December 11, 11:00 - 15:00 UTC, and the second one on December 16, 14:00 - 18:00 UTC. Flight Tracks are illustrated in Fig.1.1.

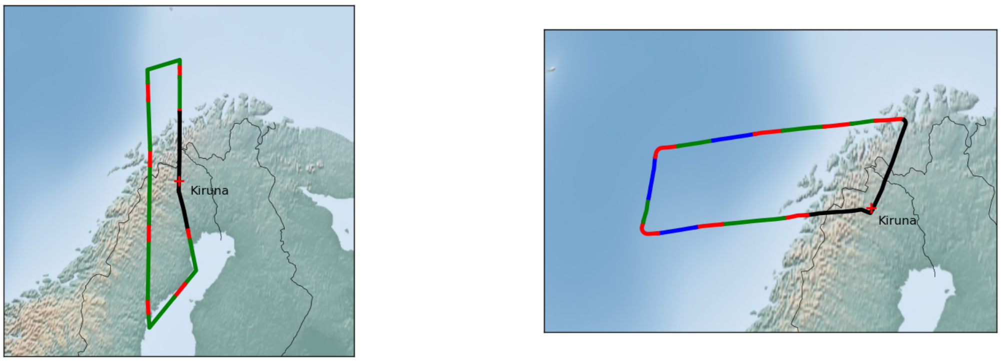

Figure 1.1.: Planned flight tracks of the Geophysica aircraft for December 11th (left) and 16th (right), 2011. Green lines mark chemistry mode measurements, blue lines dynamics mode measurement, red lines calibration sequences, and black lines indicate, that GLORIA is in parking position.

1.2.2. Instrumentation

A short description of the ESSenCe instrumentation including a brief summary of the instrument performance is given here; for details refer to the Compact Data Acquisition Report and Chapters 2, 3, and 4.

GLORIA

GLORIA is an infrared remote limb sounder which combines the high horizontal resolution of a nadir sounder (tens of km) with the altitude resolution provided by a limb-sounding instrument. This capability is achieved by combining a high resolution two-dimensional infrared detector (enabling across line-of-sight sampling), the ability to pan the line-of-sight of the instrument forward and backward, and an imaging Michelson interferometer. Precursors of GLORIA are the CRISTA (CRyogenic Infrared Spectrometers and Telescopes for the Atmosphere) and MIPAS (Michelson Interferometer for Passive Atmospheric Sounding) instruments, both of them operated on research aircraft and satellite platforms. GLORIA measurements will deliver two or three dimensional distributions of trace gases in the UTLS region.

GLORIA was developed and built by Karlsruhe Institute of Technology and Research Center Jülich.

The flight tracks of the Geophysica aircraft for Test Flights 1 and 2 as well as GLORIA measurement modes are illustrated in Fig.1.1.

MARSCHALS

MARSCHALS is a millimeter-wave spectrometer designed to measure vertical profiles of ozone, water vapor, carbon monoxide, nitrous oxide, nitric acid and other gaseous components of the Earth's atmosphere. MARSCHALS scans the atmosphere at some distance away from the aircraft to remotely measure the composition of the atmosphere. To do so, MARSCHALS measures the faint radiation emitted by molecules in the atmosphere as they cycle through perpetual changes of their internal energy levels. The specific wavelength of this radiation is such, that it can pass through thin types of clouds and still be observed at the other end. This makes the instrument particularly suitable to study the atmosphere at altitudes where clouds are often present, as it is the case with the particular region of atmosphere targeted by the ESSENCE campaign. The MARSCHALS instrument was built at and is operated by scientists from the Rutherford Appleton Laboratory in the UK. MARSCHALS measures in three bands (Band B: 297 - 305 GHz, Band C: 318 - 325.5 GHz, Band D: 342.25 - 347.25 GHz) at a resolution of 200 MHz. The standard scan sequence consists of 26 elevation angles with a nominal 1.5 km tangent height spacing from -1.5 km to flight altitude+1.5km., plus an additional +20° quasi-cold-space calibration view. Each scan angle comprises four complete calibrated measurement cycles (hot, limb and cold views). A complete elevation scan is carried out in each frequency band in turn. The total scan sequence time, for three bands, is 9 minutes.

MIPAS-STR

MIPAS-STR is the Geophysica version of the MIPAS instrument family. Like the balloon version it is a cryogenic Fourier transform spectrometer applying the limb scanning technique with high spectral resolution and radiometric sensitivity in the IR spectral region. The instrument is tailored to its operation on the Geophysica aircraft in several aspects (e.g. concerning the calibration and the input optics). As the balloon version it uses an autonomous reliable pointing system based on an GPS-aided inertial navigation system. The IR radiation is detected simultaneously in four spectral channels by sensitive lHe-cooled Si:As-BIB detectors. MIPAS-STR was involved in many international campaigns since the late 90ies.

The frequency coverage of MIPAS-STR is for Channel 1: 725–990 cm^{-1}, Channel 2: 1150–1360 cm^{-1}, Channel 3: 1560–1710 cm^{-1}, Channel 4: 1810–2100 cm^{-1}. The spectral resolution is 0.036 cm^{-1} (unapodized). Measurement integration period is 9.5s / single interferogram. The standard scan sequence includes limb-viewing geometries with tangent altitudes between 4 km and the flight level (with a vertical spacing of 1 km between 9 km and the flight level and a coarser grid between 4 and 9 km). For a typical flight altitude of 18 km, one full limb scan of the standard limb sequence (including calibration measurements) takes about 2.8 min, corresponding to a flight path of approximately 33 km. The vertical field of view diameter at the tangent point increases for the respective geometries from about 0.3 km to 3.0 km.

The atmospheric measurements are enclosed by blackbody and 'deep space' (zenith view) calibration measurements.

1.2.3. Meteorological Situation

The meteorological situation as well as model forecasts are described in detail in the Campaign Implementation Plan.

Briefly, during the first test flight, a low pressure system located over the Norwegian Sea was slowly approaching Scandinavia. Along its eastern part air from lower latitudes was moved polewards and lifted isentropically, thus transporting air with enhanced content of e.g. CO from the middle and lower troposphere upward. Connected to this frontal system high clouds appeared south of this tongue of air. On the western rim of the low pressure system air from the stratosphere was descending deep into the troposphere and coiling up cyclonically. As the low was moving eastward, this filament of stratospheric air was shifted to the east. The low pressure system passed Scandinavia on the 10th of December, 2011. CO-rich air masses moved around the low pressure systems edge cyclonically, forming a filament being almost parallel to the Norwegian coast in the afternoon. The tropopause fold at the western rim of the low pressure system moved across Scandinavia on the 11th of December with an additional northward component. This tongue of stratospheric air penetrated deep into the troposphere (down to 600 hPa). On upper levels (above 70 hPa) the polar vortex edge with cold temperatures well below 200 K was approaching northern Europe. At its edge a filament has been peeled off.

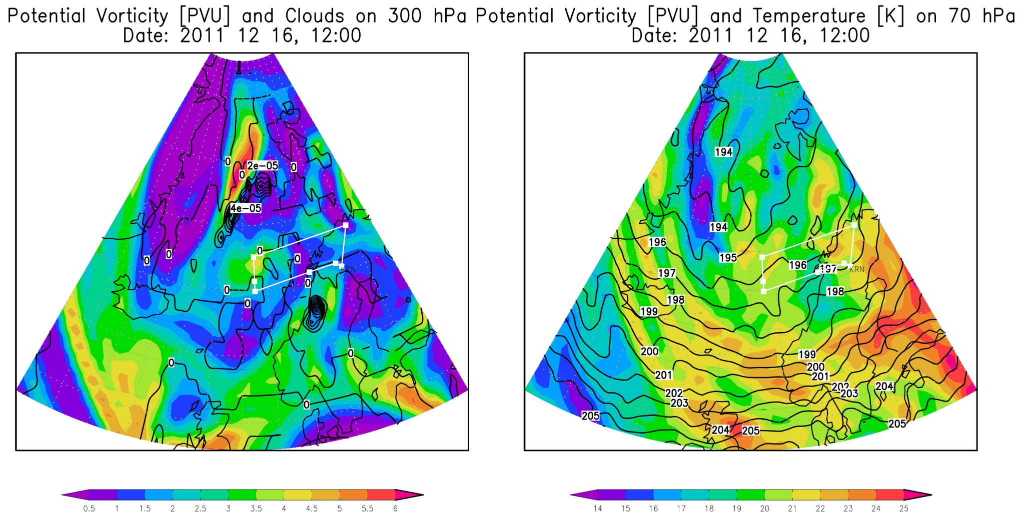

Figure 1.2.: ECMWF forecasts for ESSenCe Test Flight 2 for potential vorticity and clouds on 300 hPa (left) and potential vorticity and temperature on 70 hPa (right)

During the second test flight, the polar vortex has strengthened, showing very low core temperatures, and a wave disturbance caused it to move towards the European sector. Due to conservation of potential vorticity air from the inner vortex edge was moved polewards and coiling up, thus forming a broad intrusion of air with low PV values (Figure 1.2).

2. GLORIA Measurements

During ESSenCe, GLORIA recorded nominal atmospheric measurements including calibration measurements for more than one hour in each flight. Flight 1 covered the chemistry mode, only, while Flight 2 covered both chemistry and dynamics mode. The instrument performance was to a large extent within the specification, with a very good line of sight stabilization, a negligible interferometer shear and a nominal data acquisition. The interferometer velocity fluctuations were greater than expected due to a vibrating part in the mounting of the fixed cube corner. The problem has been identified and the mounting was modified accordingly. Because of the high velocity variations during the flights, the data processing could not be executed as expected, and some extra analysis and processing steps were required. Details are given in the ESSenCe Data Acquisition Report.

2.1. Level 0 and Level 1 Processing of GLORIA Data

2.1.1. Flight Data

In the frame of the ESSENCE project, only a subset of measured data is processed. Flight 2 of 16 December 2011 covers both chemistry and dynamics mode measurements, while Flight 1 of 11 December 2011 only contains chemistry mode measurements. Therefore data of Flight 2 has been processed with priority.

Figure 2.1 shows the interferogram maximum value of pixel [128,58] (third row from below) during Flight 2. The interferogram maximum is a proxy for the integrated radiance. Calibration sequences are color-coded. Chemistry measurements between 14:30 and 14:50 as well as dynamics mode measurements between 14:57 and 15:10 UTC have been processed. The BBc and DS measurements of calibration sequence 3 (around 16:20) have been used for radiometric calibration.

2.1.2. Data Processing

The **Level 0** processing does a resampling of the measured interferograms that are sampled equidistant in time onto an appropriate space-equidistant grid. The processing includes fringe count error (FCE) correction, spectral calibration, and non-linearity correction. FCEs are corrected through shifting of the interferogram on the abscissa such that the zero optical path difference (ZOPD) is at the same sampling point for all interferograms of one pixel. Spectral calibration is done by applying the correct laser wavelength for the calculation of the abscissa and by scaling the abscissa according to the off-axis angle of the respective pixel. The spectral

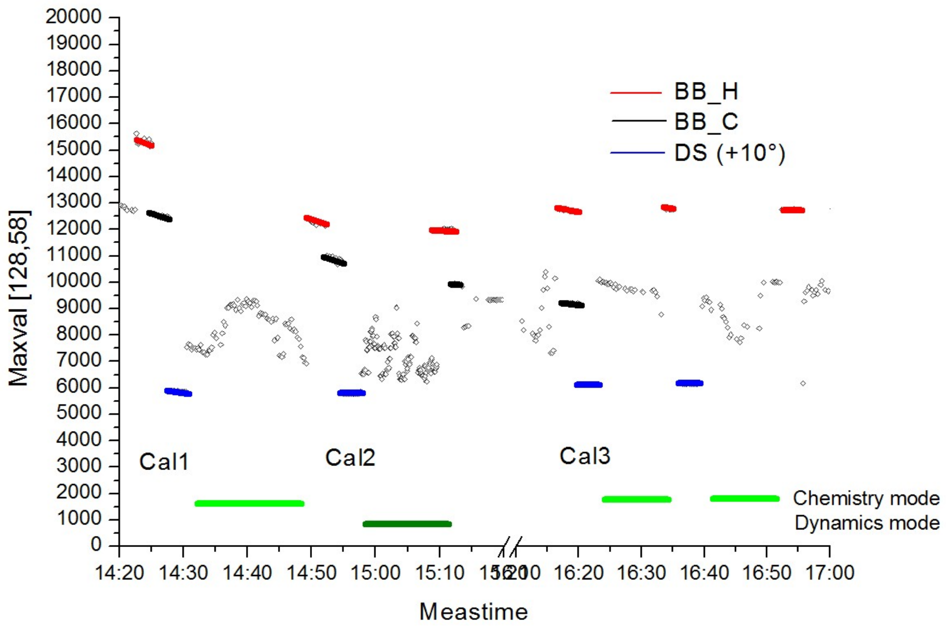

Figure 2.1.: Interferogram maximum value of pixel [128,58] during Flight 2. The interferogram maximum is a proxy for the integrated radiance. Calibration sequences are color-coded. Chemistry measurements between 14:30 and 14:50 as well as dynamics mode measurements between 14:57 and 15:10 UTC have been processed. The BBc and DS measurements of calibration sequence 3 (around 16:20) have been used for radiometric calibration.

calibration parameters are determined from the measured data (see section 2.1.3). The non-linearity of the detector system is corrected by mapping each measured interferogram value onto the value that would have been measured with a linear detector. The non-linearity curve of the detector system is determined from characterization measurements on ground (see section 2.1.4).

The **Level 1** processing performs the Fourier transform of the interferograms and applies the complex radiometric calibration. Calibration spectra are generated from blackbody and deep space measurements using a two-point calibration. Deep space measurements taken from a flight altitude of less than 20 km still contain atmospheric signatures at some wavelength regions. These should be avoided in the retrieval and cover the following regions: below 750 cm^{-1}, between 1000 and 1075 cm^{-1}, and between 1250 and 1340 cm^{-1}.

Several iteration steps are necessary to generate radiometrically and spectrally calibrated spectra:

Database info Extract relevant information for each measured data cube from the flight database (e.g. sweep direction, interferogram length, detector integration time, pointing information, blackbody temperatures).

Iteration 1 Level 0 This step consists of the Level 0 processing of all raw data (cub-files) with the idl Level 0 code (1 pixel). The purpose is to (1) identify erroneous files, (2) get an overview over velocity variations, (3) find the interferogram maximum position for each datacube for a coarse FCE correction. The interferogram maximum is determined through Fourier interpolation of the peak region on a very fine grid.

Iteration 2 Level 0 This iteration serves for the final FCE correction. The cub-files are processed for 11 x 11 pixels around the optical axis with a defined abscissa using the results from Iteration 1. For the optical axis position, a first guess is used. All interferograms are resampled on the same grid (same spacing between interferogram points), and the interferogram length with respect to the interferogram maximum is the same for each measurement mode and sweep direction. The 121 resampled interferograms are co-added to generate data with a better signal to noise ratio. The number of 121 pixels is somewhat arbitrary but provides a good compromise between signal to noise ratio and processing time. Furthermore, these pixels are close enough to the optical axis that off-axis effects (e.g. spectral shift) are negligible for the purpose of this iteration.

Iteration 2 Level 1 standard phase (blackbody) The phase of the blackbody spectra is calculated from the co-added interferograms. The mean phase over all blackbody interferograms for each sweep direction is used as standard phase (outliers are removed).

Iteration 2 Level 1 phase correction (all data) All co-added interferograms are phase corrected by fitting a linear phase to the standard phase. The slope of the linear phase is used to shift the interferograms accordingly for the next iteration (final FCE correction). The uncalibrated spectra calculated in this step allow (1) to check if the phase correction is appropriate and (2) to check the data quality. E.g. ghosts are easy to detect in the imaginary part (see Figure 2.2).

Iteration 3 Level 0 Re-process the cub-files for all pixels with a defined abscissa as deduced from Iteration 1 (ifg-maximum) and Iteration 2 (slope of the phase) using the operational processor (c code).

Iteration 3 Level 1 calibration data Calculate real and imaginary part of the uncalibrated spectra using a fixed ZOPD and no phase correction (i.e. a zero phase is applied to generate complex spectra), using a spectral resolution of 5 cm^{-1}. Several blackbody and deep-space interferograms have been recorded during flight. Spectra of the same signal and sweep direction are co-added.

Iteration 3 Level 1 atmospheric data Calculate the complex calibrated spectra. An example of a complex calibrated spectrum is shown in Figure 2.3.

Pixel binning The Level 2 processors do not use the spectra of individual pixels as input but mean spectra of horizontal pixel lines. For pixel binning, bad spectra are discarded and the other spectra are weighted according to their NESR. The binning criteria are described in more detail in section 2.1.5.

The above described processing is first done with a coarse spectral calibration, taking a first guess as laser wavelength and without applying an off-axis correction. Atmospheric chemistry spectra resulting from this processing are then used for the determination of the correct spectral calibration parameters. Once the parameters are determined, the processing is repeated using the correct spectral calibration parameters and applying an off-axis correction.

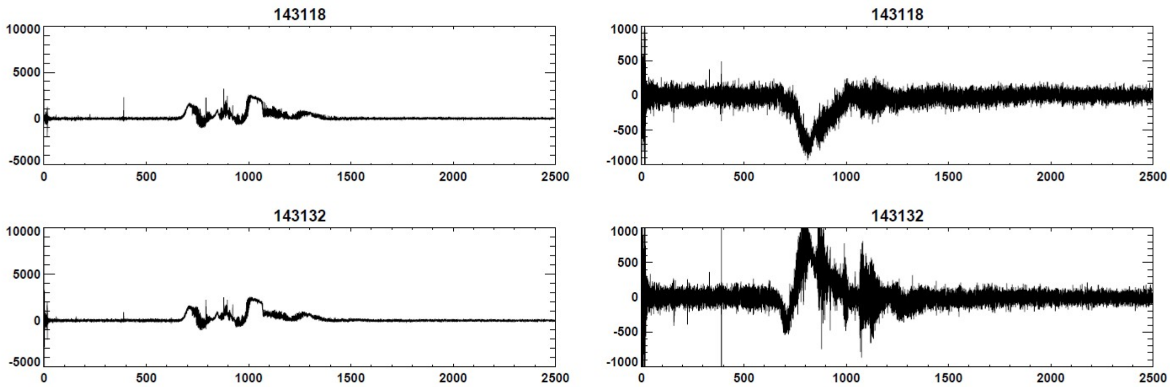

Figure 2.2.: Example of two uncalibrated but phase corrected spectra, chemistry mode.The left plot shows the real part and the right plot shows the imaginary part of the spectrum. While the imaginary part of the upper spectrum only shows the broadband beamsplitter emission, the lower spectrum shows ghost lines in the imaginary part.

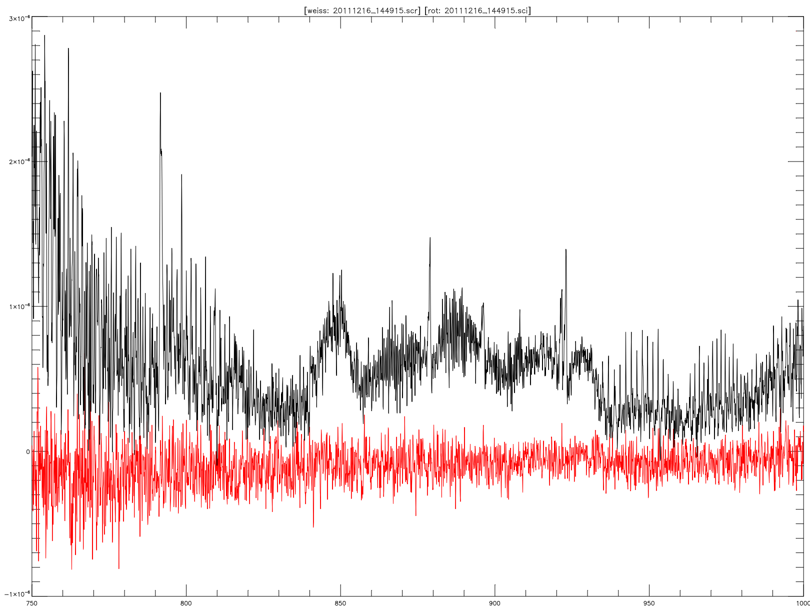

Figure 2.3.: Real (black) and imaginary part (red) of a calibrated single pixel between 750 and 1000 cm^{-1}.

2.1.3. Spectral Calibration

A simple model is applied for spectral calibration. It considers four parameters:

- The reference laser wavelength σ_0.
- The horizontal and vertical position of the optical axis (2 parameters).
- The distance between the imaging lens and the detector (image distance).

With these four parameters, the apparent laser wavelength $\sigma_{i,j}$ of each pixel [i,j] is calculated as:

$$\sigma_{i,j} = \sigma_0 \cos(\alpha) \tag{2.1}$$

and

$$\tan(\alpha) = r_{i,j}/b \tag{2.2}$$

with $r_{i,j}$ being the distance between the center of the pixel [i,j] and the optical axis and b being the image distance.

The spectral calibration parameters (position of the optical axis, image distance and reference laser wavelength) are determined from atmospheric chemistry mode measurements. All forward measurements between 14:28:55 and 14:49:15 have been co-added for noise-level reduction.

In order to find the parameters for performing spectral calibration, single isolated lines with good signal-to-noise ratio are required. The selected lines should have no or minimum overlapping of lines from other gases. The most suitable region is between 940 cm^{-1} and 970 cm^{-1} (Figure 2.4) showing well isolated CO_2 laser band lines. The spectral lines chosen for performing the spectral calibration are listed in Table 2.1.

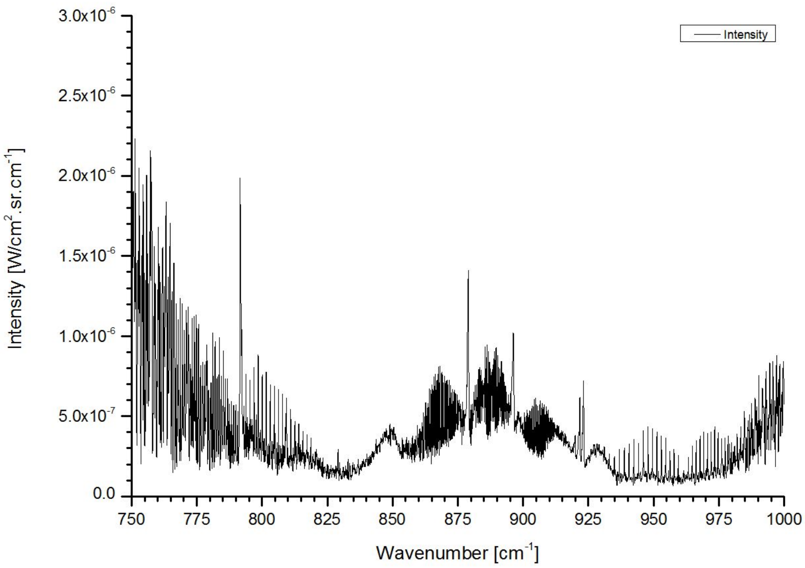

Figure 2.4.: Spectrum plot for pixel [126,124] in the range between 750 cm^{-1} to 1000 cm^{-1}

Table 2.1.: Selected lines from the Hitran database Rothman et al. (2009) used for spectral calibration

Line number	Line position	Line intensity
	cm^{-1}	$cm^{-1}/(molecule.cm^{-2})$
1	942.38334	$1.946e^{-23}$
2	947.74198	$2.209e^{-23}$
3	949.47931	$2.174e^{-23}$
4	951.19226	$2.064e^{-23}$
5	952.88085	$1.876e^{-23}$
6	954.54509	$1.612e^{-23}$
7	956.18498	$1.279e^{-23}$
8	967.70723	$1.791e^{-23}$
9	969.13955	$2.032e^{-23}$
10	970.54724	$2.195e^{-23}$
11	971.93026	$2.28e^{-23}$

Determination of Spectral Calibration Parameter

The position of the optical axis (h, v), image distance and reference laser wavelength are calculated using the line position information over the detector array. Figures 2.5, 2.6 and 2.7 show the optical axis position, the image distance, and the reference laser wavelength for the selected lines respectively. The dashed line in the plots represents the mean of the values. The mean and the standard deviation of the parameters are given in Table 2.2. The selected pixels for one spectral line used for the calculation of the parameters for spectral calibration are shown in Figure 2.8. The pixel area selected is representative for other lines as well. Pixels from the lower part of the array are completely rejected due to clouds.

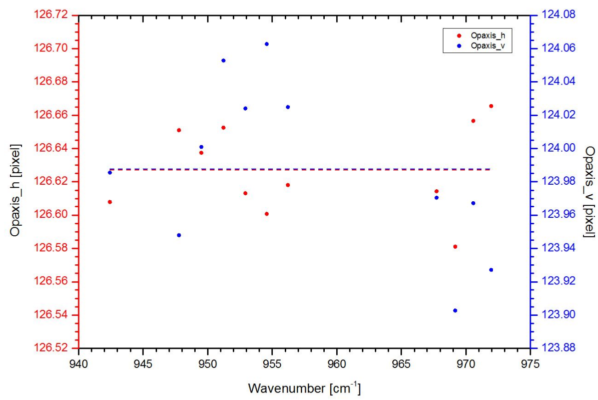

Figure 2.5.: Optical axis position horizontal (red) and vertical (blue) as calculated for the selected CO2 lines

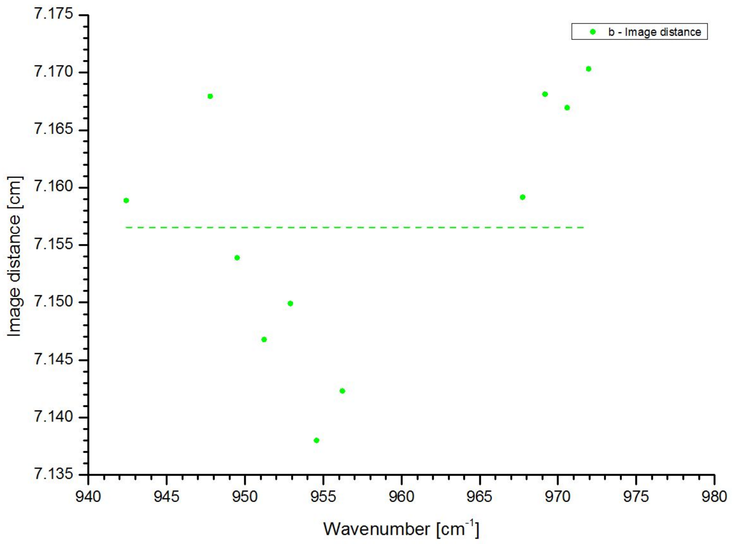

Figure 2.6.: Image distance calculated using selected atmospheric lines

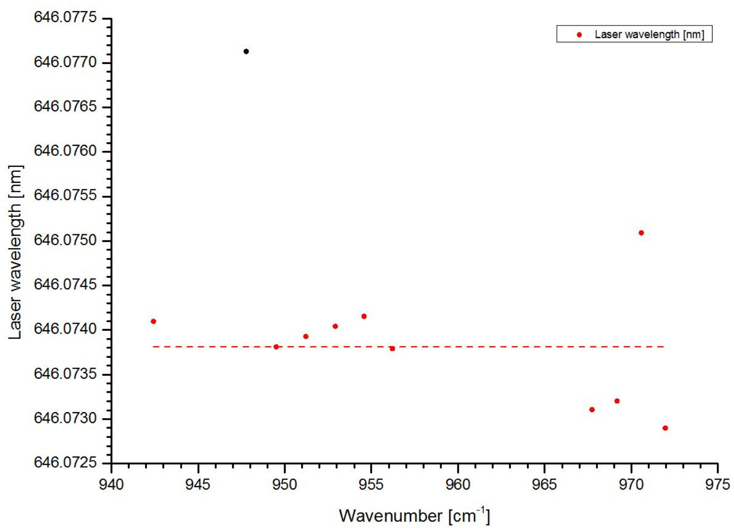

Figure 2.7.: Reference laser wavelength calculated using selected atmospheric lines, one outlier is excluded from the mean calculation.

Table 2.2.: Mean and standard deviation of the parameters calculated using the selected atmospheric lines

Parameter	Mean	sd
Optical axis h [pixel]	126.62707	0.027
Optical axis v [pixel]	123.98782	0.05094
Image distance (b) [cm]	7.15655	0.01126
Laser wavelength [nm]	646.07381	0.0006327

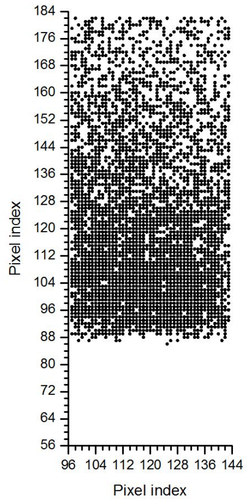

Figure 2.8.: Detector array [48 × 128] showing the pixels used for the calculation of the parameters for spectral calibration. The black dots represent the pixels used and the white dots represent the pixels rejected.

Accuracy of the Calibration Parameters

The mean of 20 measurements of spectrally and radiometrically calibrated data in the measurement time range between 14:28:55 and 14:49:15 (chemistry mode) in forward sweep direction was taken for the analysis.

The CO_2 line at 967.71 cm^{-1} is selected and the line positions over the detector array of 48×128 pixels are determined. The line position distribution over the detector array should be constant if the spectral calibration worked properly. Figure 2.9 shows the line position distribution of the selected line. All pixels below vertical index 88 are cloud contaminated and have absorption lines in the spectrum. These pixels are therefore rejected. The line position is not constant but has a slope with increasing altitude. The shift in the line position is linear and is about 0.04 cm^{-1} from pixel [96,88] to pixel [144,183]. So the total shift over the whole array [48×128] is approximately 0.05 cm^{-1}.

The residual shift shows that the simple model applied for spectral calibration does not describe the spectral behavior across the detector array sufficiently precisely. But it can be corrected by applying an additional scaling factor to each pixel. A linear 2D fit is applied to the residual shift. The determined scaling factor for each pixel is displayed in Figure 2.9 (middle). This additional scaling factor is applied in a further iteration of the processing. After this additional correction, the determined line position only shows some noise which is most likely due to the line position determination method (Figure 2.9, right)

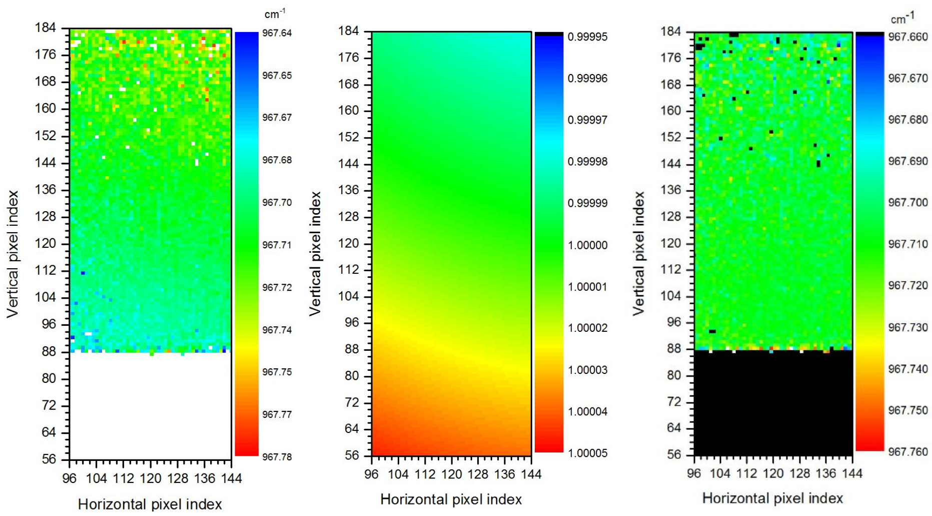

Figure 2.9.: Left: line position [cm^{-1}] plot for CO_2 line at 967.71 cm^{-1} over the detector array [48×128] after performing spectral calibration; middle: additional scaling factor for each pixel determined after the first iteration of spectral calibration; right: line position across the detector array after the additional linear correction.

2.1.4. Non-linearity Characterization

The detector system exhibits a certain non-linearity which has to be corrected prior to applying a two point calibration. On ground measurements with different integration times while looking at a constant radiation source are used for the non-linearity characterization. Figure 2.10 shows the relation between measured DC values and DC values of a virtual linear detector as deduced from measurements with different integration times. The virtual detector is a linear function of the integration time. A fourth order polynomial is fitted to the measurement points. For the non-linearity correction, each measured point of each interferogram is mapped on the virtual linear detector, using this fourth order polynomial. The corrected interferogram is thus calculated as:

$$ifg_{corr} = a_0 + a_1 ifg_{meas} + a_2 ifg_{meas}^2 + a_3 ifg_{meas}^3 + a_4 ifg_{meas}^4$$

with:

a_0=1.678802E+003, a_1=4.225276E-001, a_2=8.238717E-005, a_3=-5.849533E-009, a_4=1.687791E-013.

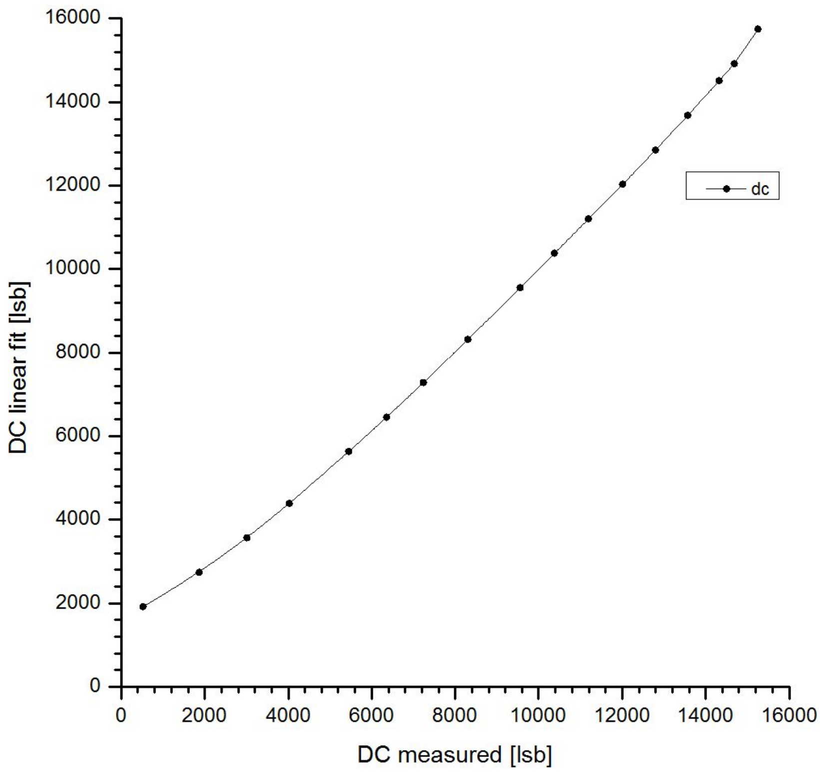

Figure 2.10.: Relation between measured DC values and DC values of a virtual linear detector as deduced from measurements with different integration times.

A non-linear response of the detector system leads to out-of-band artifacts in the spectrum. A minimization of the artifacts is thus a good quality control for the non-linearity correction. Figure 2.11 shows a magnitude spectrum of pixel [102,140] before (black) and after non-linearity correction (red) when looking at a blackbody. The maximum of the spectrum is scaled to 1. The out of band artifacts below 500 cm^{-1} and above 1600 cm^{-1} are clearly visible in the uncorrected data while the signal in these ranges after correction is dominated by noise, only.

The spectral intensity between 20 and 400 cm^{-1} is taken for the quality control of the non-linearity correction. Figure 2.12 shows the mean of the blackbody spectrum in the range between 20 to 400 cm^{-1} before and after applying the non-linearity correction. The mean value is around 250 and 50 arbitrary units respectively excluding bad pixels. The positive residual value is mainly due to the magnitude calculation, turning negative noise values into positive ones. Figure 2.12 shows that the nonlinearity correction works for most pixels. Bad pixels are discarded during pixel binning.

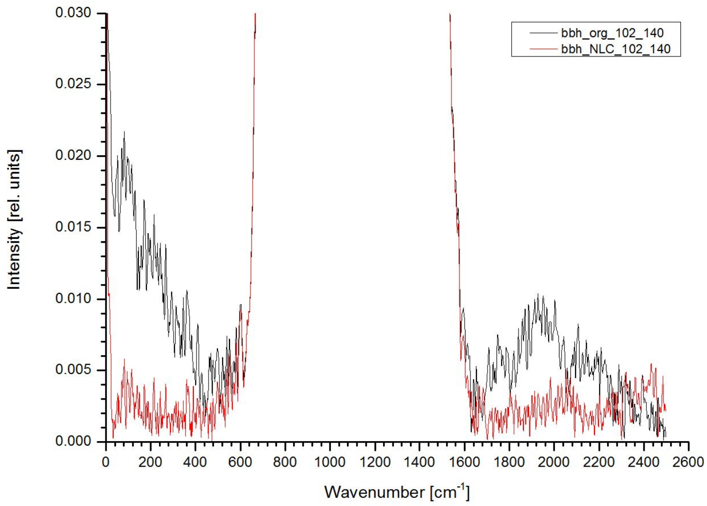

Figure 2.11.: Blackbody spectrum before (black) and after non-linearity correction (red).

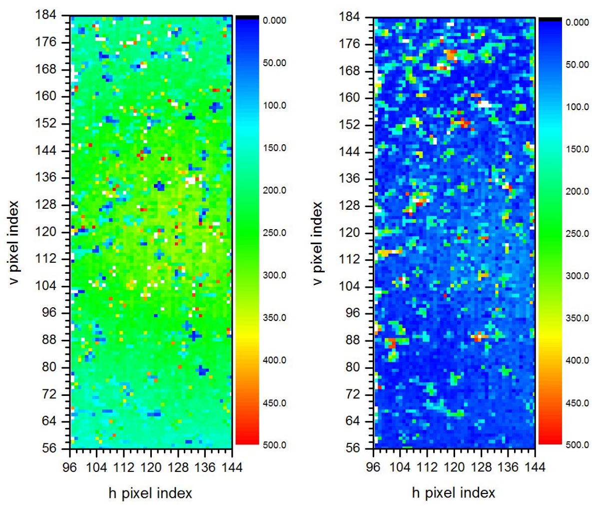

Figure 2.12.: Mean of a blackbody spectrum in the range between 20 to 400 cm^{-1} without (left) and with (right) nonlinearity correction plotted for 48 × 128 pixels. The blackbody was maintained at a temperature of 259.9 K. The mean is given in arbitrary units.

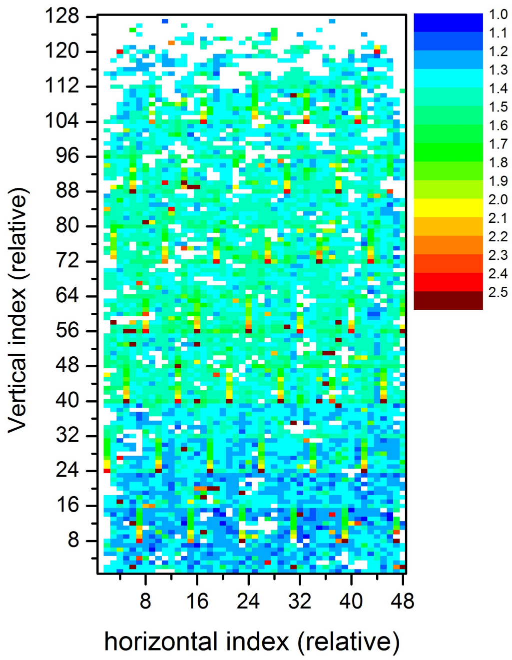

Figure 2.13.: Relative NESR for each pixel used for pixel binning. White pixels are excluded from binning.

2.1.5. Pixel Binning

The pixels of each horizontal line are binned in order to form a spatial sample. Two criteria are applied for pixel binning:

1. The radiometric error of the pixel shall not exceed 2 %.

2. The pixels are weighted according to their individual NESR.

The criteria are applied to calibrated blackbody data. For this purpose, the BBh and BBc measurements of calibration sequence 2 are taken. The blackbody temperatures are around 260 and 252 K, respectively, while the blackbody used for the generation of the calibration data (calibration sequence 3) had a temperature of about 234 K. The radiometric quality criterion is thus applied to extrapolated data, and it is expected that the actual radiometric error for the scene spectra is lower than 2 %, because the radiance level of the scene spectra is typically framed by the blackbody and deep space measurements used for calibration (see Figure 2.1). The quality criterion is applied to the mean of the spectral range between 800 and 1000 cm^{-1}.

The NESR is calculated as standard deviation of the difference between measured calibrated blackbody spectra and the corresponding Planck function. Quality check and NESR calculation are made for the co-added spectra of BBh and BBc measurements of calibration sequence 2, separately for forward and reverse interferometer sweep directions. So in total four datasets are used to generate the pixel binning mask. The quality criterion must be fulfilled for all four spectra, otherwise the pixel is rejected from binning. The NESR used to calculate the weighting factor is the mean NESR calculated from the four datasets. Note that this NESR is

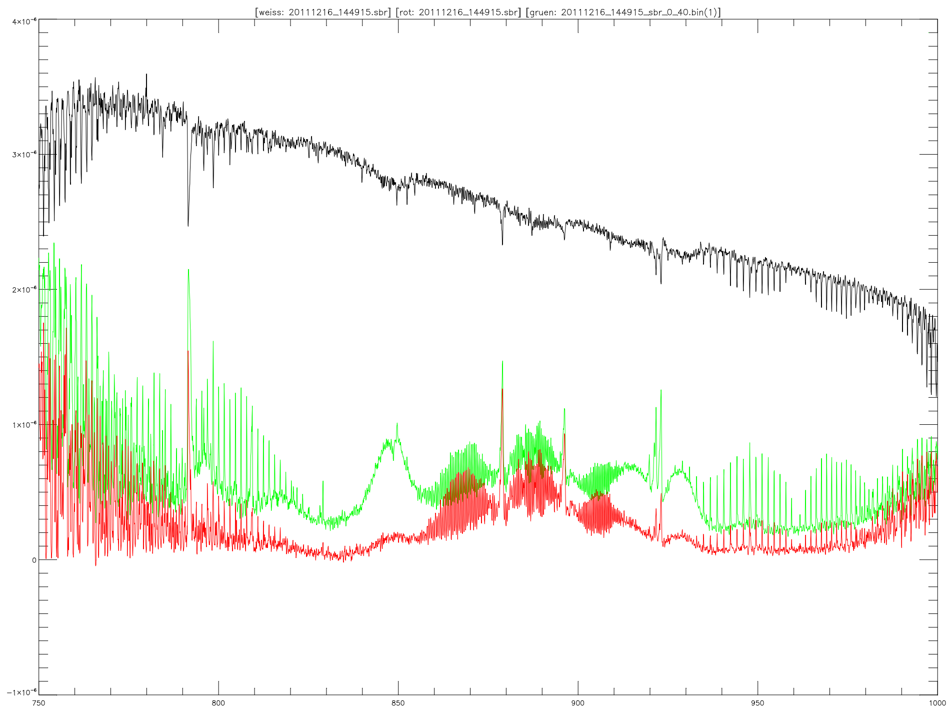

Figure 2.14.: Calibrated spectra between 750 and 1000 cm^{-1} from three different altitudes after pixel binning. Black: lowermost row, green: row #40, red: row #80.The ordinate ranges from -1·10^{-6} to +4·10^{-6} nW / cm^2 sr cm^{-1}.

a relative quantity, because a different number of spectra is co-added for each dataset. This value is only used to calculate a relative weighting factor for each pixel.

Figure 2.13 shows the relative NESR values for the individual pixels. Pixels that are excluded from binning, because they did not pass the radiometric quality criterion, are marked in white. About 20 % of the pixels are rejected because of this criterion.

It should be noted that the Level 1 data is provided on a single pixel basis and as binned data. Pixel binning can thus easily be modified and optimized using different criteria. Figure 2.14 shows spectra between 750 and 1000 cm^{-1} from three different altitudes after pixel binning.

2.2. Level 2 processing of GLORIA Chemistry Mode Data

2.2.1. Measurement Overview

In the chemistry mode, GLORIA records spectra at a maximum optical path difference of 8 cm yielding a spectral resolution of 0.125 cm^{-1} (apodized). The line of sight is fixed at 90° (starboard) with respect to the airplane flight direction. Measurement time for one image (one interferometer sweep) is 12.3 s. Individual images contain 128x48 pixels / spectra, which are averaged on a 128x1 grid (see below). Chemistry mode data analyzed here consists of 68 images acquired during the ESSenCe flight 2 between 14:30 and 14:49 UTC. This time period was chosen out of 7 chemistry mode sequences (Figure 1.1) due to the preselection described in Section 2.1. The flight track of the Geophysica aircraft with the tangent points of the analyzed GLORIA measurements is shown in Figure 2.15. Figure 2.15 also presents positions of MIPAS-STR measurements, as well as position and time of satellite and radiosonde measurements available in the vicinity of the Geophysica trajectory during the ESSENCE flight. The measurements provided atmospheric parameters enabling intercomparisons with GLORIA retrieval results (Section 2.2.4).

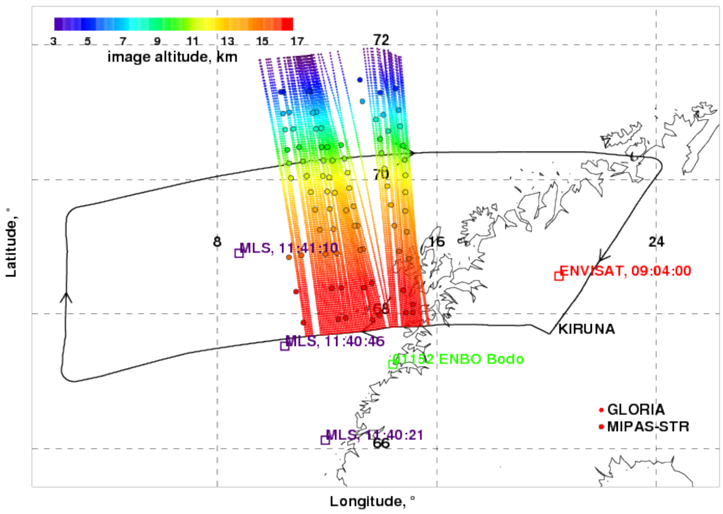

Figure 2.15.: The flight track of Geophysica aircraft from December 16th 2011 and tangent point distribution of the chemistry mode measurements. The colors of the points indicate the tangent altitudes after the line-of-sight correction (described in Section 2.2.3). The circles illustrate the tangent points of the MIPAS-STR measurements acquired during the GLORIA chemistry mode and used for the intercomparisons presented in Section 2.2.4. The color of the circle fields provides the tangent altitude information. The violet and red squares represent locations of satellite measurements applied for the comparisons with GLORIA retrieval results. The green square indicates launch position of a radiosonde providing a temperature profile plotted in Figure 2.27 and used for GLORIA retrieval examination.

2.2.2. Preprocessing

The major input for the chemistry mode retrieval chain are data-cubes of the real and the imaginary parts of calibrated spectra (spectral images). To improve the S/N for the retrieval, horizontal averages of all bins within each data-cube are used, i.e., after a pixel selection process all selected pixels within a row have been averaged.

On the basis of these binned 1-dimensional limb-views a cloud detection is performed and only the cloud-free part is handed over to the non-linear retrieval process.

Pixel Binning

Before the spectra of each image row are co-added, a pixel selection is performed. This is based on the standard deviation of the imaginary spectra. In the ideal case these imaginary spectra should only contain noise. However, various effects (e.g. a non-optimal phase correction) can easily be detected also in the imaginary spectra. The top part of Figure 2.16 shows an example for an image of the standard deviation of the imaginary spectra (STDIS) within the 800-949 cm^{-1} spectral range. Obvious outliers are easily detectable even by eye (mainly colored orange-red). For automatic recognition of these pixels we have applied a median filter for each pixel row separately: all pixels of a row with values of STDIS larger than the median(STDIS) plus three times the standard deviation of STDIS are removed (Figure 2.16). Before co-adding of pixel-rows a 'bad-pixel-mask' from L1-analysis (Section 2.1.5) is applied. Averaging of selected pixels is then performed by Gaussian weighting on the basis of the STDIS values.

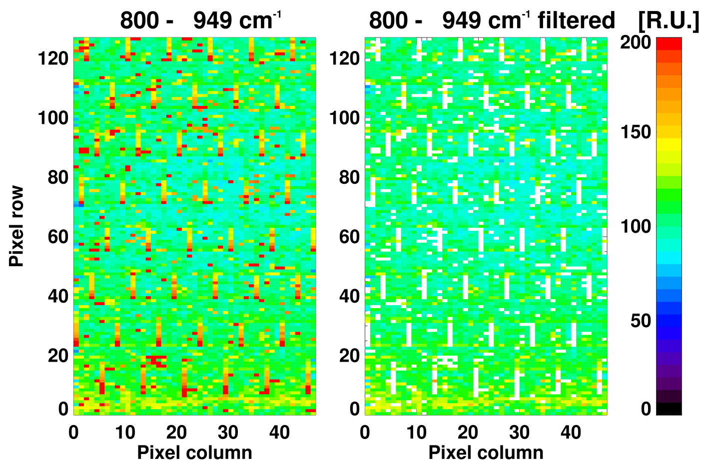

Figure 2.16.: Image of the standard deviation of the imaginary part of the spectra between 800-949 cm^{-1} for one data cube. Left: without selection, right: rejected pixels colored white.

Cloud Identification

Different approaches for the identification of clouds in mid infrared spectra have been developed (e.g. Spang et al., 2004; Kleinert and Glatthor, 2011). The differential approach of Kleinert and Glatthor (2011) is most robust with respect to uncertainties in instrument characterization and has been chosen for chemistry mode cloud detection.

On the left part of Figure 2.17 we show the altitude profile of the radiances integrated within the spectral range 800-949 cm^{-1}. Obviously below a certain pixel row the radiances increase strongly. This increase is due to clouds which enhance the broadband spectral signal. The middle and the right part of Figure 2.17 show the first and second derivative of the integrated radiances with altitude. These curves indicate clearly the sudden change in radiance at the point of reaching the cloud top. In principle all of those curves could be applied for cloud top detection. Here we have used the 2nd derivative: starting from top, the actual value of the 2nd derivative is compared with the mean of the 2nd derivative values above. In case the mean is exceeded by five times the standard deviation of the values above, the relevant altitude is identified as the cloud top. This threshold corresponds to a cloud index as defined in the dynamics mode analysis (Section 2.3.3) of 1.6–1.8.

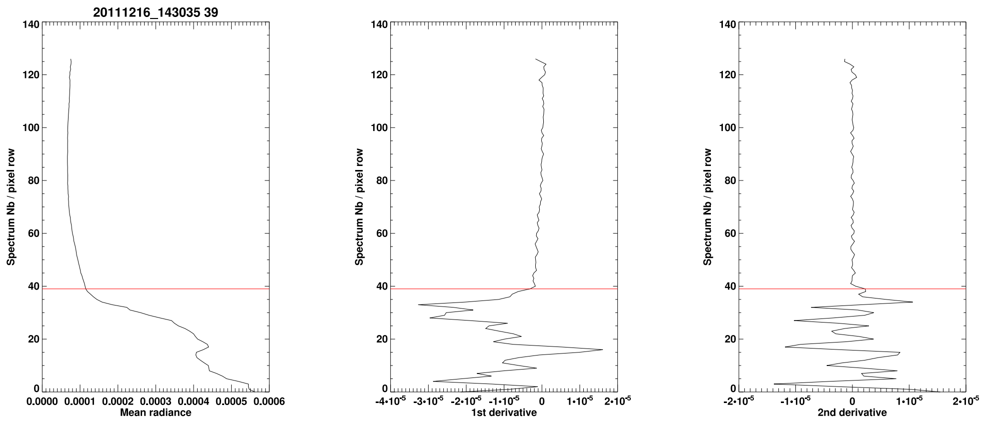

Figure 2.17.: Vertical profile of integrated radiance (left), the first derivative of integrated radiance (800-949 cm^{-1}) with respect to row number (middle), and the second derivative of integrated radiance with respect to row number (right).

2.2.3. Retrieval

The retrieval of altitude profiles of atmospheric parameters from GLORIA chemistry-mode limb-radiance spectra is performed for cloud-free pixel, only. Retrieval tool is KOPRAFIT developed at Karlsruhe Institute of Technology (KIT). The kernel of KOPRAFIT is the fast line-by-line radiative transfer algorithm KOPRA (Stiller, 2000). KOPRAFIT is the standard tool at KIT-IMK applied for the retrieval of altitude profiles from balloon and aircraft (e.g., Woiwode et al., 2012).

The retrieval scheme is a constrained global fit approach using all tangent altitudes of one limb-scan with averaged spectra simultaneously. Atmospheric and instrumental parameters are combined in the vector $\vec{x}$, which is determined in a Newtonian iteration process (Rodgers, 2000; von Clarmann et al., 2003):

$$\begin{aligned} \vec{x}_{i+1} &= \vec{x}_i + (\mathbf{K}_i^T \mathbf{S}_y^{-1} \mathbf{K}_i + \mathbf{R})^{-1} \\ &\quad \times \left[\mathbf{K}_i^T \mathbf{S}_y^{-1} (\vec{y}_{\mathrm{meas}} - \vec{y}(\vec{x}_i)) - \mathbf{R}(\vec{x}_i - \vec{x}_a) \right]. \end{aligned} \tag{2.3}$$

$\vec{y}_{\mathrm{meas}}$ is the vector of selected measured spectral radiances of all tangent altitudes under investigation, and $\mathbf{S}_y$ is the related noise covariance matrix. $\vec{y}(\vec{x}_i)$ contains the spectral radiances calculated with the radiative transfer model KOPRA using the best guess atmospheric state parameters $\vec{x}_i$ of iteration number i. $\mathbf{K}_i$ is the Jacobian matrix, i.e. the partial derivatives $\partial\vec{y}(\vec{x}_i)/\partial\vec{x}_i$ calculated also with the radiative transfer model. $\mathbf{R}$ is the regularization matrix and $\vec{x}_a$ the a-priori information.

The retrieval of the atmospheric parameters was performed on a grid with 0.25 km level spacing up to 20 km and increasing grid distance above. A first-order smoothing constraint $\mathbf{R} = \gamma \mathbf{L}^T \mathbf{L}$ with the altitude-independent but species-dependent regularisation parameters γ has been applied. $\mathbf{L}$ is a first order finite differences operator (Tikhonov, 1963).

For initial guess and a-priori values of temperature ECMWF analysis data (Dee et al., 2011) has been chosen while climatological profiles have been used in case of trace gases. The regularization strength was chosen such as to just avoid oscillatory structures in the retrieved profiles of all atmospheric parameters. For instrumental join-fit parameters like spectral shift, radiance offset or line-of-sight (LOS), no regularisation has been applied.

Table 2.3 provides an overview of the atmospheric parameters retrieved from the GLORIA data with corresponding microwindows and fitted parameters. The results of the retrievals presented in the next two sections are selected by applying the image quality mask mentioned in Section 2.1. This section provides results of the LOS, temperature and vmr retrievals, whereas the next one includes intercomparisons of the GLORIA, remote sensing and in-situ vmr and temperature profiles.

Line-of-Sight

The upper panel of Figure 2.18 presents a comparison of GLORIA and MIPAS-STR radiances (c.f. Section 4.1). The elevation levels at which GLORIA radiance enhancement due to clouds is observed are inconsistent with the measurements of MIPAS-STR. The decrease in GLORIA radiances is located at larger elevation than the decrease measured by MIPAS-STR and indicates a higher cloud top. To estimate an accurate elevation and further also the tangent altitudes, the LOS correction was retrieved and implemented into the atmospheric parameter retrievals listed in Table 2.3.

The line-of-sight retrieval takes ECMWF temperatures as a-priori data to model the CO_2 signature between 957 and 965.5 cm^{-1}. Retrieval target is a constant line-of-sight offset for all images in the chemistry mode sequence. The results of the retrieval are shown in Figure 2.19 with the mean LOS offset equal to 0.002 radians (0.115°). The GLORIA radiances after the

Target parameter	**Microwindow in cm^{-1}**	**Co-fits**
LOS correction	957-965.5	shift, cont.
Temperature	957-965.5	shift, cont.
O_3	778-782.5	T, H_2O, $ClONO_2$, shift, offset
$ClONO_2$	778-782.5	T, H_2O, O_3, shift, offset
HNO_3	876-880	H_2O, CFC-12, shift, offset, cont.
CFC-12	915-925	CO_2, HNO_3, CFC-113, shift, offset, cont.
H_2O	795.625-796.25 848.0-855.0	CFC-11, shift, offset, cont.

Table 2.3.: Retrieval overview. Shift corresponds to spectral shift, offset to a spectral constant radiance offset per microwindow and cont. to continuum. In the O_3 and $ClONO_2$ retrieval, the offset was calculated for each pixel. For the retrievals with continuum co-fit, one mean offset estimation was provided for each image.

LOS correction are presented in the bottom panel of Figure 2.18 and show a good agreement with the MIPAS-STR data.

Temperature

Individual temperature profiles are retrieved after applying the line-of-sight correction. The same microwindows as for the line-of-sight retrieval are applied. The results of the horizontal flight part are plotted in the top left panel of Figure 2.20. The corresponding initial guess data set based on the ECMWF data and implemented in the calculations is given in the top right panel. The black areas indicate clouds or altitudes above the flight track (with pixel elevation larger than 90°). The error due to spectral noise of the plotted retrieval result is in the 0.6 - 1.1 K range and the vertical resolution is better than 0.8 km. Both are presented in Figure 2.20 in the middle left and right panel respectively. The differences between the measured and the calculated spectra are presented for each pixel in the form of root-mean-square (RMS). The RMS analysis shows values below 40 nW/(cm^2 sr cm^{-1}).

Ozone

Ozone and chlorine nitrate are retrieved together in the 778-782.5 cm^{-1} microwindow (Figure 2.21). In Figure 2.21 only the images with mean RMS<100 nW/(cm^2 sr cm^{-1}) are shown. The RMS corresponds to the root-mean-square of a difference between measured and expected (simulated) GLORIA spectra at defined geolocation (superpixel). As an example why results are selected after the retrieval two situations with different RMS values are displayed in Figure 2.22. In the top panel simulated and measured spectra corresponding to the tangent altitude of 12.439 km (14:38 UTC) are plotted. In the panel directly below the resulting differences are shown. The RMS derived for the analysed superpixel equals around 33 nW/(cm^2 sr cm^{-1}). For the second example (two lower panels) a superpixel with tangent altitude of 12.248 km (14:32 UTC) was chosen. In this case the differences between the two spectra are clearly

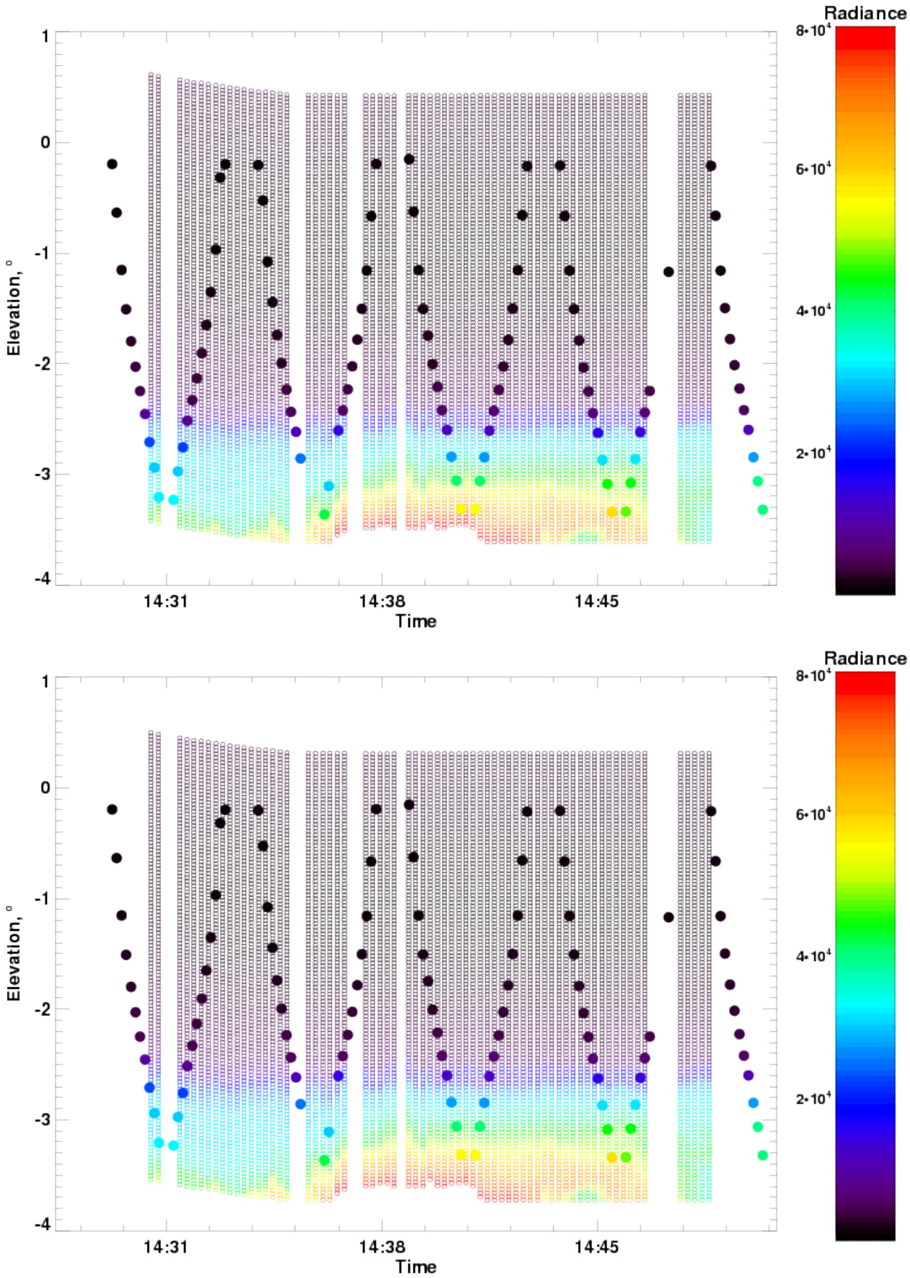

Figure 2.18.: MIPAS-STR - GLORIA radiance (nW/cm^{2}sr) comparison for the chemical mode measurements in the wavenumber region between 949 and 969 cm^{-1}. Tiny squares represent GLORIA data, whereas the full circles correspond to MIPAS-STR measurements (c.f. Section 4.1). MIPAS measurements have been corrected for a line-of-sight offset of 0.0833° due to its line-of-sight retrieval. The upper (lower) panel shows GLORIA data without (with) the retrieved line-of-sight correction.

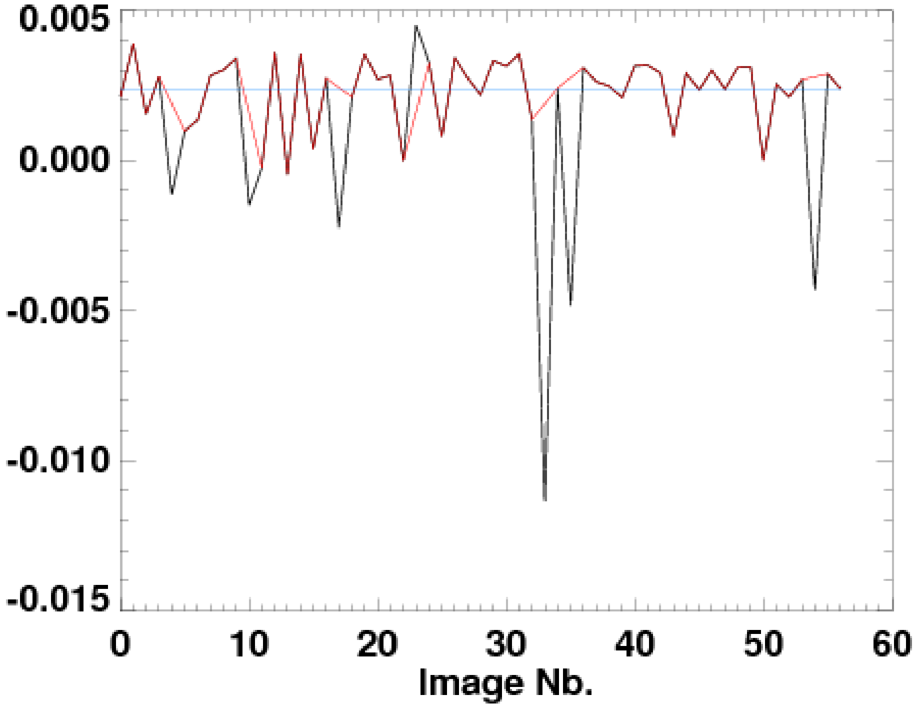

Figure 2.19.: Line-of-sight retrieval result in radian. The black line represents the LOS offset retrieved for the images. The red line shows the offsets used for the mean LOS correction estimation and corresponds to the offsets smaller than standard deviation. The obtained mean LOS offset of 0.002 radians is plotted with the blue line.

larger providing the RMS of approximately 104 nW/(cm^2 sr cm^{-1}). This hints at undetected problems in the calibrated spectra which are probably the reason for the high RMS values in those few cases. In the analysis of the retrieval results, we use the RMS to control the retrieval quality and to avoid employing of erroneous images in e.g. the vmr profiles estimation. For the O_3 and $ClONO_2$ retrieval 4 images are rejected due to high mean RMS values. For the O_3 retrieval results with RMS<100 nW/(cm^2 sr cm^{-1}) the mean noise error equals 0.1 ppm and the vertical resolution is between 0.2 - 1.1 km (Figure 2.21).

$ClONO_2$

The distribution of vmr profiles shows a structure of enhanced chlorine nitrite at altitudes between 15 and 17 km (cf. Figure 2.23). The mean noise error of the result is estimated to 0.03 ppb and the vertical resolution is 1.0 - 2.2 km.

The retrieval of $ClONO_2$ is based on a minor spectral signal at these very low $ClONO_2$ values. Thus, we attribute most of the patchy structure of $ClONO_2$ along the flight track mainly to instrumental artifacts rather than to atmospheric variability.

HNO_3

Nitric acid was retrieved from the 876-880 cm^{-1} range. The results shown in Figure 2.24 are characterized by a mean error of 0.1 ppb, a vertical resolution of 0.4 - 1.1 km and radiance RMS below 40 nW/(cm^2 sr cm^{-1}).

CFC-12

The Freon 12 (CFC-12) retrieval (Figure 2.25) was carried out for the microwindow between 915 and 925 cm^{-1}. The noise error analysis shows a relatively homogeneous distribution with mean errors around 6 ppt. The two spikes observed at 13°E and 15°E in the error plot appear also in the resolution and the radiance RMS contour indicating images with larger instrumental errors and hence with relatively low retrieval quality. The mean vertical resolution is around 1 km and the radiance RMS less than 40 nW/(cm^2 sr cm^{-1}).

H_2O

The results of GLORIA retrievals for water vapor are shown in Figure 2.26. The calculations are made for the 795.625-796.25 and 848.0-855.0 cm^{-1} ranges and provide results with mean errors of 0.25 ppm and a vertical resolution of up to 2.4 km. Mind that for this first analysis of H_2O from GLORIA spectra only windows below 1000 cm^{-1} have been adopted. Though we have selected two of the stronger H_2O lines here, their signal is still rather small which is reflected in the estimated values of noise error and vertical resolution. Due to the weak signal, even small instrumental errors (apart of spectral noise) are visible. These probably lead to an inhomogeneous distribution along the flight track for H_2O, similar as in the case of $ClONO_2$.

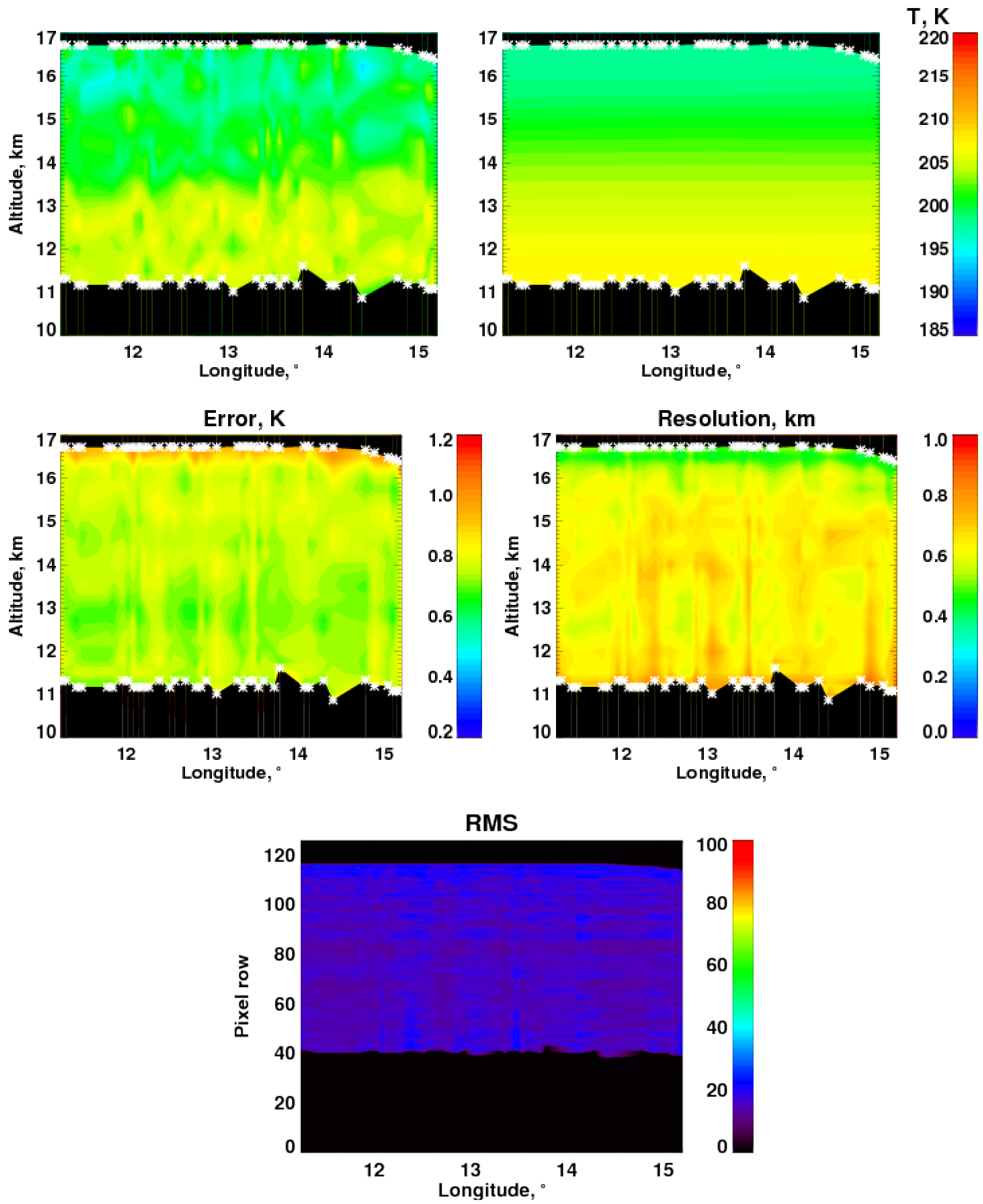

Figure 2.20.: Temperature retrieval result (top left), initial guess (top right), error (middle left), resolution (middle right) and RMS of spectra in nW/(cm^2 sr cm^{-1}) (bottom) plotted against longitude. The white stars represent position of profiles resulting from GLORIA measurements. The regions between the stars are interpolated. Cloud layer is indicated with the bottom black area, the upper black areas represent altitudes above the Geophysica flight altitude (cf. Section 2.2.2).

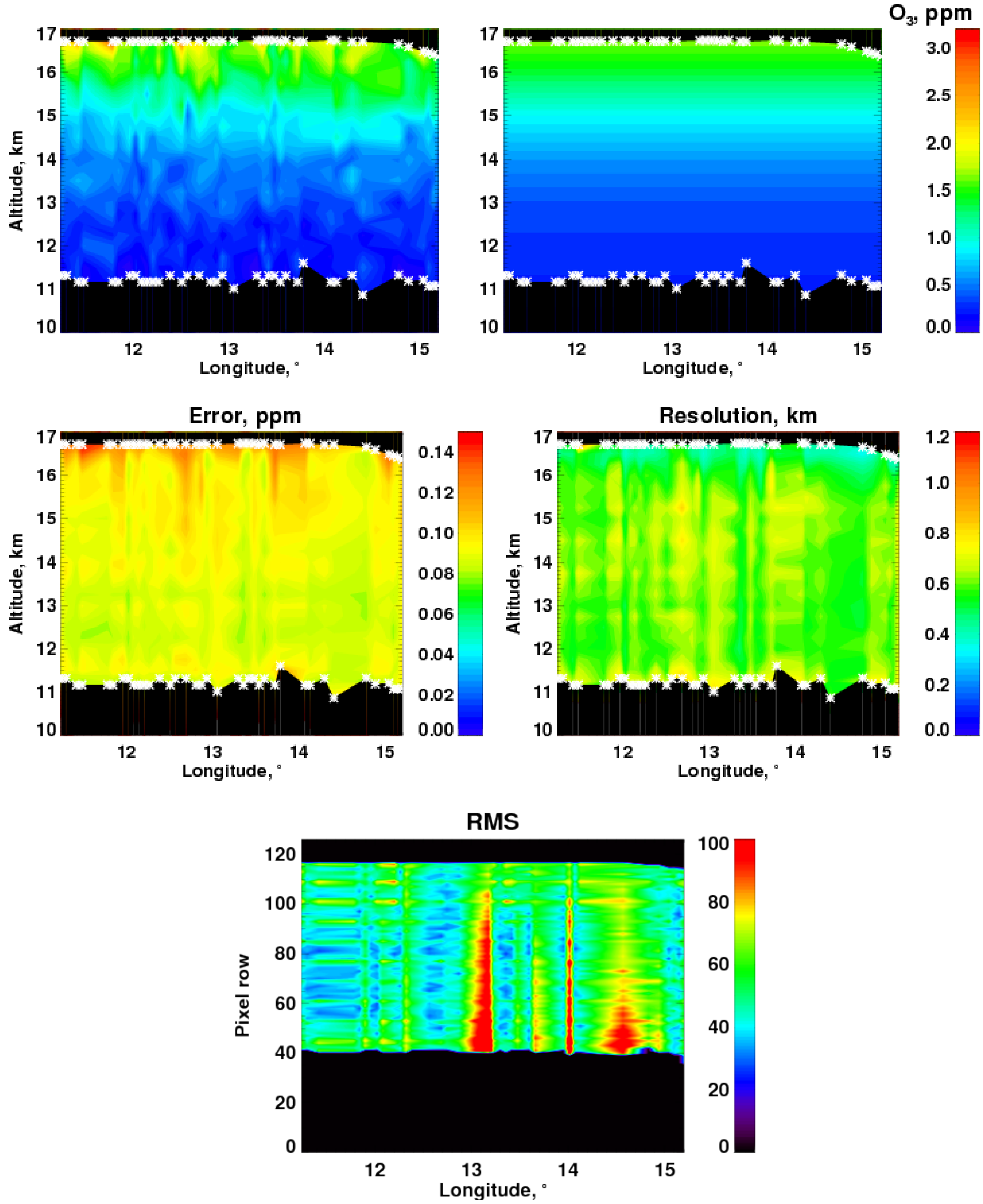

Figure 2.21.: Ozone retrieval result (top left), initial guess (top right), error (middle left), resolution (middle right) and RMS of spectra (bottom) plotted against longitude. Detailed figure description as in Figure 2.20.

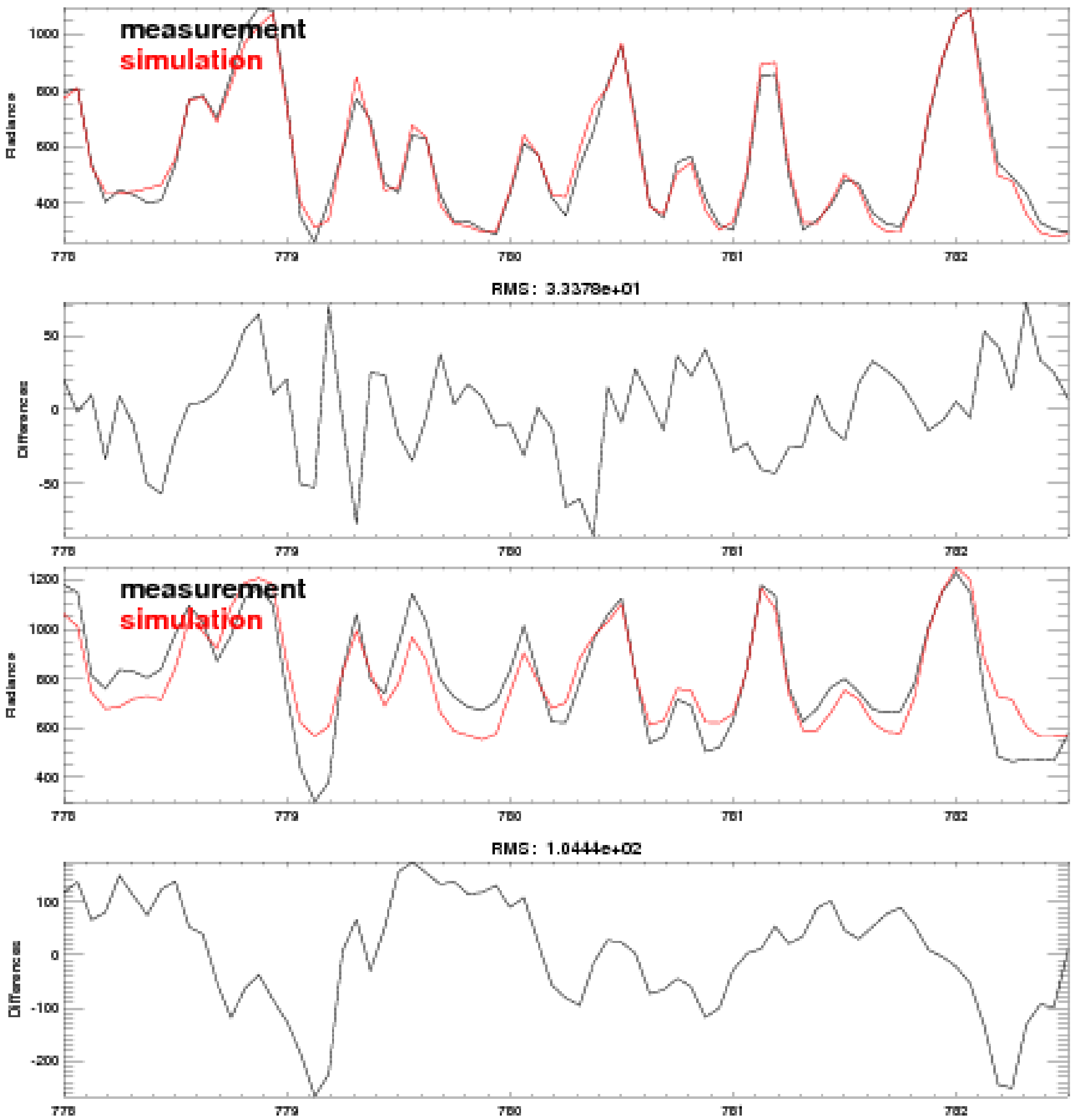

Figure 2.22.: Spectra comparison used for RMS estimation. The top plot shows an example of measured and simulated spectra corresponding to the 778-782.5 cm^{-1} microwindow and 12.439 km tangent altitude. In the second plot from the top the differences of the two spectra are displayed. The root-mean-square (RMS) equals here 33.38. In the bottom panels the two spectra and the differences are plotted for another image (tangent altitude 12.248 km). The RMS in this case equals 104.44. All values are expressed in $\mathrm{nW/(cm^2\,sr\,cm^{-1})}$.

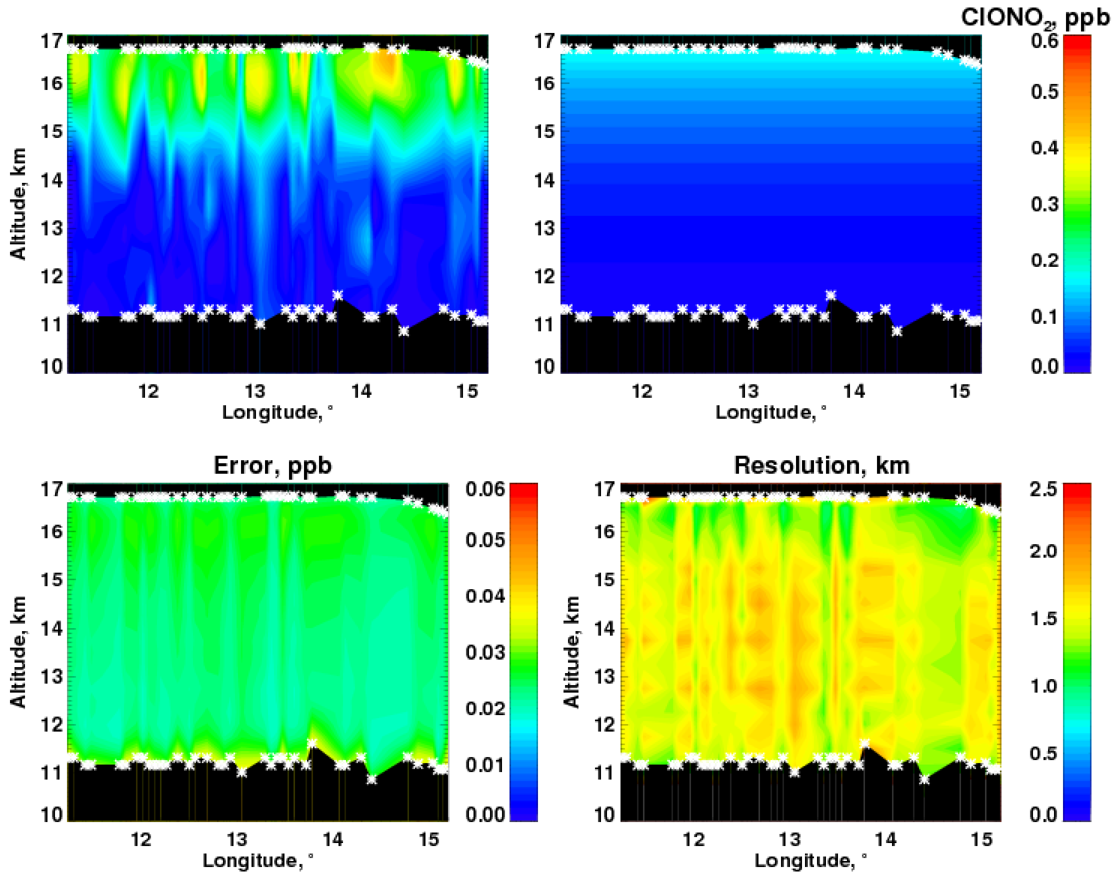

Figure 2.23.: Chlorine nitrate retrieval result (top left), initial guess (top right), error (middle left), resolution (middle right). Since the $ClONO_2$ is a co-fit in the O_3 retrieval, the RMS of the O_3 spectra (bottom plot in Figure 2.21) is also valid for this retrieval. Detailed figure description as in Figure 2.20.

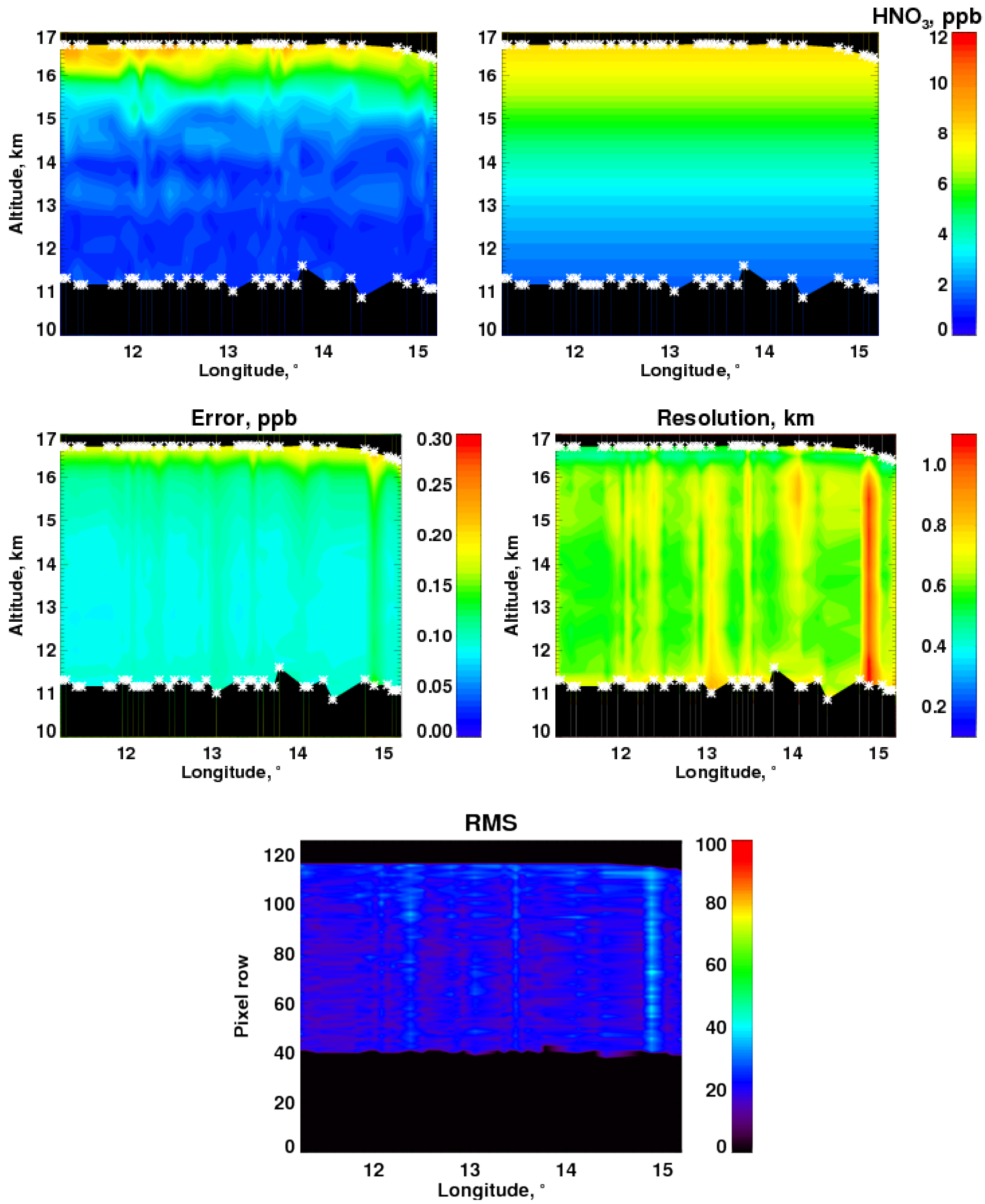

Figure 2.24.: Nitric acid retrieval result (top left), initial guess (top right), error (middle left), resolution (middle right) and radiance RMS of spectra (bottom) plotted against longitude. Detailed figure description as in Figure 2.20.

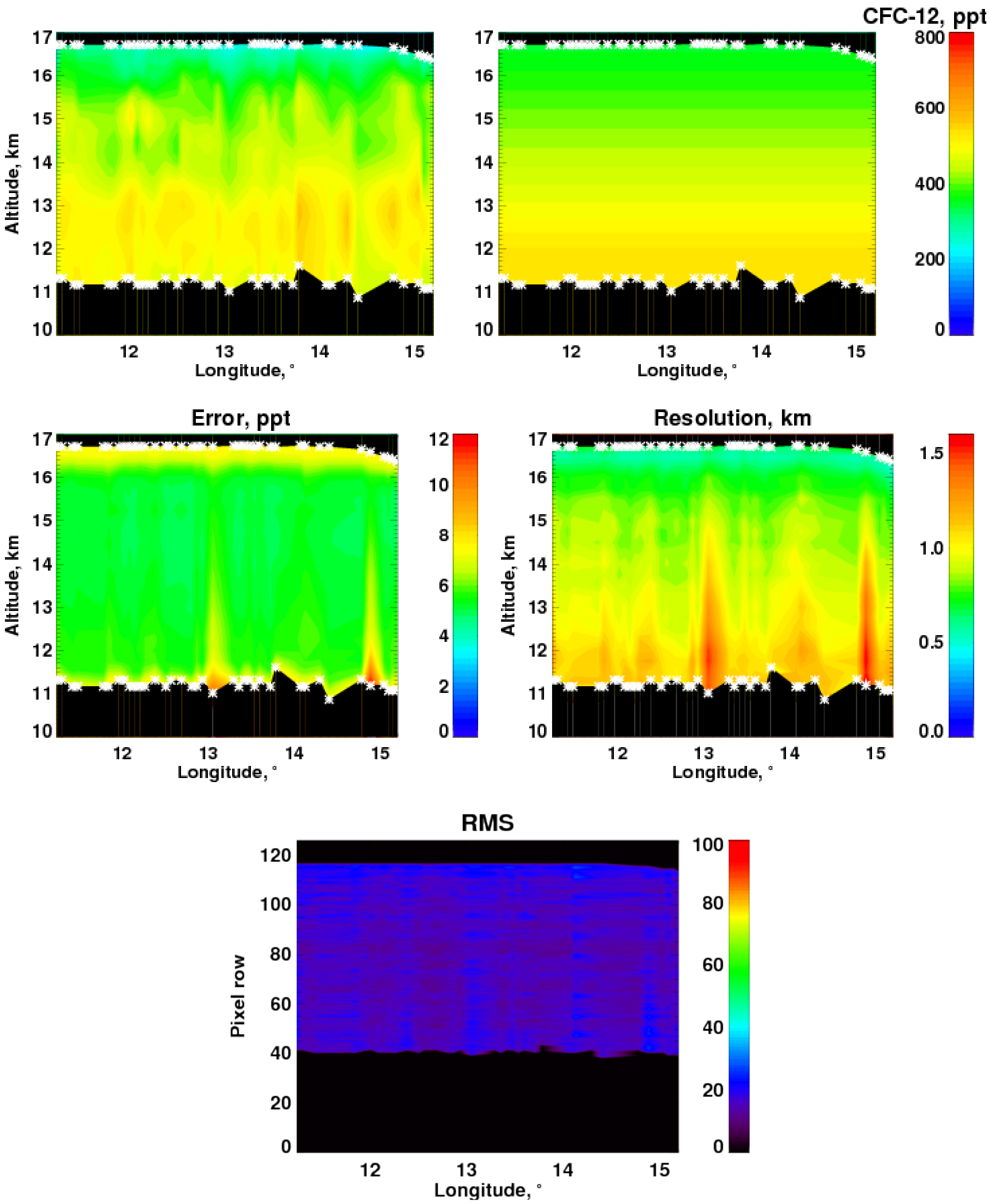

Figure 2.25.: CFC-12 retrieval result (top left), initial guess (top right), error (middle left), resolution (middle right) and radiance RMS of spectra (bottom) plotted against longitude. Detailed figure description as in Figure 2.20

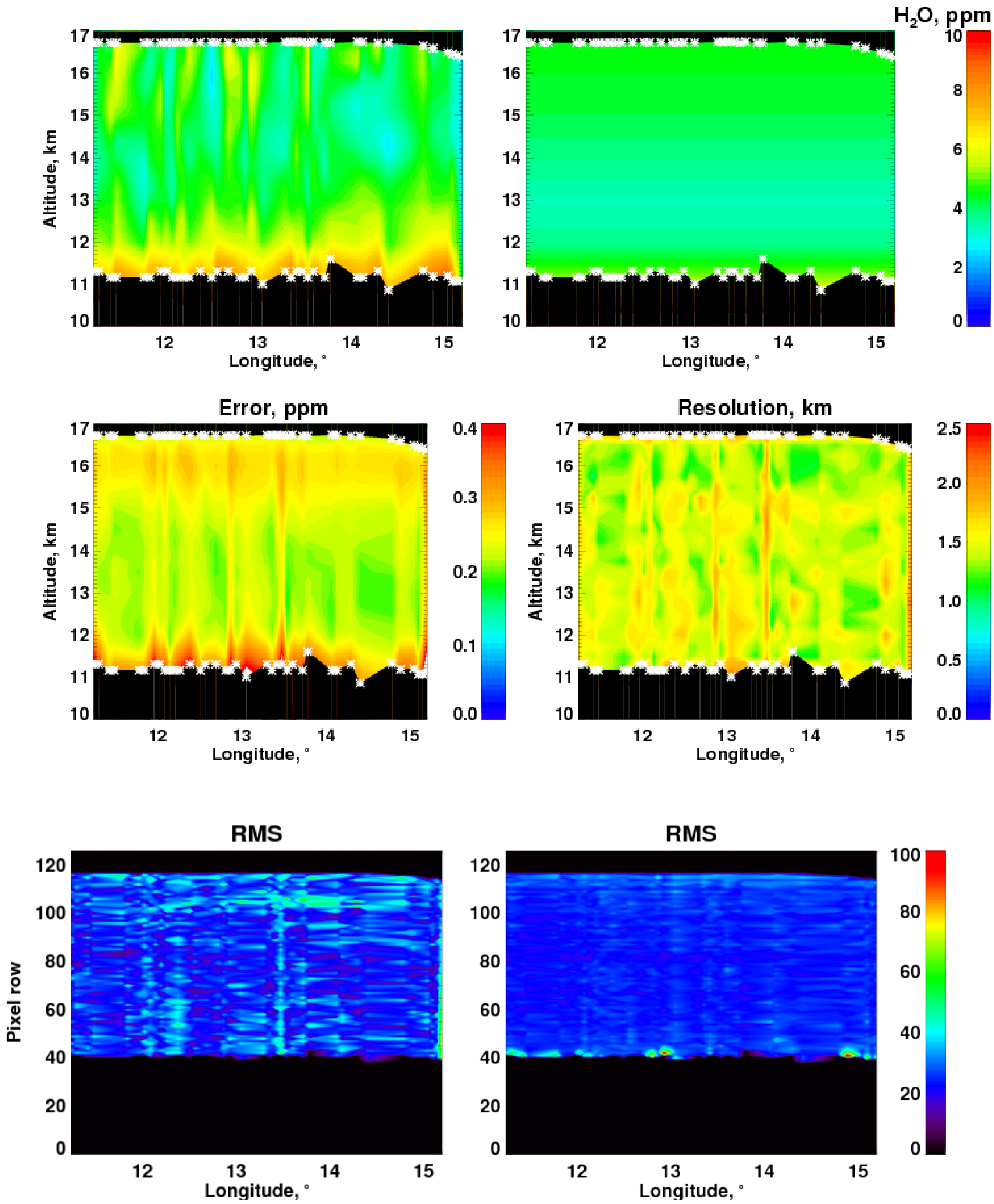

Figure 2.26.: Water vapor retrieval result (top left), initial guess (top right), error (middle left), resolution (middle right) and radiance RMS of spectra for the 795.625-796.25 and 848.0-855.0 cm^{-1} microwindows (bottom) plotted against longitude. Detailed figure description as in Figure 2.20

2.2.4. Intercomparisons

The GLORIA retrieval results are compared with available satellite (MIPAS ENVISAT, MLS), airborne remote sensing (MIPAS-STR) and in-situ (commercial Rosemount sensor placed on board Geophysica, i.e. UCSE data, radiosonde, HAGAR, FISH) data (Table 2.4).

Instrument	**Position °E, °N**	**Time UTC**	**Parameters**
MIPAS-STR	flight track	flight time	T, O_3, HNO_3, $ClONO_2$, CFC-12, H_2O
MIPAS ENVISAT	20.45, 68.56	09:04:00	T, O_3, HNO_3, $ClONO_2$, CFC-12, H_2O
MLS	11.94, 66.12 10.46, 67.52 8.80, 68.90	11:40:21 11:40:46 11:41:10	T, O_3, HNO_3, H_2O
Radiosonde	14.40, 67.25	12:00:00	T
Rosemount sensor UCSE data	flight track	flight time	T
HAGAR	flight track	flight time	CFC-12
FISH	flight track	flight time	H_2O

Table 2.4.: Intercomparison overview. The T parameter corresponds to the temperature.

The GLORIA profiles plotted in this section are mean values of the retrieved images (Figure 2.20, 2.21, 2.24, etc.). To eliminate the deficient images (cf. O_3, $ClONO_2$ retrieval sections) from the mean profiles used for the intercomparisons, a RMS<60 nW/(cm^2 sr cm^{-1}) filter was applied.

The plotted error bars result from gain, line-of-sight and noise analysis. The uncertainty of gain was estimated to be about 2%, of LOS correction at 10% and the noise error was taken from the retrieval diagnostics (middle left panels in Figure 2.20, 2.21, 2.23, 2.24, etc.). Mind that these assumed values adopted for gain and LOS errors are crude estimates and merely should indicate the sensitivity of our retrieval to those instrumental uncertainties. To estimate the effect of calibration gain and LOS errors, new retrievals are carried out and their results are compared with the initial retrieval result. The resulting differences are combined with the spectral noise by the root of the square sum

$$\Delta x = \sqrt{\Delta x_{gain}^2 + \Delta x_{los}^2 + \Delta x_{noise}^2} \tag{2.4}$$

providing 1σ error for each superpixel (von Clarmann et al. 2003). The plotted error bars correspond to the Δx of all superpixels at each altitude.

From MIPAS-STR, 8 profiles acquired in the same time as the GLORIA profiles are chosen for the comparison. The azimuthal direction of GLORIA and MIPAS-STR measurements is very similar (cf. Figure 2.18). The retrieval of the MIPAS-STR data is described in detail in Section 4.1.

The MIPAS ENVISAT data is retrieved at KIT (von Clarmann et al. 2009) and the MLS profiles are taken from the MLS/Aura Online Visualization and Analysis System (Froidevaux et al., 2008). For the temperature comparison the radiosonde data published on the University of Wyoming website (http://weather.uwyo.edu/upperair/sounding.html) are used. One profile provided by the radiosonde launched from the station located nearest to the GLORIA measurements (01152 ENBO Bodo) was chosen. Additionally, the temperature measured on board of Geophysica with the commercial Rosemount sensor was considered. The temperature profiles are plotted in Figure 2.27. The CFC-12 and H_2O profiles are compared with HAGAR and FISH data respectively. The FISH (Fast In-situ Stratospheric Hygrometer, Zöger et al. 1999) instrument is operated by Forschungszentrum Jülich and, during the ESSenCe campaign, provided H_2O with an accuracy equal to 6% of the measured value plus 0.1 ppm (priv. comm. with N. Spelten). For the measurements of HAGAR (Hight Altitude Gas AnalyzeR, University Wuppertal) the total error is estimated to 2% (Volk et al. 2000). The in-situ data displayed here are preliminary.

From the comparisons shown in this section, those between GLORIA and MIPAS-STR are the most essential, due to the resembling data acquisition method and matching geolocation of the measurements (cf. Figure 2.15). The atmosphere in the vicinity of the flight track was not homogeneous with possible polar stratospheric clouds appearance. Therefore, the intercomparisons with the in-situ and satellite measurements have to be analyzed with caution.

For all intercomparisons the original data of each instrument are shown without application of averaging kernels. To enable estimation of the differences plotted in the left panels of Figures 2.27 - 2.32, the data sets were interpolated on the GLORIA altitude grid.

Temperature

The GLORIA temperature mean profile (Figure 2.27) shows a relatively good consistency with the MIPAS-STR data between 11 and 13.5 km and between 14.5 and 16 km. At approximately 14 km and at the flight altitudes the differences are larger than the GLORIA error bars, but still below 2 K. Similar characteristics are shown by the comparison with the UCSE data, except for the region around 13 km where a significant decrease in the UCSE profile is observed. The comparison with satellite temperature data shows agreement at lower altitudes and at the flight level. The ascent profile from the radiosonde is consistent with the GLORIA mean profile between 12.5-13.5 and 15-16.5 km.

Ozone

The ozone GLORIA mean profile (Figure 2.28) and the corresponding MIPAS-STR retrieval results present similar ozone distribution. Below approximately 15 km also the MLS data set shows good consistency, above this level the MLS ozone is relatively low and fits neither the GLORIA nor the MIPAS-STR profiles. In contrast with the low MLS data, the MIPAS ENVISAT ozone values are exceptionally large.

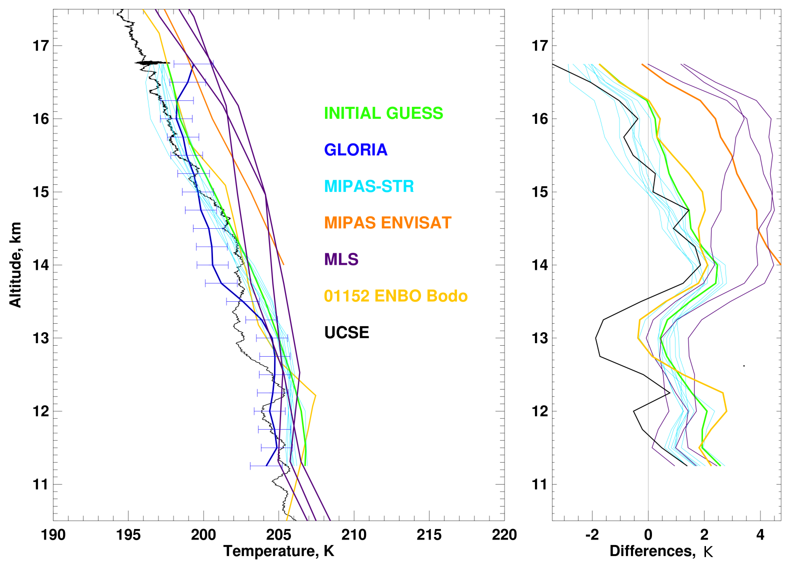

Figure 2.27.: Temperature intercomparison.

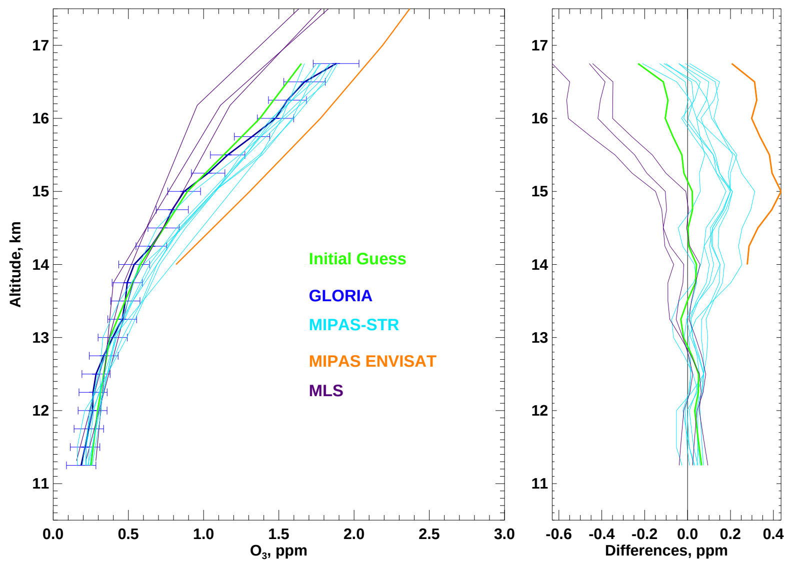

Figure 2.28.: O_3 intercomparison.

$ClONO_2$

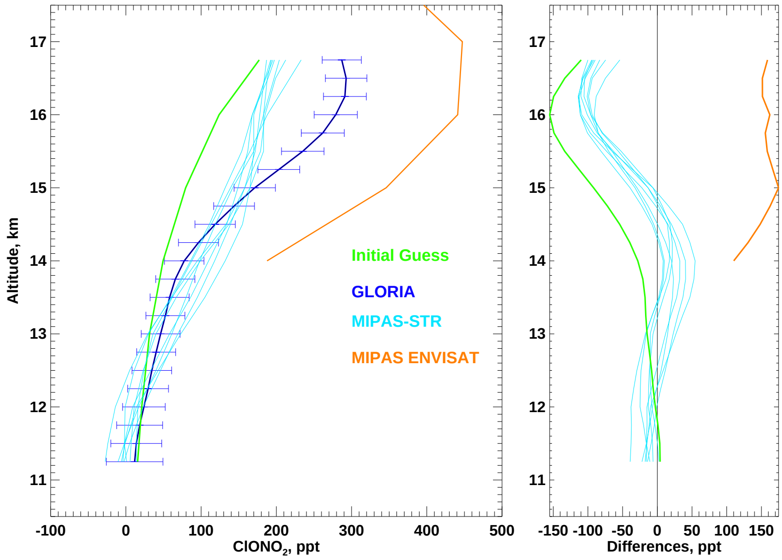

Figure 2.29.: $ClONO_2$ intercomparison.

The comparison of the $ClONO_2$ GLORIA retrieval results with the MIPAS-STR profiles shows a good consistency below 15 km. Above this level the GLORIA mixing ratios start to rise and exceed significantly the MIPAS-STR values. At about 16.5 km altitude the GLORIA values decrease replicating the shape of the MIPAS ENVISAT profile (cf. Figure 2.29).

HNO_3

Figure 2.30 presents the HNO_3 intercomparison. The small error bars of the GLORIA data provide good agreement with the MIPAS-STR profiles below 13.5 km and above 16 km. Between those altitude levels the GLORIA mean profile shows lower values. The MLS data set provides smaller mixing ratios than the GLORIA retrieval results, whereas the MIPAS ENVISAT data are larger than any of the profiles available for the intercomparison.

CFC-12

Figure 2.31 shows that the GLORIA CFC-12 data are consistent within the error bars with the MIPAS-STR CFC-12 profiles. It illustrates also that the HAGAR data are in good agreement with the GLORIA mixing ratios within the whole altitude range except the region around 14 km. The MIPAS ENVISAT profile fits the GLORIA retrieval results above 15 km, below the altitude its values are larger.

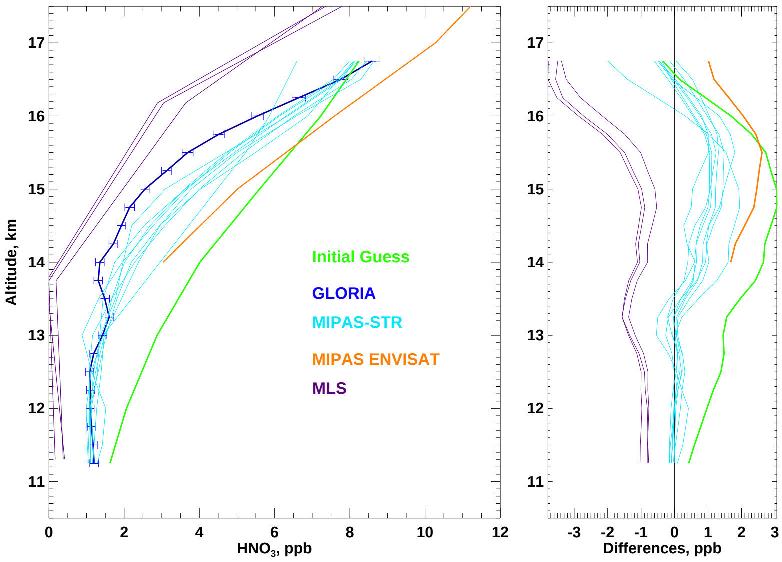

Figure 2.30.: HNO_3 intercomparison.

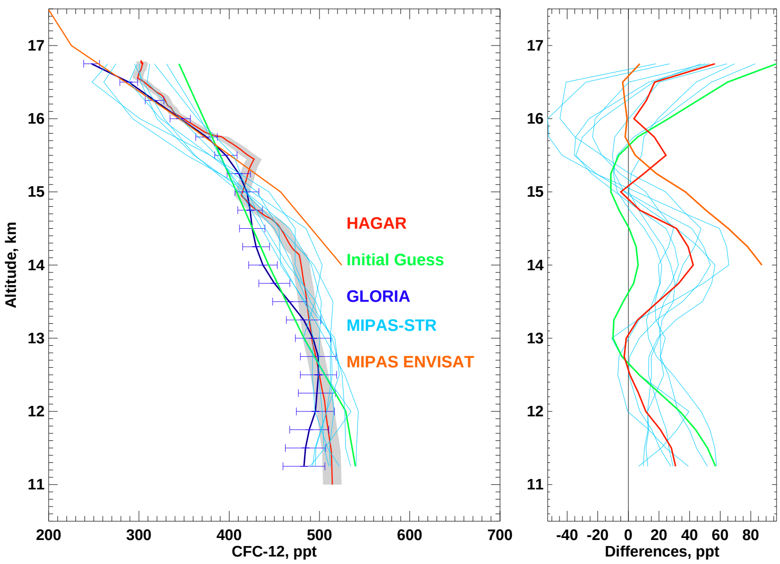

Figure 2.31.: CFC-12 intercomparison. The gray color corresponds to HAGAR CFC-12 measurement uncertainties.

H_2O

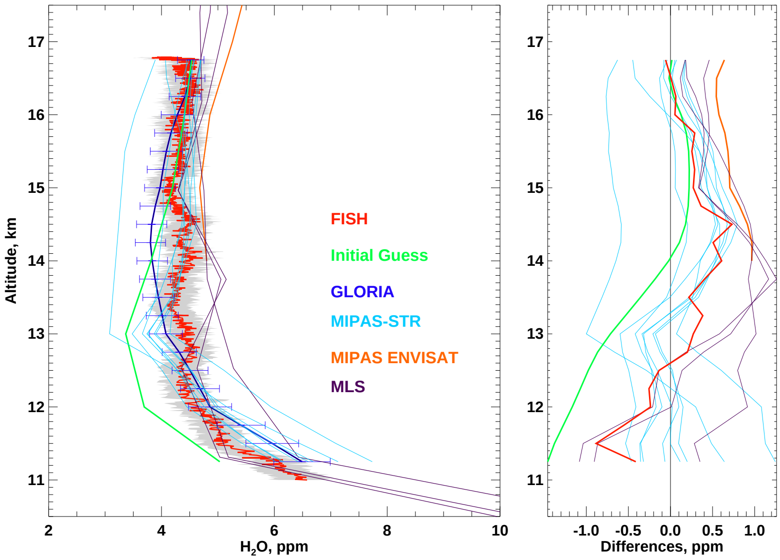

Figure 2.32.: H_2O intercomparison. The gray color corresponds to FISH H_2O measurement uncertainties.

The GLORIA H_2O mean profile and MIPAS-STR profiles are compared in Figure 2.32. The differences between the two data sets are smaller than the GLORIA error bars. The comparison with FISH profiles provides an agreement within the error bars at the altitudes above 12.5 km. The MIPAS-ENVISAT profile yields larger values than GLORIA, whereas the MLS data fit within the error bars above 15 km or below 12.5 km depending on the profile.

2.3. Level 2 processing of GLORIA Dynamics Mode Data

2.3.1. Measurement Overview

In dynamics mode, GLORIA records spectra at a maximum optical path difference of 1.8 cm yielding a spectral sampling of 0.3125 cm^{-1}. The line of sight is panned from 45° to 135° with respect to the airplane flight direction in 4 degree steps. Measurement time for one image (one interferometer sweep) is 2.8 s; two images are recorded for each viewing direction. Dynamics mode data was recorded during ESSenCe Flight 2 from 14:58 to 15:10. Individual images contain 128x48 pixels / spectra, which are averaged on a 128x1 grid, as described below. The total dynamics mode sequence consists of 121 individual images.

2.3.2. Pixel Binning

In dynamics mode, no averaging in the vertical direction of the image is applied. In the horizontal, all pixels in a detector row are averaged. Broken (deviation of more than 2σ from the line average) or 'cloudy' pixels are removed. Entire detector rows are ignored if more than 75% of the pixels are marked as broken or cloudy. Weighting of individual pixels is based on the noise analysis of black body spectra (c.f. Section 2.1.5). Typical GLORIA dynamics mode spectra for the binned data are illustrated in Figure 2.33.

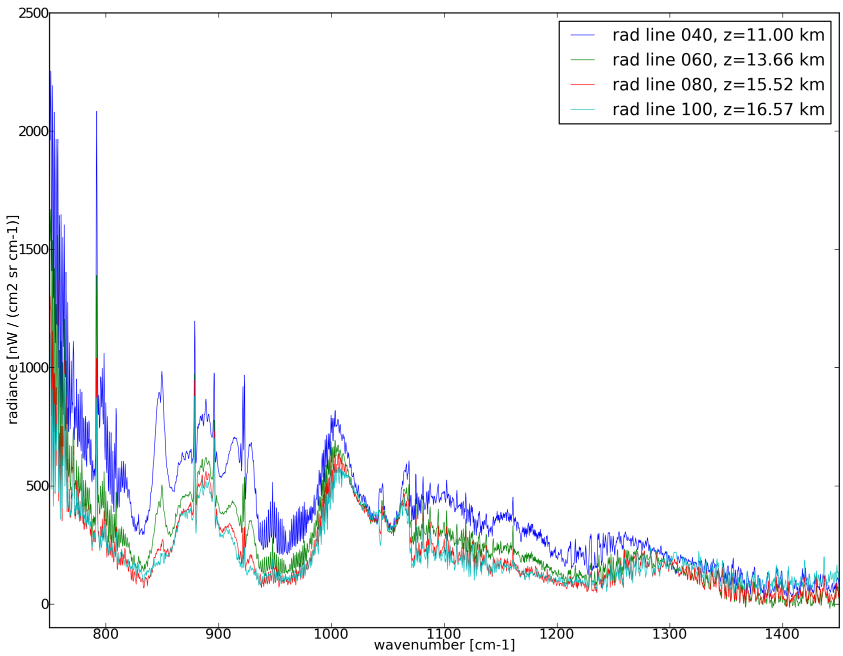

Figure 2.33.: A reduced selection of horizontally averaged spectra for a single GLORIA dynamics mode measurement (image 120, measured at 15:09:14 UTC, 67.35° N, 6.25° E), after pixel weighting and filtering.

2.3.3. Cloud Identification

For the cloud identification in dynamics mode, cloud indices (CI) as defined by Spang et al. (2004) have been calculated. This index exploits the relative change of atmospheric window radiance (832–835 cm^{-1}) levels compared to a strong emission line (788–797 cm^{-1}; Figure 2.34). The window radiance is elevated by the cloud's thermal radiation while the emission line is much less affected.

Cloud pollution is indicated by a low value of CI. A conservative threshold value of CI_{thresh} = 2.5 is used for the removal of cloudy pixels from the detector array for every single dynamics mode image, compared with e.g. the value of 1.8 used for CRISTA-NF in (Spang et al., 2004).

Cloud indices recorded during the dynamics mode sequence are illustrated in Figure 2.35. The four segments, separated by thin white lines, represent four distinct azimuth scans. Relative to the aircraft's heading, the scans start at 45 degrees and stop at 135 degrees.

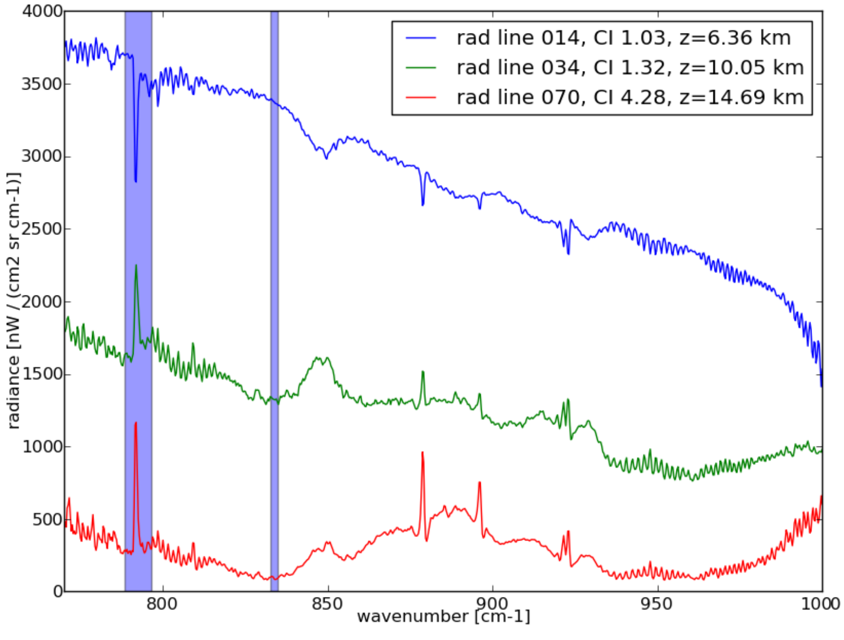

Figure 2.34.: Horizontally averaged spectra obtained from a non-cloud-filtered image. Highlighted in blue are the microwindows used for cloud indexing.

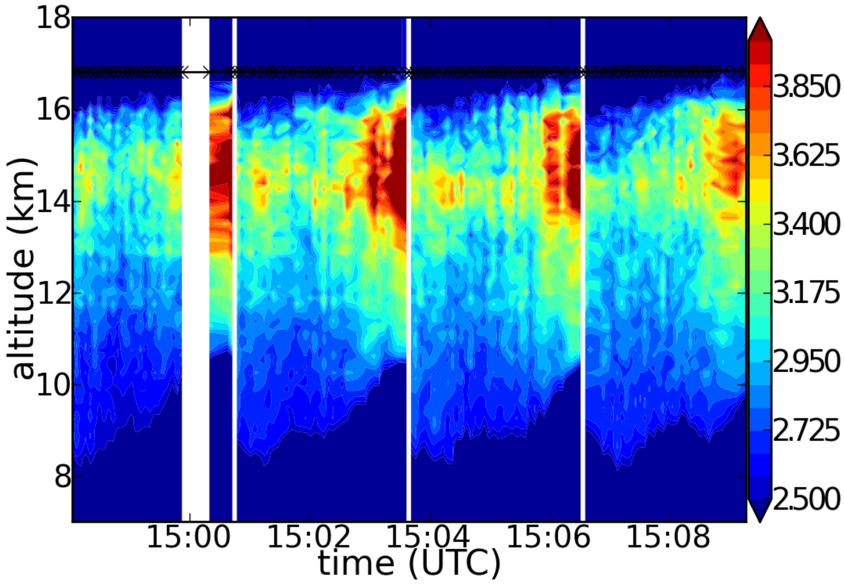

Figure 2.35.: Cloud index values for the GLORIA dynamics mode measurements, interpolated on a spatial grid. The thin white lines serve to separate the four azimuth scans. The "gap" within the first scan is a time frame with no valid measurements. Values are only significant below flight altitude, indicated by the black line between 16 and 18 km.

It follows that the leftmost parts of each segment represent areas that are, at the time of measurement, still to be passed by the aircraft. The right portions, on the other hand, are already behind the plane.

Apart from the high-CI values in the right section of the segments, all targeted volumes exhibit some degree of cloud or aerosol pollution. In addition, there is a particularly suspicious structure of low indices at flight altitude that extends further downwards in subsequent scans. A comparison of GLORIA dynamics mode cloud indices with cloud indices as observed by the MIPAS-STR instrument (Figure 4.3) exhibit very similar structures: during the calibration sequence separating the GLORIA chemistry and dynamics mode measurements (c.f. Figure 1.2), the aircraft has passed an elevation in cloud top height. Furthermore, the low CI values at flight altitude, especially when looking forward, point to the possible presence of polar stratospheric clouds. In addition, almost all of the target volume seems to be at least polluted with aerosol to some degree. These observations are important to consider in the interpretation of retrieval results.

2.3.4. Line of Sight Correction

Dynamics mode data exhibits a similar elevation offset as chemistry mode data and the same LOS correction is applied (c.f. Section 2.2.2).

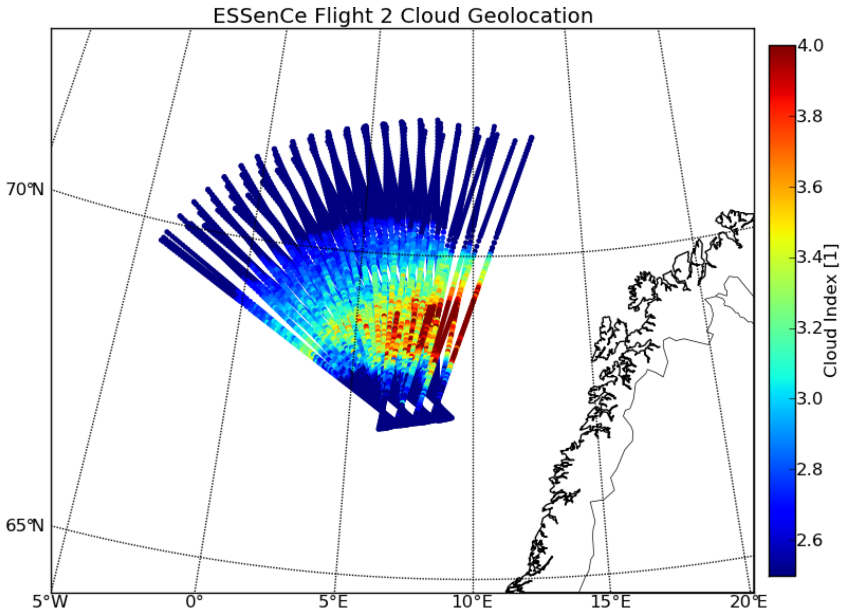

Figure 2.36.: GLORIA cloud indices at the tangent points of dynamics mode measurements

2.3.5. Retrieval Setup

The GLORIA dynamics mode retrieval is a constrained global fit approach, similar to the approach utilized for the chemistry mode.

The GLORIA dynamics mode retrieval processor is a modular system consisting of a very fast forward model and a suite of general non-linear inversion algorithms (Ungermann et al., 2011). It works on tabulated, spectrally-averaged emissivities instead of line-by-line data. This method is over three orders of magnitudes faster than conventional line-by-line models. The accuracy of this method is better than 99.5% in comparison to line-by-line calculations, provided that dedicated regression factors are applied.

Measurement error covariance matrices as utilized in the minimization process are assumed to be diagonal and consider measurement noise (26 nW / cm^2 sr cm^{-1}), only. However, for the analysis of retrieval uncertainties (Section 2.3.7), other sources of uncertainty are considered as well.

The retrieval is weakly regularized by constraining the first derivative of the retrieval targets to some a-priori data (see below). For numerical reasons we also include a small amount of zeroth order regularisation, which has very little to no influence on the retrieval result.

Dynamics mode prime targets are temperature, ozone, CFC-12 and HNO_3. To consider atmospheric aerosols, contamination by minor species (not considered in the retrieval setup) or instrumental effects, absorption cross section profiles are fitted every 60 cm^{-1} as well (c.f. Table 2.5). These cross sections are assumed to be wavelength-independent within these 60 cm^{-1} spectral intervals.

A-priori data for $ClONO_2$ is taken from a ClaMS model run (Grooß et al., 2005). This model was initialized for the ESSenCe campaign using ECMWF ERA-Interim data (Dee et al., 2011). PAN and water vapor were taken from a WACCM4 model run (Garcia et al., 2007).

spectral range (cm^{-1})			retrieval target
785.3125	-	786.5625	Aerosol 1
790.9375	-	793.125	Temperature
877.8125	-	879.6875	HNO_3
894.375	-	896.5625	HNO_3
920.9375	-	923.125	CFC-12
941.25	-	943.4375	Aerosol 2
955.625	-	956.875	Aerosol 3
994.375	-	996.5625	O_3

Table 2.5.: ISWs selected for the ESSenCe retrievals with main contributions. Three aerosol profiles are fitted simultaneously

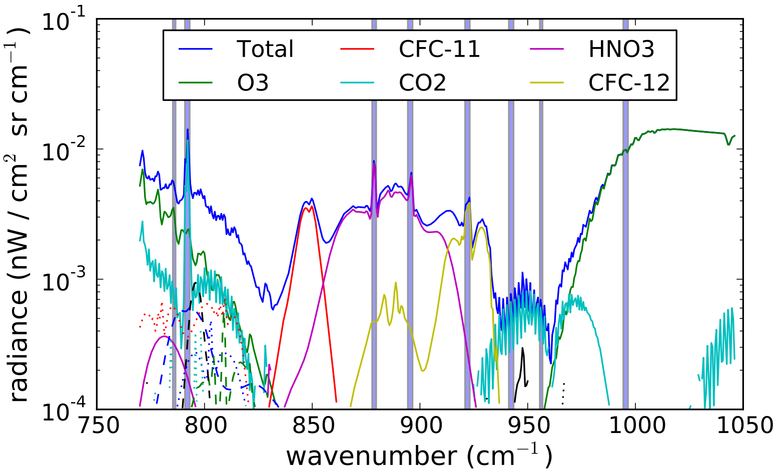

Figure 2.37.: ISWs selected for the ESSenCe retrieval. For reference, simulated spectra of the polar MIPAS reference atmosphere at 16 km tangent altitude are shown.

Values for pressure were taken from the ECMWF ERA-Interim dataset. All other data was taken from the MIPAS reference atmospheres (Remedios et al., 2007); CO_2 volume mixing ratios were updated using Mauna Loa CO_2 data (www.esrl.noaa.gov/gmd/ccgg/trends/).

The selection of integrated spectral windows (ISW) for the retrieval is performed in two steps. In the first step, spectral intervals for the retrieval of temperature and ozone as well as two aerosol profiles are selected, which cover the 12.6 μm CO_2 Q-branch and in the 10 μm O_3 band. Error analysis for this selection shows that it is possible to retrieve both quantities without significant interference by other trace gases. In the second step, HNO_3 and CFC-12 are added as retrieval targets. Spectral samples are optimized for both gases separately under the assumption that O_3 and temperature are known. The combined setup can be seen in in Figure 2.37 and Table 2.5.

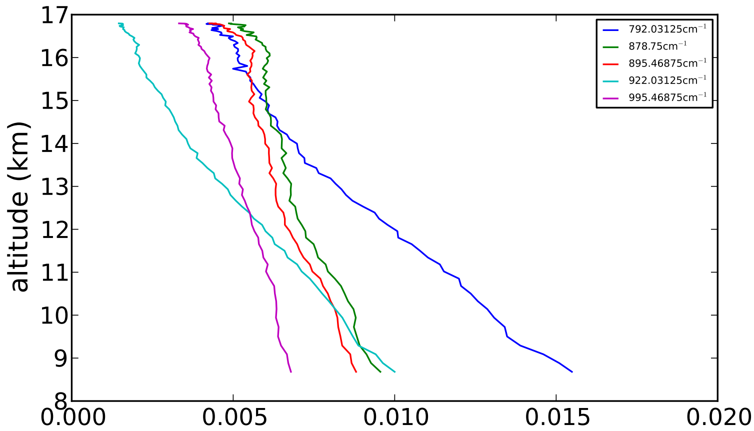

Figure 2.38.: Radiance profiles for selected integrated spectral windows (image 120, measured at 15:09:14 UTC, 67.35° N, 6.25° E).

2.3.6. Retrieval Results

Individual spectra, altitude profiles for integrated spectral windows, and retrieved atmospheric parameters are illustrated in Figure 2.33, Figure 2.38, and Figure 2.39, respectively. This data is from image 120 (measured at 15:09:14 UTC, 67.35° N, 6.25° E) at the end of the dynamics mode sequence, looking into relatively clear air.

The radiance data of image 120 exhibit a pronounced change in the altitude gradient between 14 and 16 km, correlating with clear maxima/minima in retrieved parameters at these altitudes. These structures are significant with respect to instrumental and retrieval uncertainties.

Two dimensional views of dynamics mode retrieval targets are illustrated in Figures 2.40 and 2.41. The data covers four horizontal swaths, as indicated by the vertical blue lines. About 75% of each swath / section cover the same air volume as the previous one, but with different viewing angles. Overall the atmospheric situation is very homogeneous in the horizontal direction.

The structure between 14 and 15 km altitude and the sharp decrease in HNO_3 as observed in image 120 (Figure 2.39) is visible in most images and points to a filamentary structure in the atmosphere.

2.3.7. Retrieval Performance

The quality of the GLORIA dynamics mode retrieval is analyzed by means of the random and systematic error budget, spatial resolution, and by comparing retrieval results with collocated measurements.

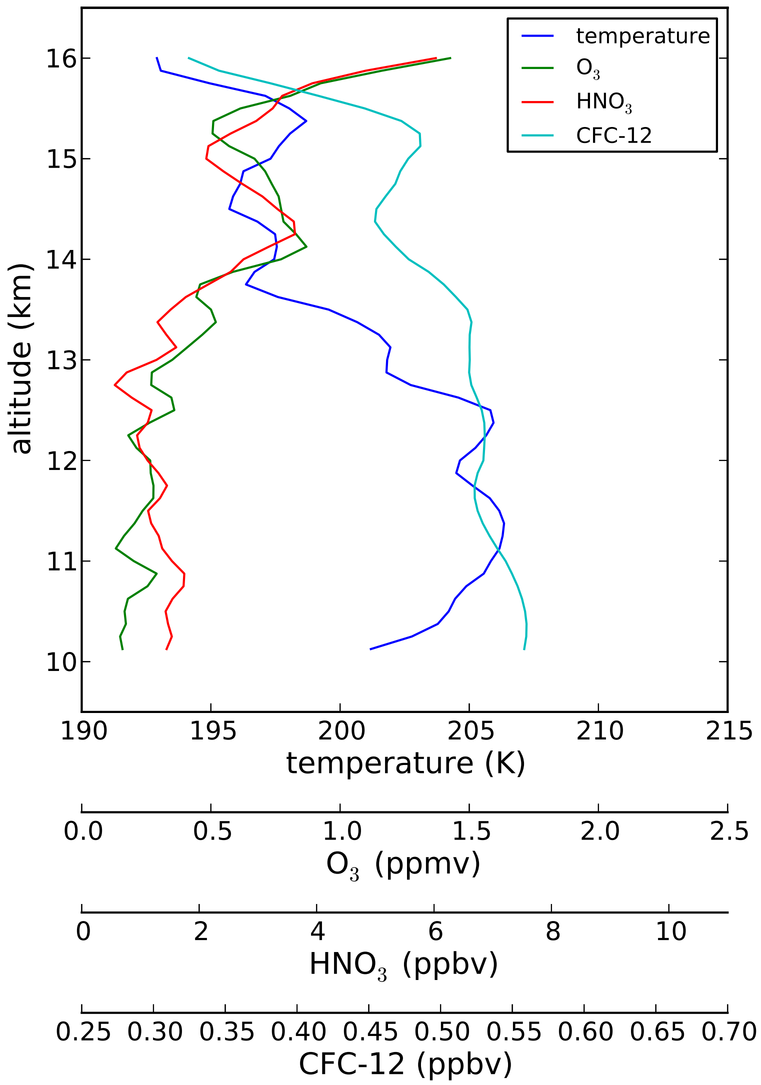

Figure 2.39.: Retrieval results for image 120.

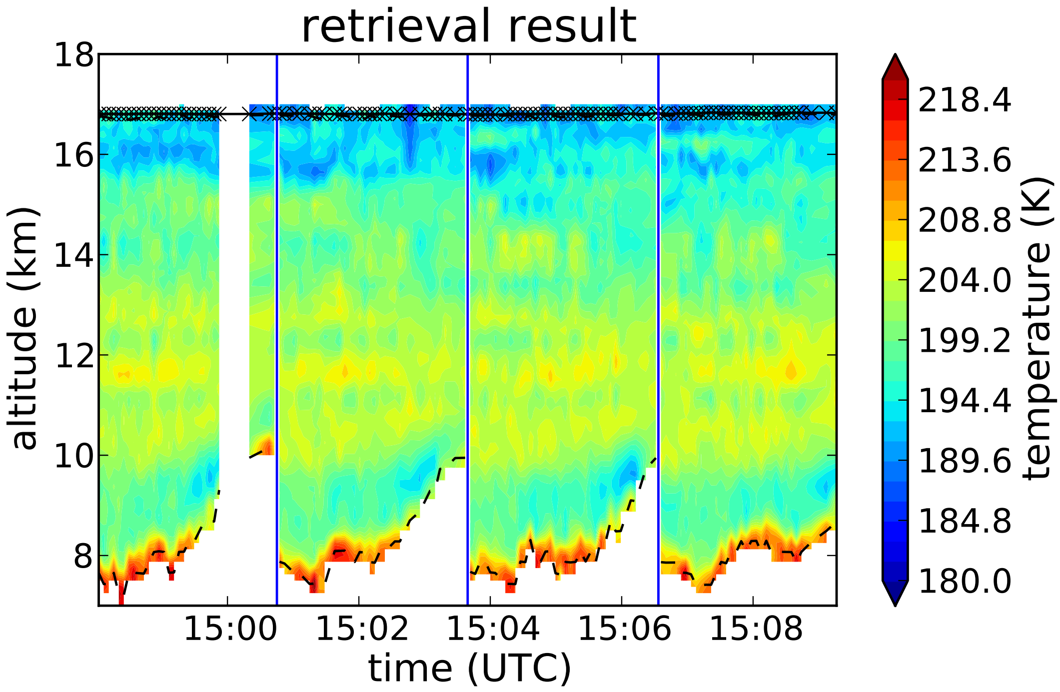

(a) Temperature

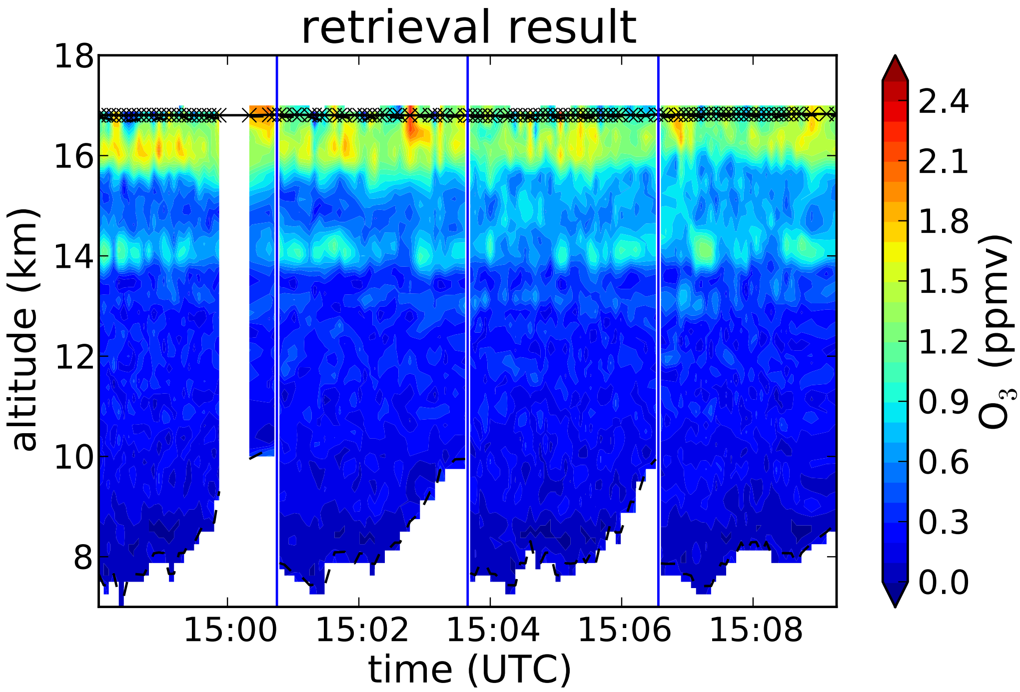

(b) O_3

Figure 2.40.: Retrieved data for the GLORIA dynamics mode sequence

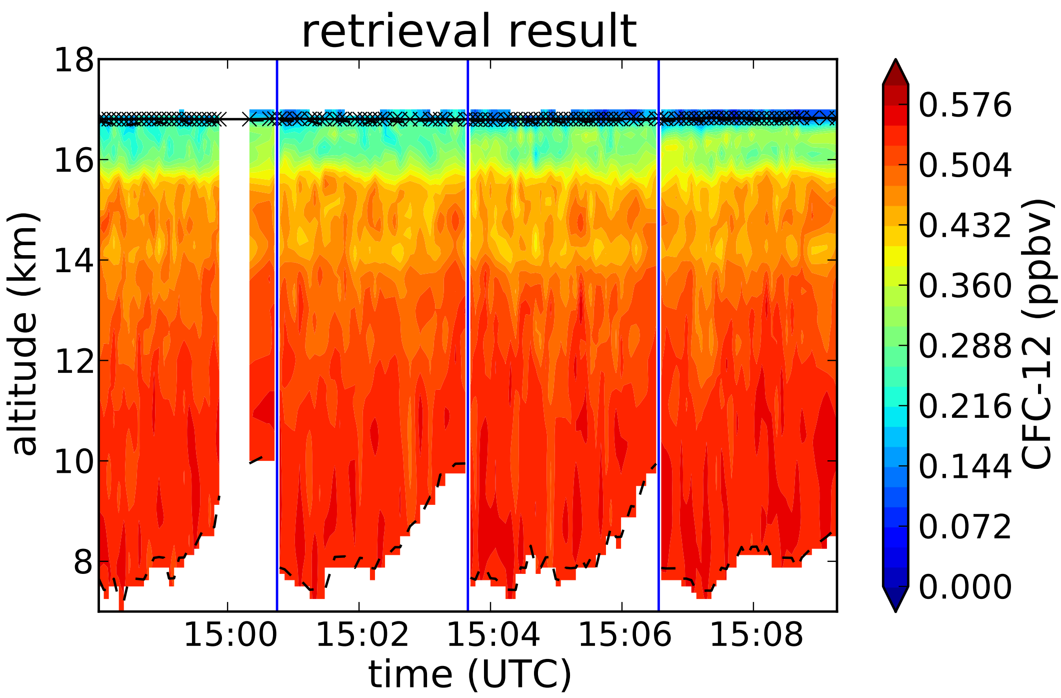

(a) CFC-12

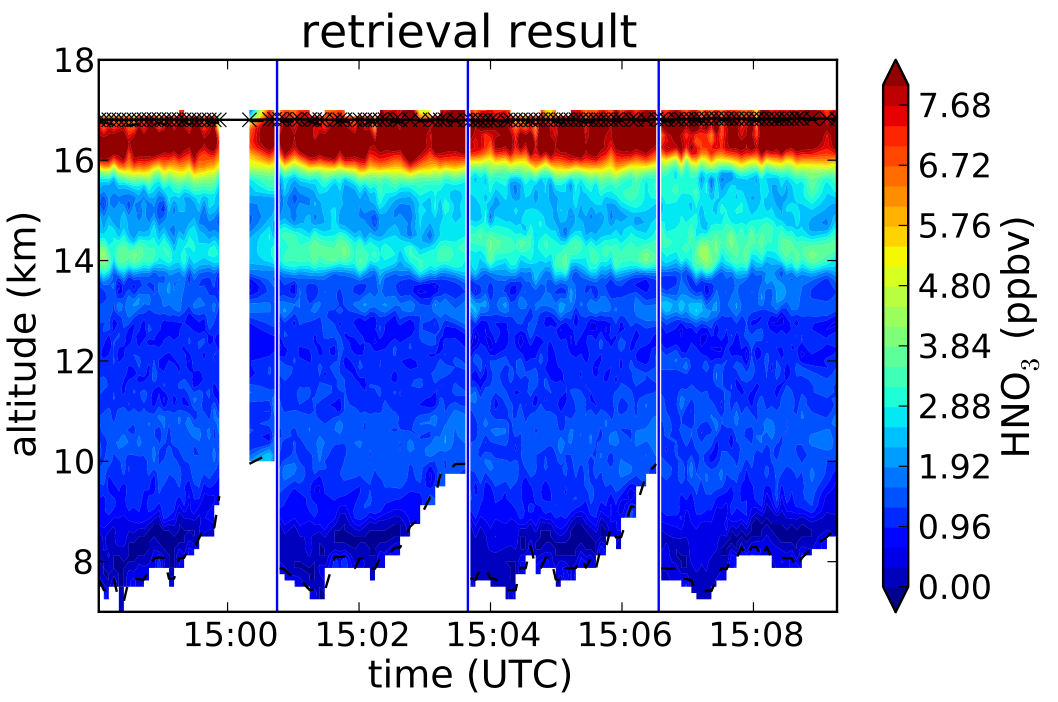

(b) HNO$_3$

Figure 2.41.: Retrieved data for the GLORIA dynamics mode sequence

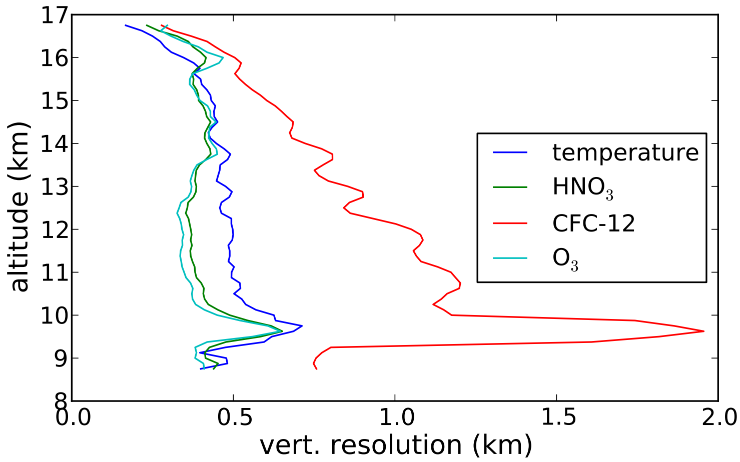

Figure 2.42.: Vertical resolution (image 120)

Error Budget

For the error analysis we consider inaccuracies introduced by other trace gases, instrument noise, detector-gain, and uncertainties in elevation stability (Table 2.6)

The vertical resolution (Figure 2.42) of all species is excellent for a passive remote sensing instrument; typical values are 300–500 m for temperature, ozone, and HNO_3, and 500–1000 m for CFC-12.

The combination of noise and gain error limits temperature to a precision of 1.5 Kelvin (Figure 2.43). Uncertainties in the trace gas retrievals are dominated by instrument noise (Figure 2.44-2.46). Typical values are 0.1 ppmv for ozone, 0.04 ppbv for CFC-12 and 0.4 ppbv for HNO_3.

entity	uncertainty
Temperature	5% of the climatological mean
Pressure	0.3% of the climatological mean
PAN	100%
other species	Std. deviations from MIPAS reference atmospheres
Instrument noise	26.51 nW/(cm^{2}cm^{-1}sr)
Gain	2%
Elevation stability	0.023°

Table 2.6.: Uncertainties for a-priori or ’unknown’ atmospheric and instrumental parameters, as considered in the error analysis

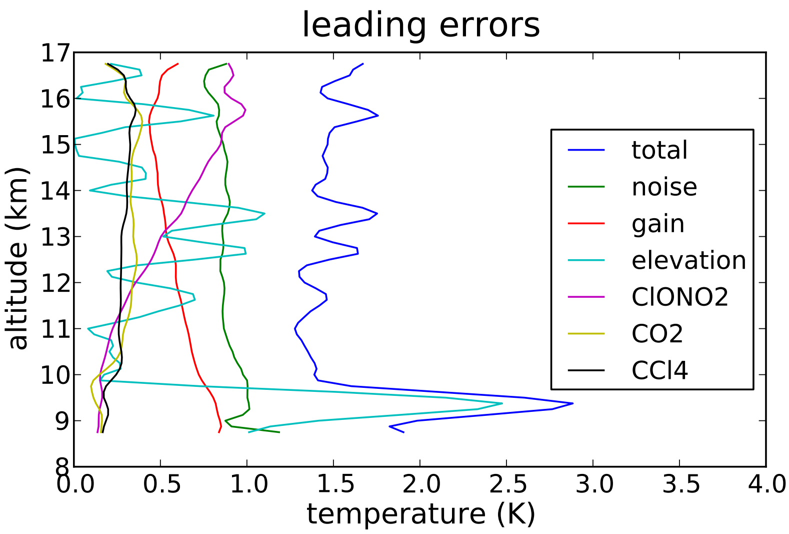

Figure 2.43.: Error analysis for Temperature (image 120)

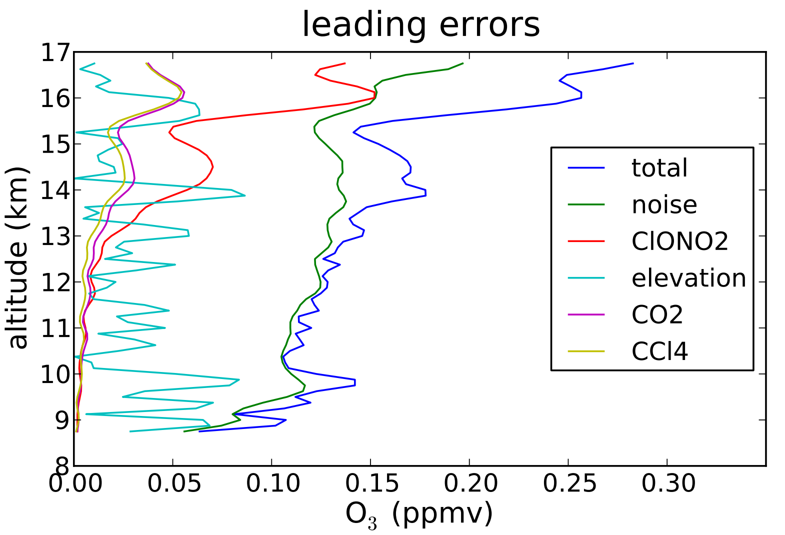

Figure 2.44.: Error analysis for O_3 (image 120)

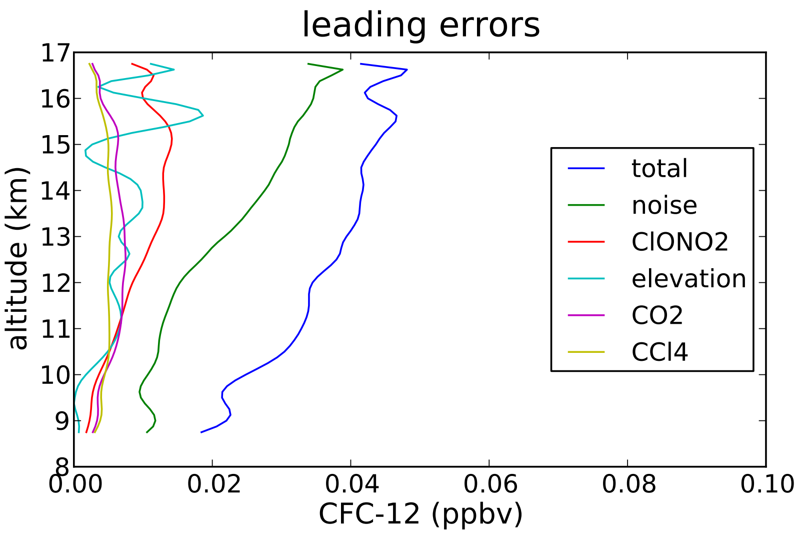

Figure 2.45.: Error analysis for CFC-12 (image 120)

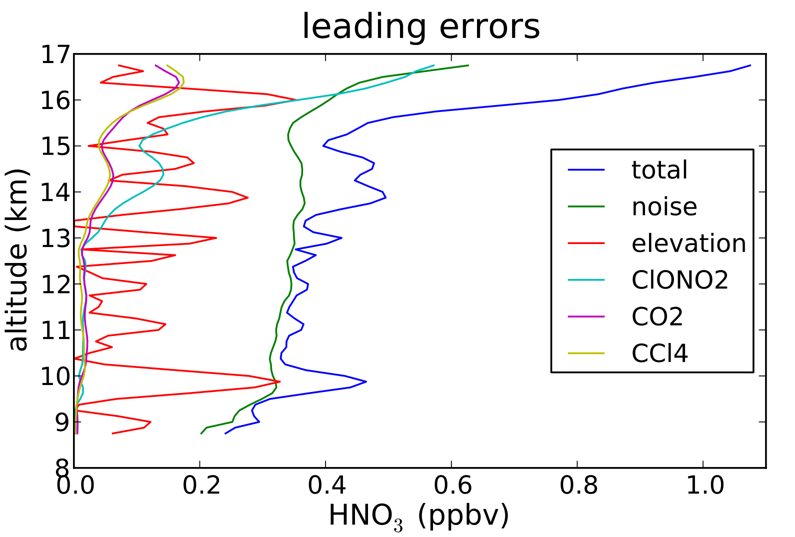

Figure 2.46.: Error analysis for HNO_3 (image 120)

Comparison to Other Measurements

To validate dynamics mode retrieval results we compare retrieved data to several other instruments. Most notable are the MIPAS-STR and MIPAS-Envisat instruments, the EOS Aura MLS instrument (Froidevaux et al., 2008), as well as several in-situ and ground-based instruments. Since some measurements have a large horizontal footprint compared to GLORIA or exhibit a notable miss-distance, we use the average of all dynamics mode profiles for the comparison (Figure 2.47). We also included data from a radiosonde launched at Bodø, Norway. During ascent and descent of the aircraft measurements of CFC-12 and temperature where taken by in-situ instruments. Table 2.7 lists the different datasets used for comparison. For the comparison with MIPAS-STR, we include only those GLORIA profiles with a line of sight nearly perpendicular to the flight direction.

Figure 2.48-Figure 2.51 show comparisons for the different species. Whereas the left panel shows the data 'as it is', the right panels show differences between GLORIA and other instruments considering the effect of different averaging kernels. This affects the comparison with the MIPAS-Envisat and AURA-MLS datasets with their relatively broad averaging kernels.

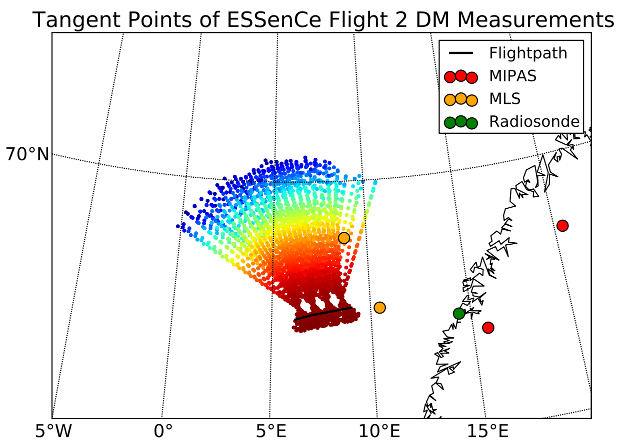

Figure 2.47.: GLORIA tangent points and locations of other measurements used for validation

Instruments	Parameters
Envisat MIPAS	Temperature, O_3, HNO_3, CFC-12
MIPAS-STR	Temperature, O_3, HNO_3, CFC-12
EOS Aura MLS	Temperature, O_3
Radiosonde	Temperature
HAGAR	CFC-12
WAS	CFC-12

Table 2.7.: Instruments used for validation

Temperature

GLORIA and correlative temperature datasets agree within 5 K (Figure 2.48). GLORIA dynamics mode data seems to have a cold bias of 1–3 K with respect to most other datasets. Further investigation is needed.

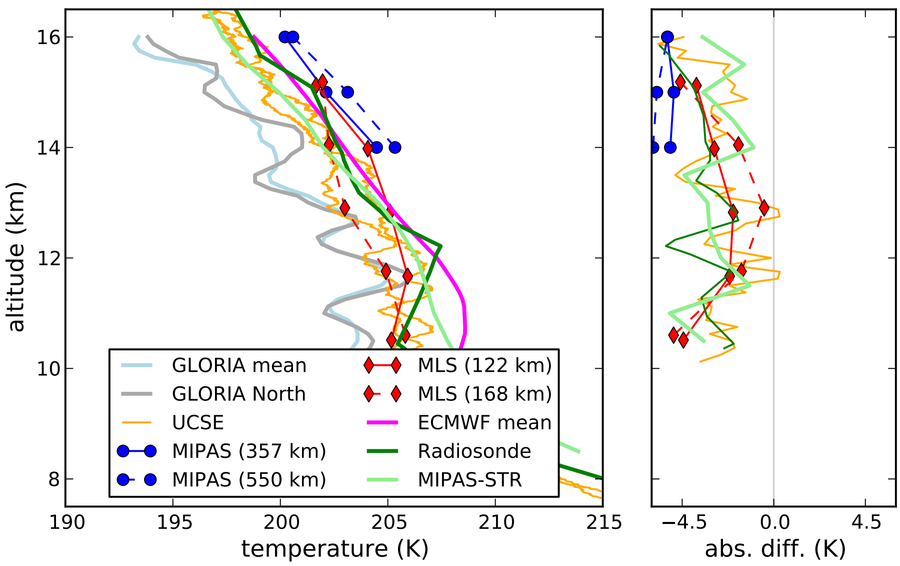

Figure 2.48.: Absolute and relative differences of temperature between GLORIA and other instruments. 'GLORIA mean' represents the mean of all dynamic mode sweeps, whereas 'GLORIA North' considers viewing angles of 90°, only. Differences between GLORIA and other instruments are shown in the right panel. Differences to MIPAS-STR include GLORIA viewing angles of 90°, only. Averaging kernels of the MIPAS-Envisat and MLS datasets have been considered for the calculation of the corresponding differences.

Nitric Acid

GLORIA dynamics mode retrieval results and MIPAS-STR data (Figure 2.49) are in good agreement. The visibility of the filamentary structure between 14 km and 16 km is clearly visible in the GLORIA data, whereas MIPAS with its broad field of view does not show it.

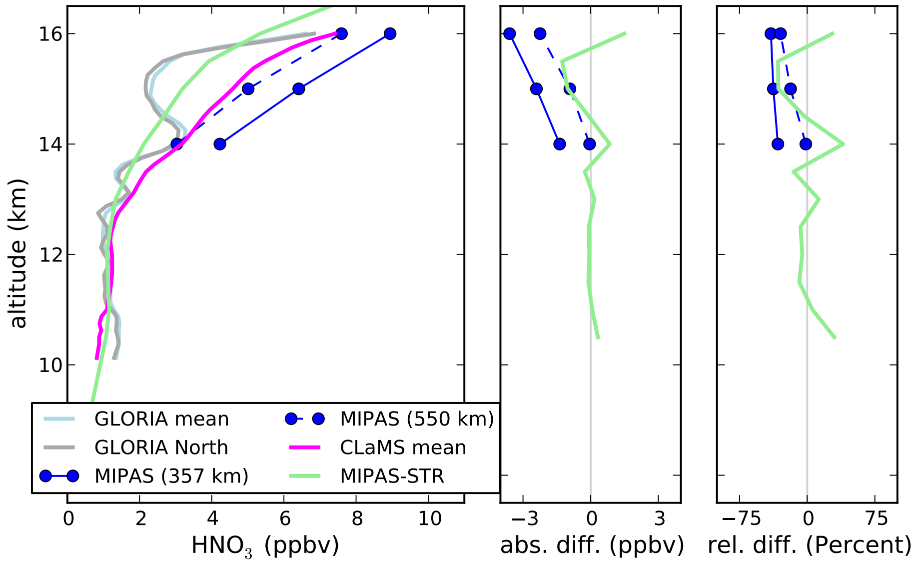

Figure 2.49.: Absolute and relative differences of nitric acid between GLORIA and other instruments. For details see Figure 2.48

Ozone

GLORIA ozone data agrees well with MIPAS-STR at lower altitudes, but exhibits a small low bias at higher altitudes (Figure 2.50). This deficit may be related to the existence of clouds in most scans or point to a systematic bias of GLORIA 10 μm radiances related to the radiometric calibration procedure. Further investigations are needed.

CFC-12

CFC-12 mixing ratios agree well with MIPAS-STR data and datapoints from in-situ instruments (Figure 2.51). Again, the slight high-bias GLORIA CFC-12 data may point to some remaining instrumental or retrieval effects.

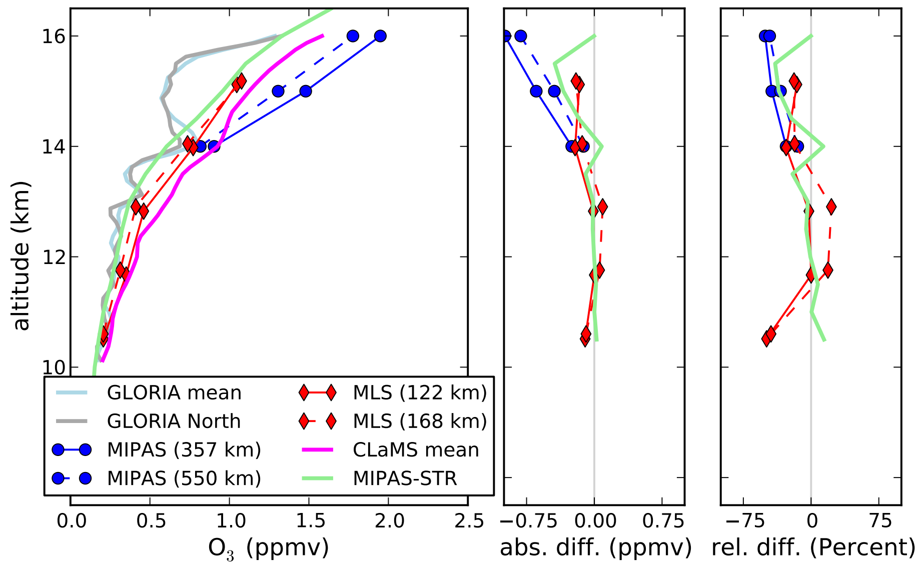

Figure 2.50.: Absolute and relative differences of ozone between GLORIA and other instruments. For details see Figure 2.48

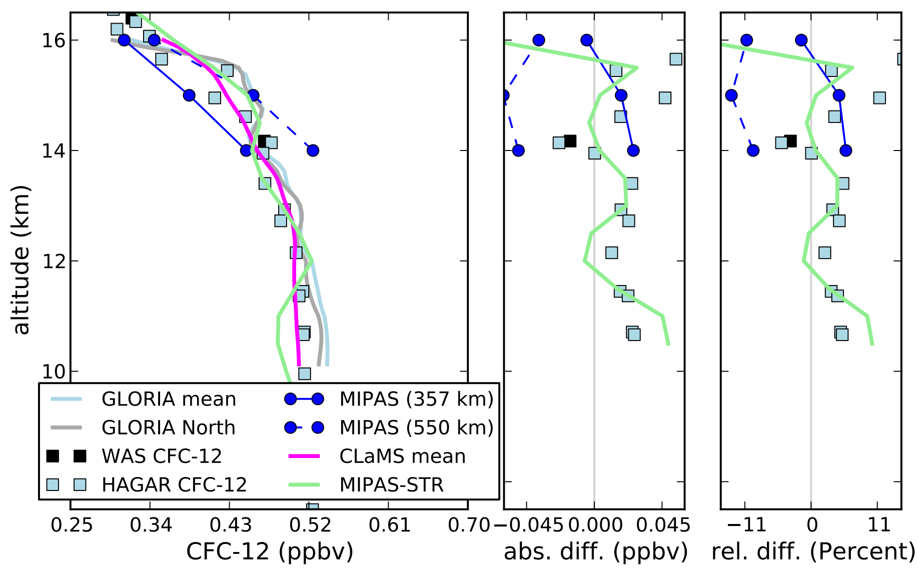

Figure 2.51.: Absolute and relative differences of CFC-12 between GLORIA and other instruments. For details see Figure 2.48

3. MARSCHALS Measurements

3.1. Level 1 Processing

The processing of MARSCHALS Level 0 data up to Level 1b had been finished ahead of the Data Acquisition Meeting on the 22nd March 2012 and the acquired flight spectra are discussed in the ESSenCe Data Acquisition Report (DAQR) to which we refer for details. However, the following two updates should be mentioned:

3.1.1. 16-Bit Wrapping of the ADC

The Level 1 processing is performing the radiometric calibration of the measurements. Additional steps required are the unwrapping of count series due to the 16-bit wrapping steps of the ADC, the post-flight correction of the gyro bias and the computation of the correct measurement errors that are only possible once the 16-bit unwrapping has been performed. The final data product after all these steps is what we call Level 1b data. It was found that on a few occasions in the ESSenCe data of Flight 2 the 16-bit unwrapping did not work correctly. This was remedied in a re-processed version of Level 1b data that has been distributed. For most of the cases this issue could be resolved, however for a select case where the wrapping spans two or more wrap ranges the algorithm has no possibility to determine the correct wrap range unambiguously.

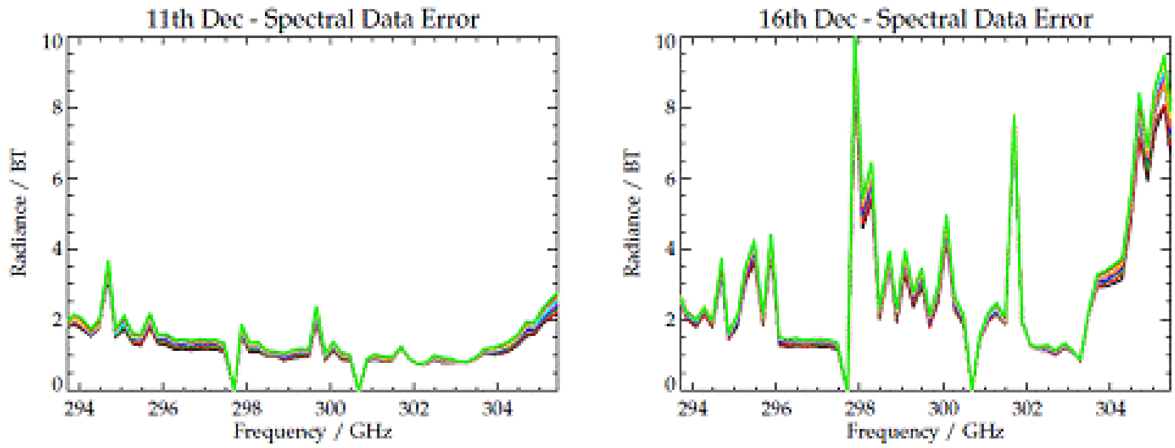

Figure 3.1.: 16-bit wrapping artefacts in original Level 1b data of Flight 2 measurement error.

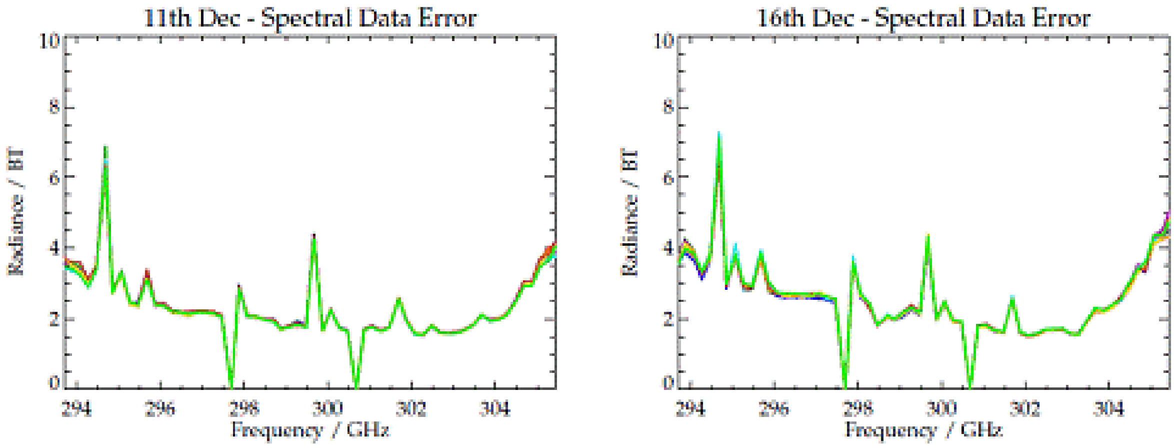

Figure 3.2.: 16-bit wrapping issues in Flight 2 measurement error fixed.

3.1.2. First/Last Scan in Flight

It was noted that in the DAQR we have not shown the first and the last scan in each flight. The reason for leaving out the last scan is that it is never complete. That is because the instrument shut down is triggered by the aircraft descending below a target altitude (generally 14 km) and this usually happens in the middle of an atmospheric scan and not at the end.

The first scan is left out because of a data quality issue affecting the first few measurements after instrument start up. The first couple of measurements after the start of the measurement cycle are not usable. The reason for this is not 100% established, but it is consistent for every flight and only lasts a couple of seconds. It could therefore be argued that - when filtering out the first couple of bad measurements - the rest of the scan could still be used for analysis. We have therefore started to include this scan in our analysis as well.

However our finding is that retrieval results of this scan don't look particularly good (the scan get filtered out later in our plotting procedure). This is certainly also due to the fact that the aircraft is still in full ascent after the shutter opening at 14 km, and the inconsistent platform altitude at the beginning of the flight is obviously detrimental to limb-sounding.

We would therefore advise to treat this first scan of each flight (which is a Band C scan in the current scan sequence for PREMIER-Ex and ESSenCe) with careful scrutiny.

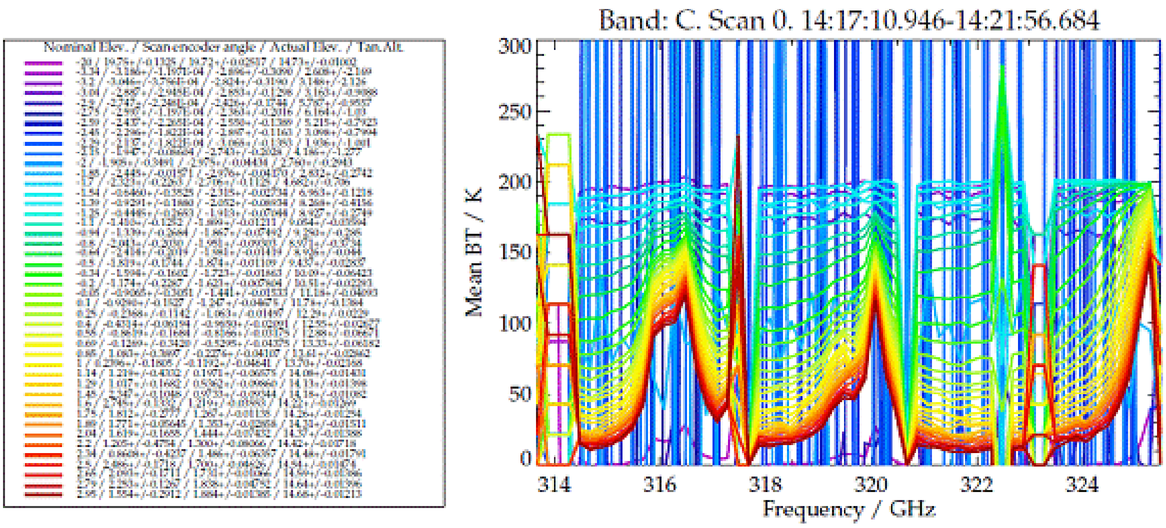

Figure 3.3.: The first scan of each flight was previously left out because of a number of bad measurements immediately after instrument start-up, but this plot shows that the second part of the scan can potentially be exploited.

3.2. Instrument Pointing

ESSenCe uncovered an issue in the MARSCHALS pointing system. The instrument pointing after the first flight was biased towards ground views, i.e. the nominal scan range seemed to have an offset towards low off-nadir angles.

3.2.1. UCSE Roll Angle Data

Immediately after the campaign we have noted that the UCSE roll-angle for this flight also showed a systematic bias at an angle of +0.5 deg. This wasn't intuitive because during its box shaped flight loop the aircraft experiences wind from all directions in turns, so a wind-induced effect should manifest with different signs for different flight legs. A quick look at UCSE data recorded on the apron during EMC tests and during the roll test on the runway seemed to confirm the presence of a systematic 0.5 deg bias.

3.2.2. Updated Scan Sequence for Flight 2

Our reaction on site was to compute a new extended and slightly oversampled scan sequence which would correct for the negative offset of the pointing correction, allowing for some fluctuations in the possible magnitude of the phenomenon. This proofed to work pretty much as expected, although it has to be noted that due to the almost completed absence of the initial roll-angle bias the scan in Flight 2 is now over-sampling the upper atmosphere quite heavily.

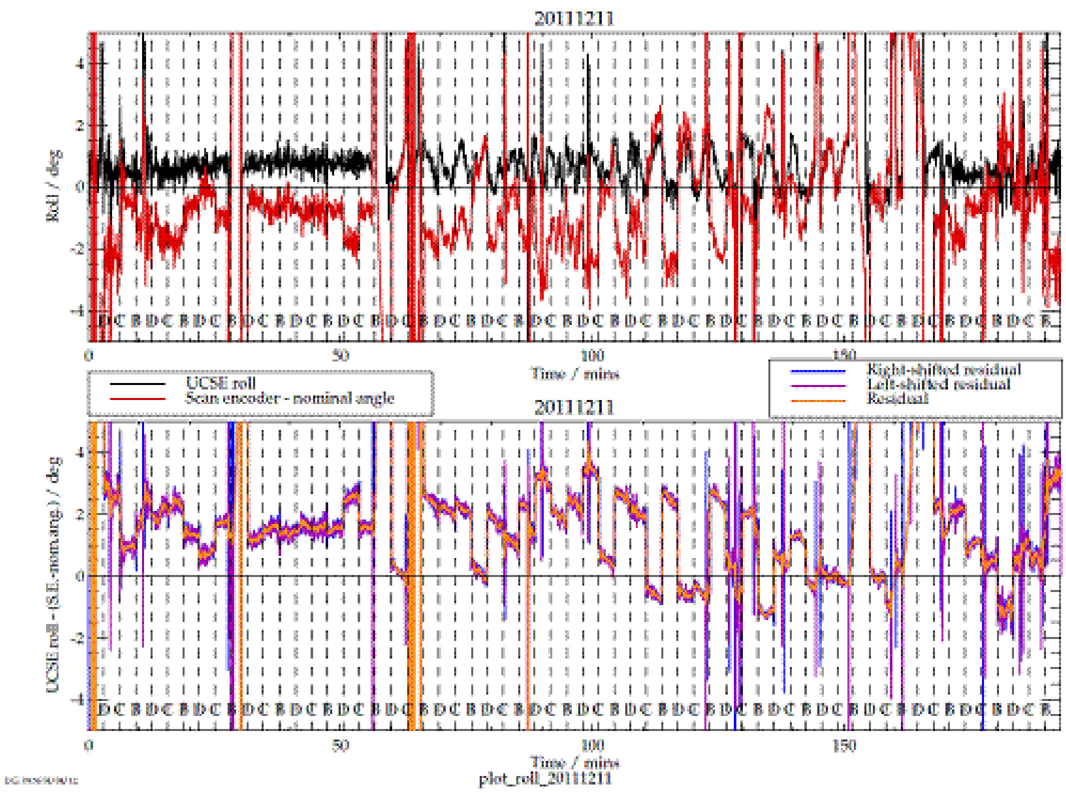

Figure 3.4.: UCSE roll-angle (black) and MARSCHALS roll-angle correction (red) from the commanded pointing update. A positive UCSE bias seems to result in a negative bias to the pointing correction, which in turn incurs a systematic negative bias of the scan range.

3.2.3. Post-Campaign Analysis of Aircraft Roll-Angle

A retrospective analysis of all available roll-angle data has now shown that our initial doubts on the accuracy of the UCSE roll-angle were unfunded and that the aircraft was indeed nudged to starboard for the full duration of the flight.

First of all this was confirmed by an independent analysis of aircraft attitude by our colleagues from the MIPAS team, and secondly we found out that the initial hints of a permanent bias in the UCSE data had to be rejected after looking after collecting additional evidence. The 0.5 deg roll-angle baseline in the UCSE data of the EMC test is simply due to the fact that the apron is sloped by (uncannily enough) exactly that amount to the east. This was confirmed by looking at the PREMIER-Ex data of EMC tests, where the UCSE roll-angle on the apron - in the identical parking position of the Geophysica - also read out a constant 0.5 deg (and obviously during the PREMIER-Ex flight no such pointing problems had manifested).

The further analysis of UCSE data taken during the roll test on the runway also dowsed any previous signs of a smoking gun. When plotting the aircraft roll-angle versus the aircraft

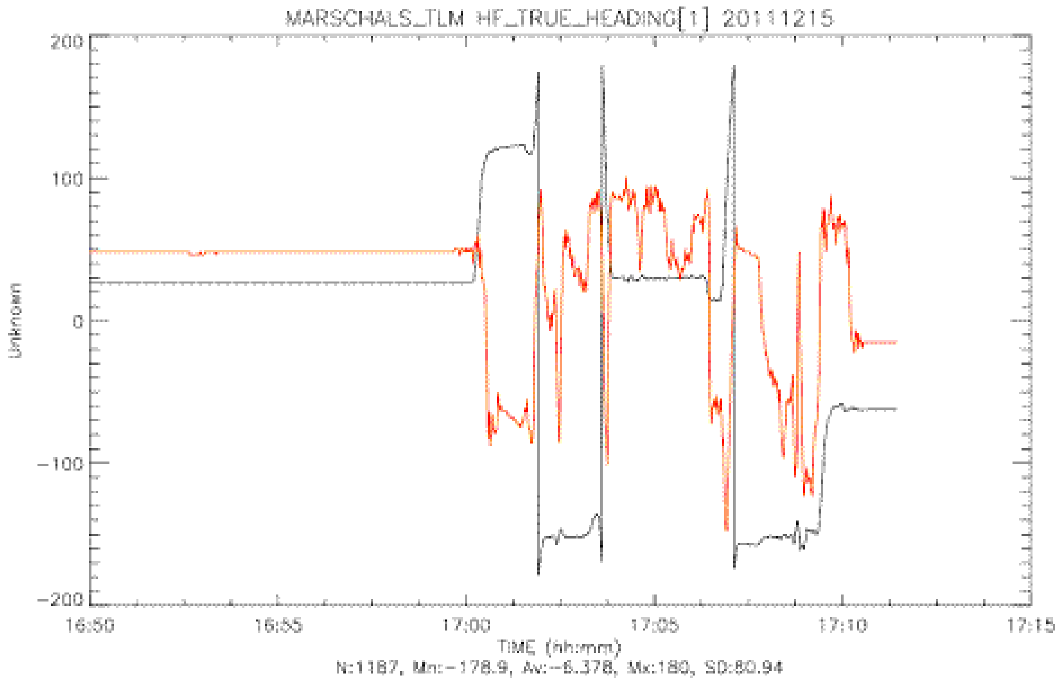

Figure 3.5.: UCSE heading (black) versus UCSE roll-angle multiplied by a factor of 100 (orange) during a breaks test on the runway. A roll-angle of 0.5 correlates to the heading on the apron of 30 deg N, but other instances seem to be purely random.

heading, we found that the stretches where the roll-angle was reading 0.5 deg were limited to that part of the test run where the heading was the same as on the apron, which we have now established to slope by exactly 0.5 deg. Other parts of the roll test seem to indicate for a tendency towards positive roll-angles, but on closer inspection the random fluctuations from the shaking aircraft seem to dominate the behaviour for the period the aircraft was rolling along or manoeuvring around the runway.

Our final conclusion is therefore that we must have an error in our pointing update code which makes that the calculated gyro correction is applied in the wrong direction of the roll-angle deviation from horizontal. If the aircraft is flying perfectly horizontal - as was the case for PREMIER-Ex - this does not matter because the term in the correction of the gyro angle which accounts for aircraft roll will be zero. In the case of ESSenCe Flight 1 however the fact that the aircraft was flying at a permanent non-zero roll-angle for all (or at least most) instances of the commanded gyro updates meant that the gyro was adjusted to non-zero 'reference horizon', which evidently meant that the subsequent scan was not perfectly centred on the limb range.

In absolute terms this doesn't matter because the post flight gyro correction we are performing is correctly reconstructing the true view angles and tangent point altitudes for each measurements, it just means that the atmospheric sampling is less than ideal.

The reason for the skewed flight attitude in the first ESSenCe flight is not clear. First consultation with the pilot on site revealed that a 0.5 deg roll would be unnoticeable to the pilot in flight and it's not something he would worry about.

Clearly this is something we need to remedy before the next deployment, but on the up side this is likely to be a trivial bug to fix. On the same occasion there are some additional ideas we have that could improve the pointing is to use a running mean of the roll-angle over a couple of seconds as a measure for the applied correction to be less sensitive to roll-angle noise, although we will have to evaluate if or how this could be possible (unfortunately the person who devised the MARSCHALS pointing control system is no longer working at RAL, so we'll first have to re-acquire some lost know-how).

3.3. Level 2 Processing

3.3.1. Averaging of Consecutive Views

The MARSCHALS scan sequence contains 4 consecutive measurements at each nominal scan altitude. This is done to increase integration time and thereby to reduce the noise equivalent Brightness Temperature (NEBT). In our analysis of campaign data we average these views together to a single measurement, for which the retrieval is run. For most situations the automatic pointing control will ascertain that these four views are perfectly collocated, but because of the rather unsteady flight attitude in ESSenCe Flight 1 in particular we have to allow for changes in view angles during the acquisition of the four measurements. This is done as follows: The four views at the same nominal view angle are averaged and a new measurement error for the averaged measurements calculated from the measurement error of a single measurements, reduced by a factor of SQRT(4) from statistical averaging.

We also calculate the standard deviation of the averaging process, which will be small if the four spectra are very similar, but large if one ore more spectra are significantly different than the average spectrum (would be the case i.e. if the aircraft made a brisk movement that the automatic pointing system would fail to correct for). The measurement error of the averaged spectrum is then defined for each individual spectral point as the larger value of either the averaged down spectral error, or the standard deviation of the averaging process.

3.3.2. Quality Filtering

Channelisers

The quality control for the channelisers is currently handled at Level 1b, i.e. known bad measurements (mostly bad channels) are correctively flagged with very large measurements errors of 1000K. The affected channels are listed in the ESSenCe Data Acquisition Report (and are also reproduced in the table below). This way the retrieval won't even try to fit these bad measurements and we can forgo additional filtering in the Level 2 processing. The only thing we are introducing on top of that is that we ignore fully opaque views at the bottom range of the atmosphere. These views don't contribute any spectral information, but they could potentially confuse the retrieval (indistinguishable measurements for very different view angles).

The criterion for opaqueness is simply the minimum Brightness Temperature value of the spectrum, and the threshold values we've experimented with are 180K, 190K and 200K. 180K is a conservative choice which works well for all bands, although the more transparent Band B (and less so Band C) also seems to work well with the higher thresholds.

```
Bad Channels ESSenCe Flight 1
------------------------------------------------------
Dead channels:   20           (all bands, all scans)
                 35           (all bands, all scans)

Out of dynamic range:
  Band B: none                           (all scans)
  Band C: 0,1,2,19,47,48,59              (all scans)
  Band D: none                           (all scans)

High noise:
  Band B: none
  Band C:   03                           (all scans)
             4                        (scans 0,2,5)
            23                    (scans 0,1,3,4,6)
            44                           (scan 23)
  Band D:    3,5,29,40                   (all scans)
            22                          (scans 2,6)
------------------------------------------------------
```

```
Bad Channels ESSenCe Flight 2
------------------------------------------------------
Dead channels:   20           (all bands, all scans)
                 35           (all bands, all scans)

Out of dynamic range:
  Band B: none                           (all scans)
  Band C: 0,1,2,19,47,48,59              (all scans)
  Band D: none                           (all scans)

High noise:
  Band B:    0                           (all scans)
  Band C:   44            scans 0,4,5,6,7,8,9,10,11)
            46                       (scans 9,10,11)
  Band D:    1                             (scan 3)
             3,5,29,40                   (all scans)
            21,22                          (scan 5)

------------------------------------------------------
```

Individual Scans

Not all scans are of equal quality when it comes to the data processing. This is at first order related to aircraft movements. The platform is not always very stable during flight, and level flight attitude is of paramount importance for scanning remote sensing instruments. The following figures show a sample of these analyses for Band B in Flight 2. We have been looking at the residuals between measurements and simulations after the retrieval and the standard deviation thereof and the measurement noise. We have then compared these to the standard deviations of parameters like roll-angle, tangent point altitude and the spectral variability of individual channels for the averaging process of the 4 views at the same nominal elevation angle.

In some cases this allows us to draw a parallel between features in the retrieval statistics and features from the view averaging. For example for Band B in Flight 2 the larger than normal measurement errors in scan 4 correlate with increased fluctuation of the radiance in that channel, which is term is explained by an extraordinary tangent point variation of several 100 metres for some of the views in this scan.

These comparisons are the basis for the selection criterion we apply in our results. I.e. for the presented case of Band B Flight 2 we would reject scan 6 which was acquired during a turn and contains no valid measurements, and we would probably reject scan 1 which doesn't cover the lower atmosphere. Scan 4 is expected to be potentially problematic because of the large tangent altitude fluctuations in the averaged views, however these variations are accounted for in the increased measurement error of the averaged views so a retrieval is still possible in principle.

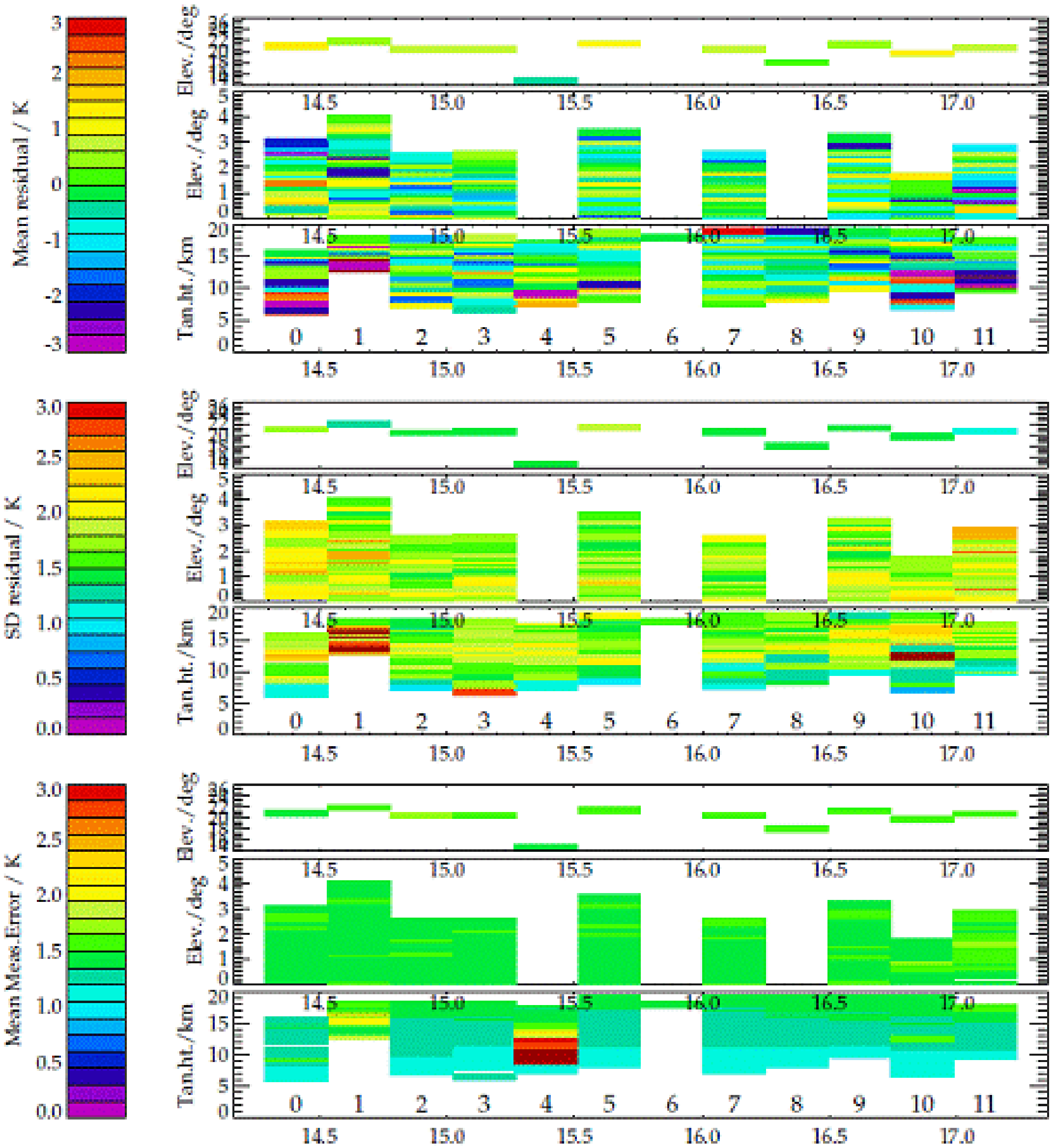

Figure 3.6.: Residuals and StdDev from a Band B retrieval of Flight 2. Scan 1 has reduced altitude coverage, scan 4 shows above average spectral errors and scan 6 is lost to a turn. As seen in Figure 3.9 the measurement error for scan 4 is dominated by fluctuations in the tangent altitude for the four consecutive scans. In this example, scan 4 can still be processed because the increased measurements errors are accounted for at Level 1b, which scans 1 and 6 lack information content due to missing measurements linked to aircraft manoeuvres.

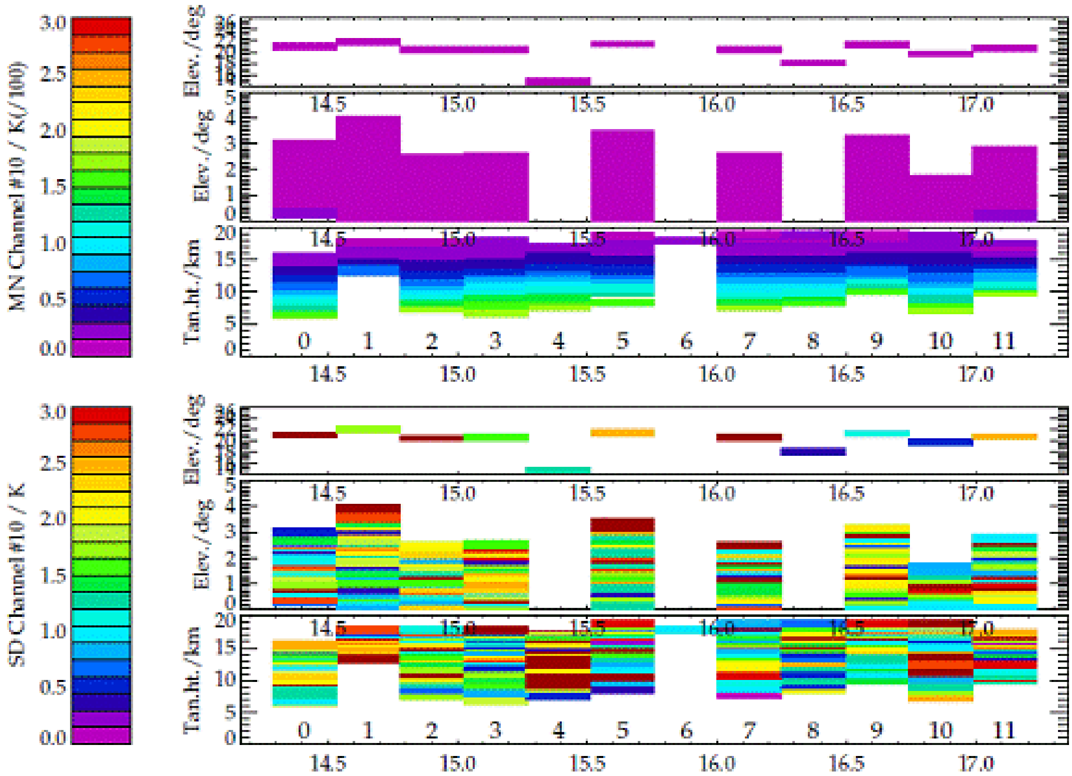

Figure 3.7.: Mean and StdDev for a random channel of Band B Flight 2. The Brightness Temperature profiles of the individual scans are well aligned, which confirms that the active pointing control does its job. Variations in the standard deviation of the four-view-averaging are nevertheless most likely due to aircraft movement between the individual measurements, as seen for scan 4 (compare to Figure 3.9).

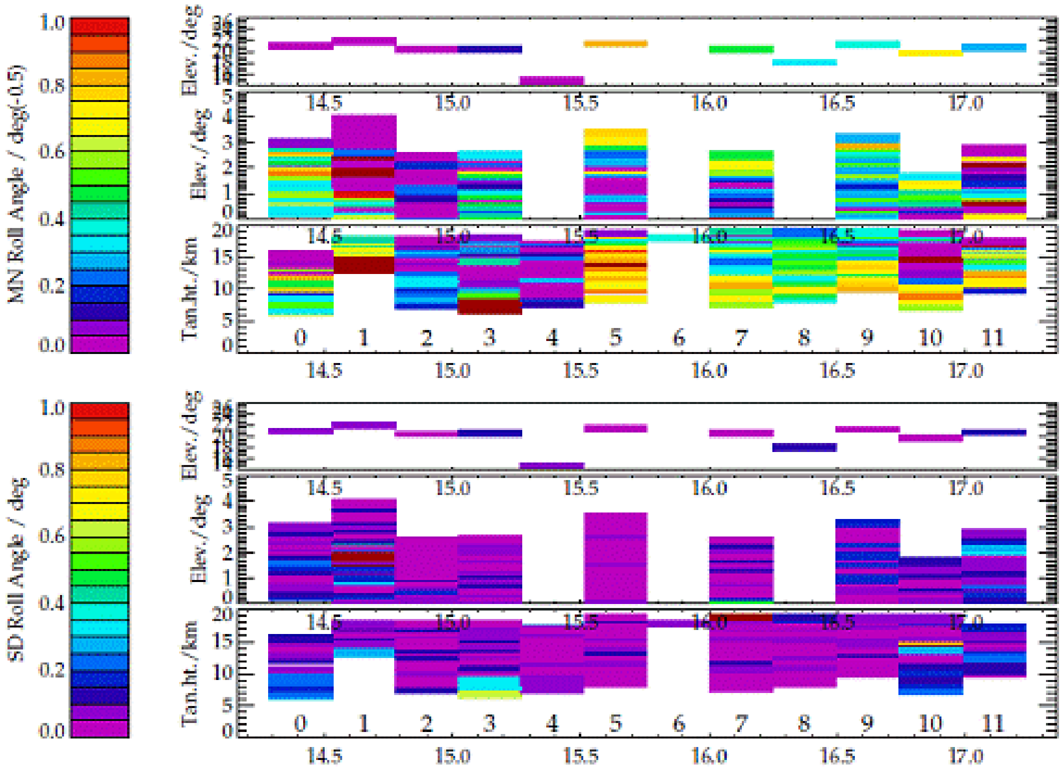

Figure 3.8.: Roll angle fluctuations during the view averaging. Despite difference in absolute flight attitude the fluctuations during a 4 view averaging are generally less than 0.1 deg. This is an illustration of the correct functioning of the active pointing control.

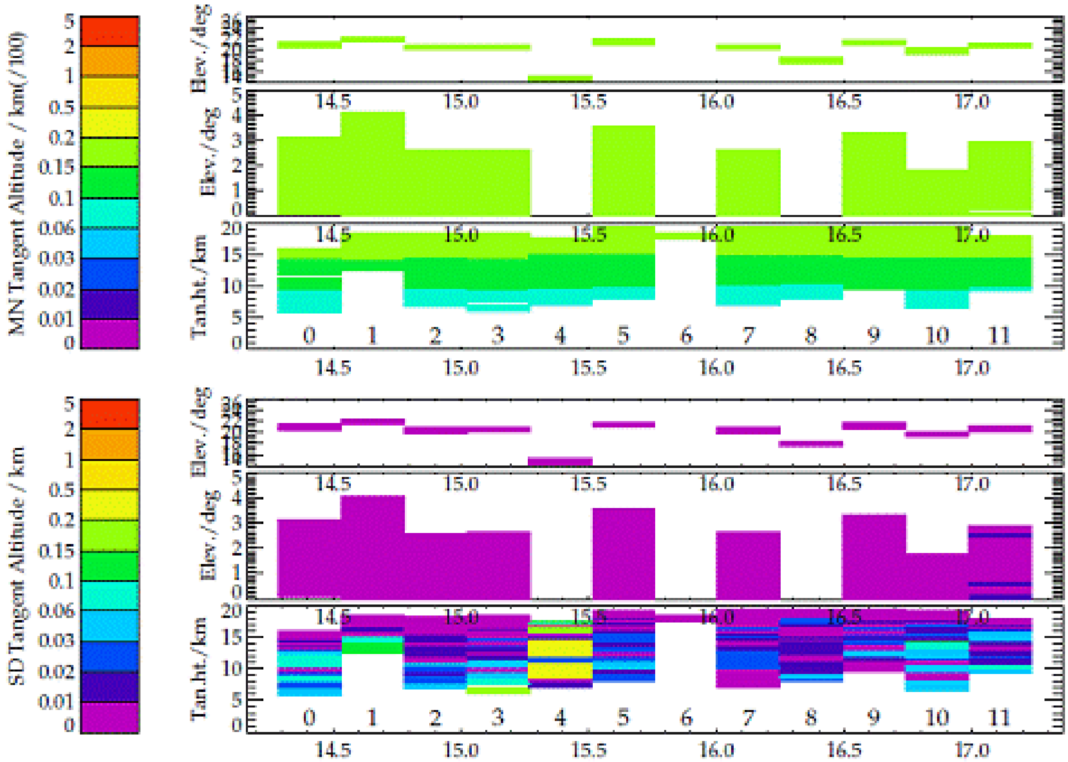

Figure 3.9.: Mean and StdDev for the refracted tangent altitudes. The smooth line up of tangent altitudes of the individual scans demonstrates the functioning of the active pointing control. Scan 4 shows larger than normal fluctuations for tangent altitudes of the four nominally identical views. These are responsible for the increased measurement error in scan 4 (see Figure 3.6) but that doesn't seem to impact the average.

3.3.3. Original Retrieval Settings

The retrievals have initially been performed with an algorithm based on the setting we have found to work well for the analysis of PremierEx data (with campaign specific adaptations for a priori profiles, a new analysis of the spectral performance of the channelisers to mask bad channels, etc.). However, with the availability of the retrieval result from GLORIA, we now had a high-resolution reference profile that we could use to improve our own retrieval settings. The GLORIA measurements indicated the presence of a very thin (less than 1km) layer in O_3 and HNO_3 mixing ratios at an altitude of ca. 14km. In our previous retrievals we used a 2km retrieval grid. This grid was too coarse to resolve such a fine layer. We have sub sequentially tried to refine the retrieval grid spacing until we could resolve this filament ourselves. Furthermore, we could use the height of the filament as a proxy to study our pointing bias retrievals. This has allowed us to reach a conclusion on this open issue.

Initial Retrievals

The same basic retrieval settings have been used as in PREMIER-Ex, although this has to be seen as a starting point and all these settings are open to further modifications if evidence suggests so. ECMWF analysis serves both as a priori and first guess. We can optionally use the corresponding ECMWF profile for each scan, but per default we are using a flat a priori for the whole flight (currently this is scan 4 from Band C; This selection is somewhat arbitrary as it dates back to the PREMIER-Ex settings as well, but in first order we expect this choice to be of no direct consequence on the retrieval).

The retrieval grid is spaced at a minimum of 2km for most species (0km, 2km, 4km ,6km, 8km, 10km, 12km, 14km, 16km, 18km, 23km, 30km, 40km), with a coarser spacing applied for CO (4km, 8km, 12km, 18km, 23km). Different scenarios for a priori errors are 10%, 30% and 100% and different vertical correlation lengths are 0km, 2km and 4km. Our best results are for 10-30% a priori error and no vertical correlation length.

Plots of these results are shown in Figures 3.10-3.18. Results of the new and improved retrieval setting for the scan collocated with the GLORIA measurements are shown and discussed in more depth in the following Section 3.5.

Initial Retrieval Results - Flight 1

The main feature of Flight 1 is a tropopause fold at the beginning of the flight. This is very visible in the ozone cross section and in nitric acid. It's less visible in water vapour, but then again the same is true for the model data.

There is an interesting feature in nitric acid in the third part of the flight, a sort of downward facing intrusion, that is present in the retrievals and in SLIMCAT, but not confirmed by

CLaMS. Nitrous oxide and carbon monoxide are added for the sake of completeness, but the signal to noise ration doesn't allow for a good retrieval of these species.

All of the plots shown are based on a retrieval that makes use of the pre-retrieved pointing bias. We believe that for Band B at least this produces slightly better results. For the other bands no such statement can be made at this time. This is therefore not the final release of MARSCHALS data and we will improve on these results in the near future.

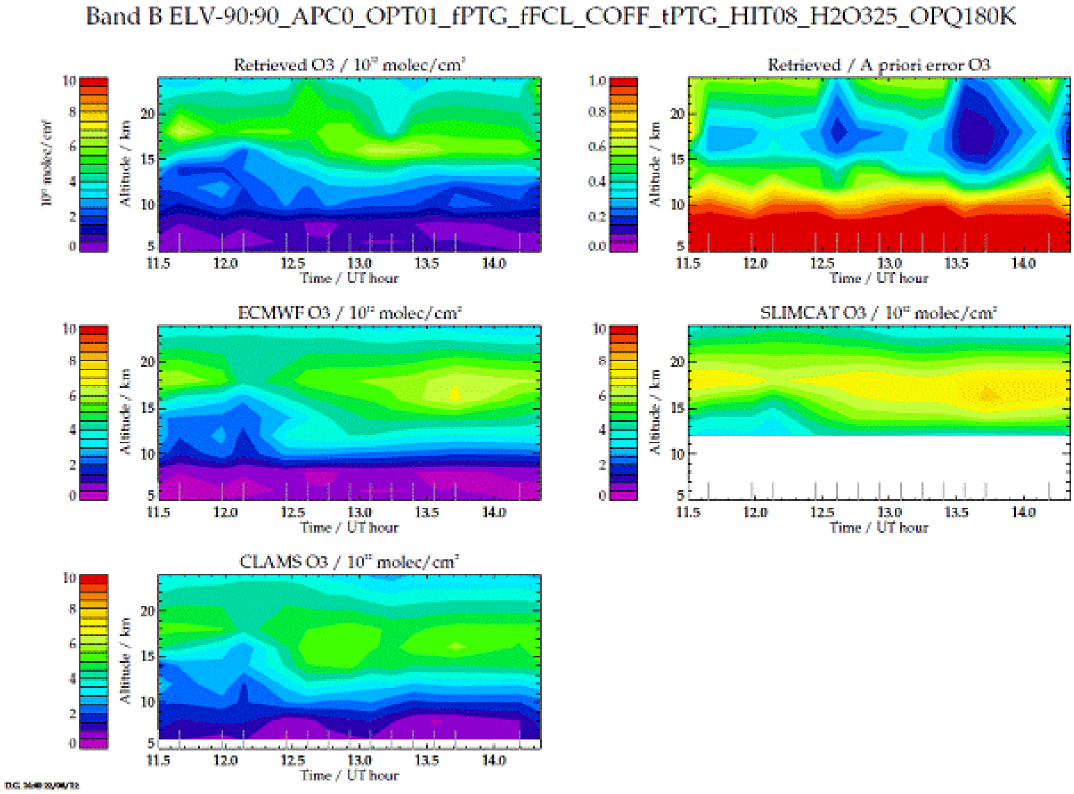

Figure 3.10.: Band B ozone from Flight 1.

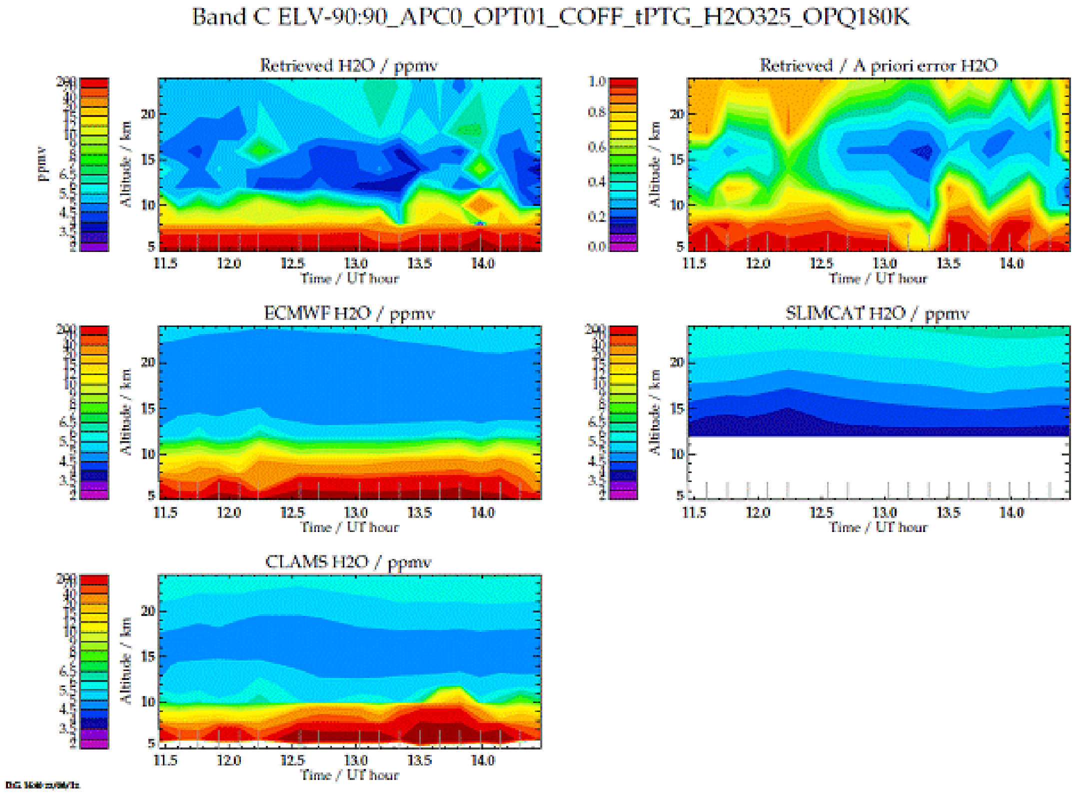

Figure 3.11.: Band C water vapour from Flight 1.

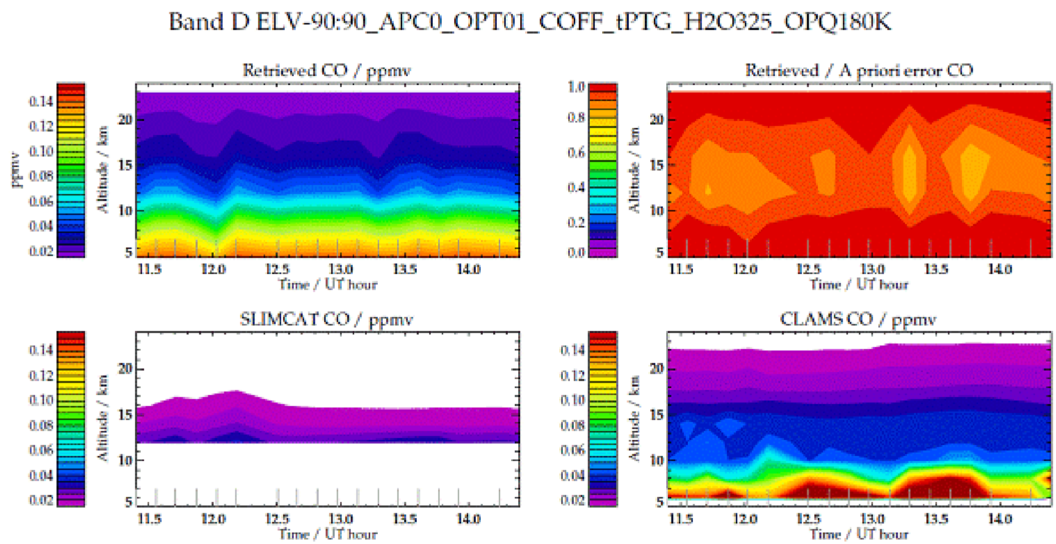

Figure 3.12.: Band D carbon monoxide from Flight 1.

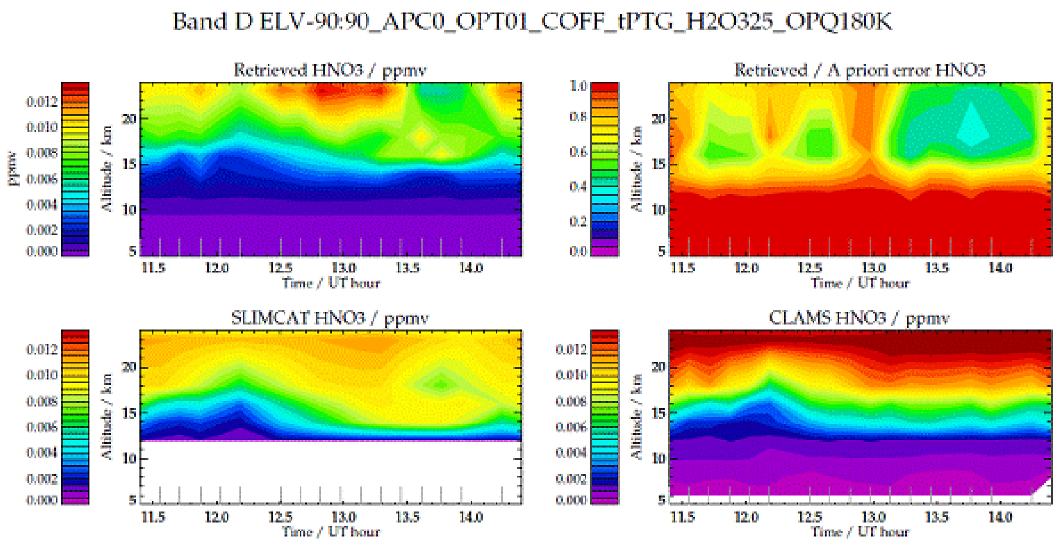

Figure 3.13.: Band D nitric acid from Flight 1.

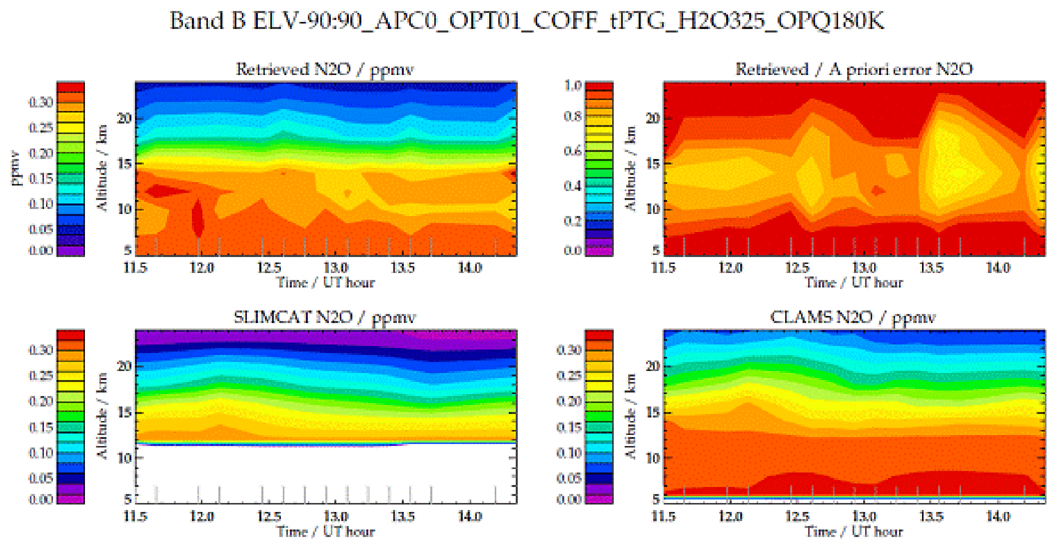

Figure 3.14.: Band B nitrous oxide from Flight 1.

Initial Retrieval Results - Flight 2

The main characteristic of Flight 2 is its lack of characteristics. The atmosphere was evenly stratified with little features in the cross sections predicted, by the models, nor indeed measured by the instruments. For Flight 2 we have included the MIPAS-STR data in our comparison. There is however one interesting feature, again in nitric acid, namely a thin layer below the bulk of the stratospheric distribution.

This layer is predicted by the models at an altitude of 16 km, but both MARSCHALS and MIPAS-STR seem to put this layer at 18 km. Also the following depression in HNO_3 is put at higher altitudes by MARSCHALS (outside the plot range of MIPAS-STR). We believe that the two measurements endorse each other quite nicely in this case.

As in Flight 1, nitrous oxide and carbon monoxide don't exceed a signal to noise level which would allow a usable retrieval.

All of the plots shown are based on a retrieval that makes use of the pre-retrieved pointing bias. We believe that for Band B at least this produces slightly better results. For the other bands no such statement can be made at this time. This is therefore not the final release of MARSCHALS data and we will improve on these results in the near future.

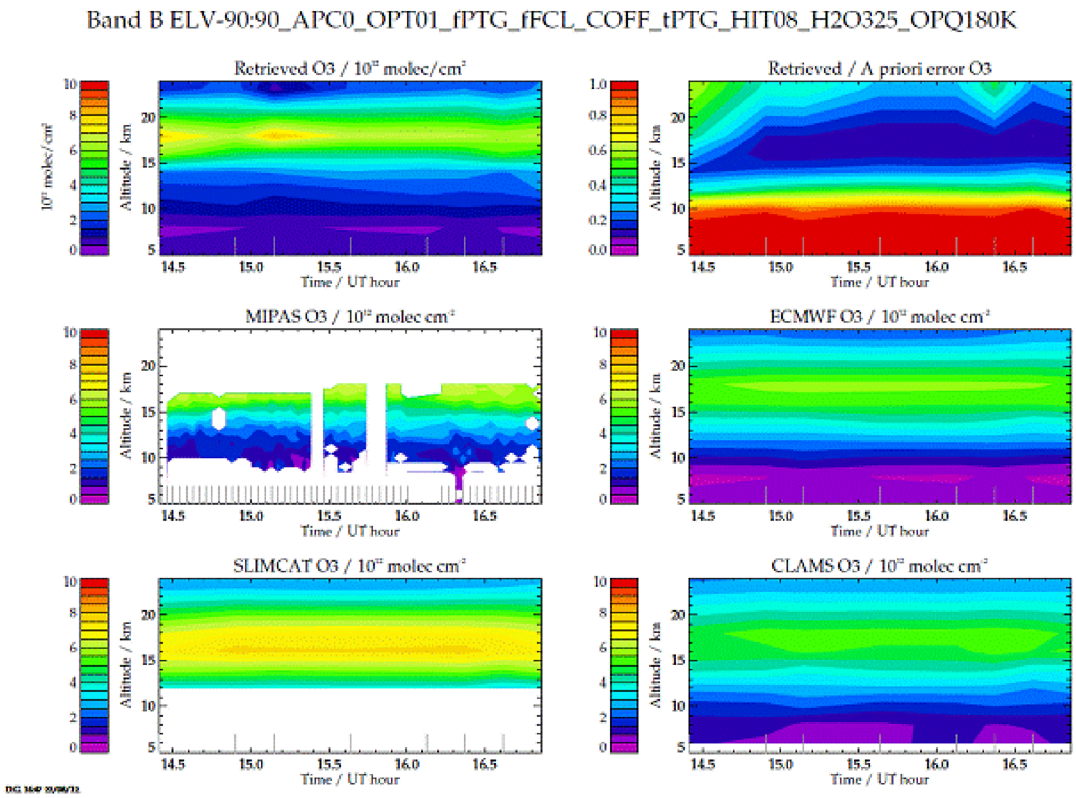

Figure 3.15.: Band B ozone from Flight 2.

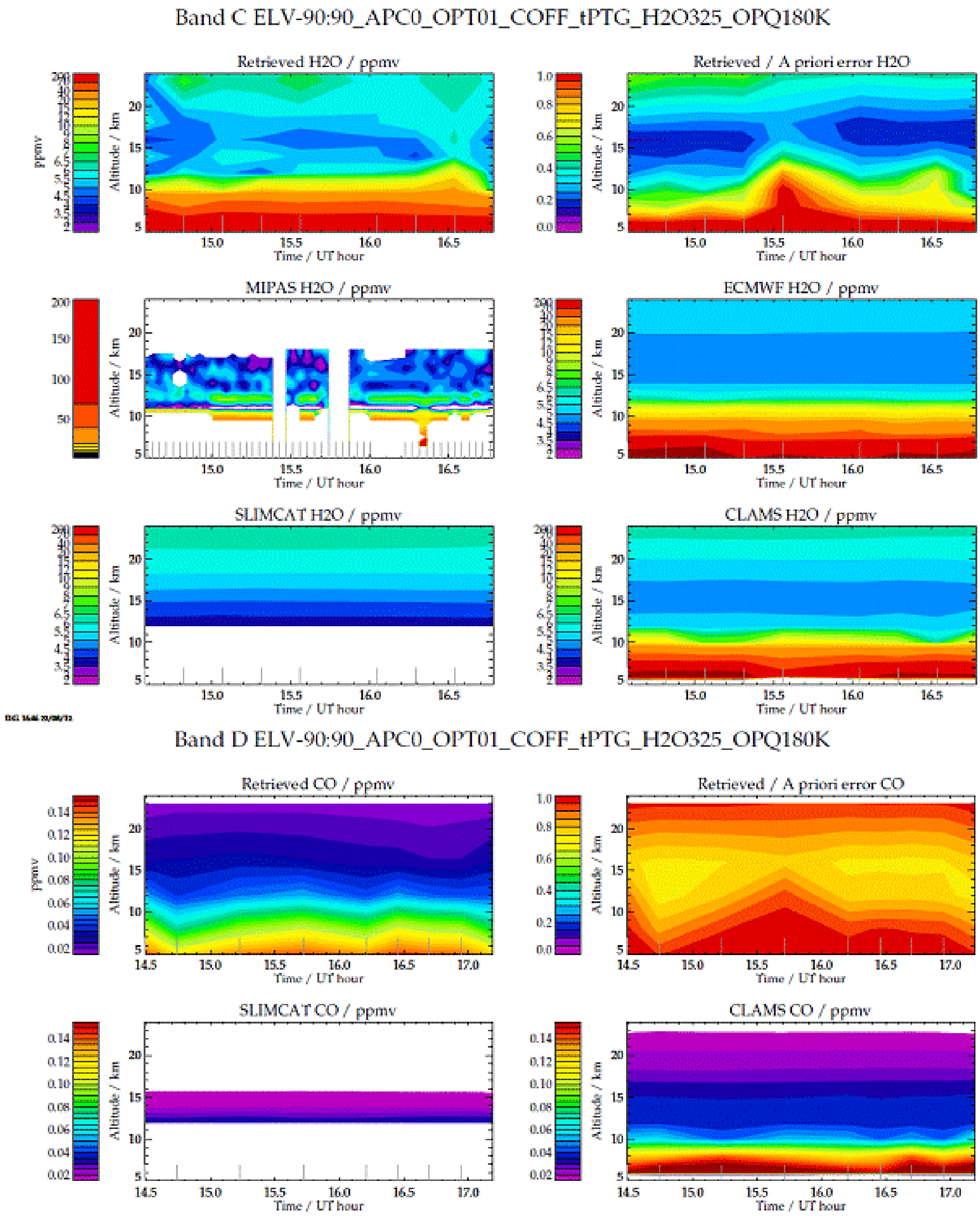

Figure 3.16.: Band C water vapour and Band D carbon monoxide from Flight 2.

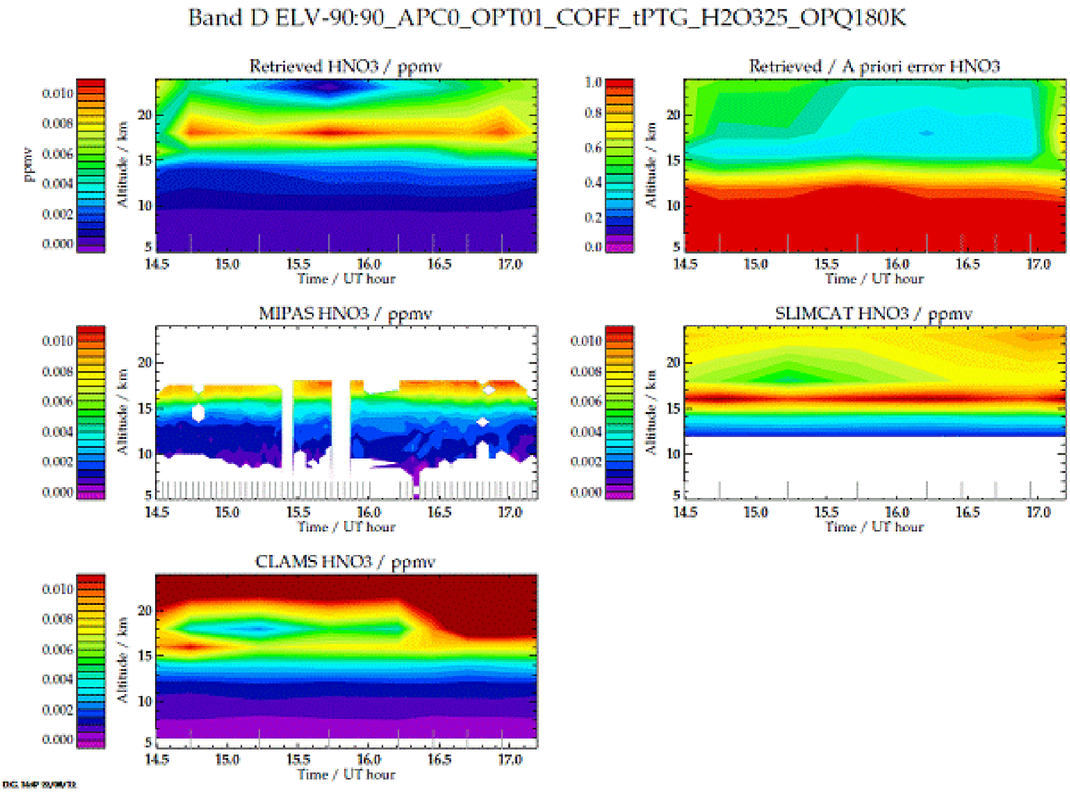

Figure 3.17.: Band D nitric acid from Flight 2.

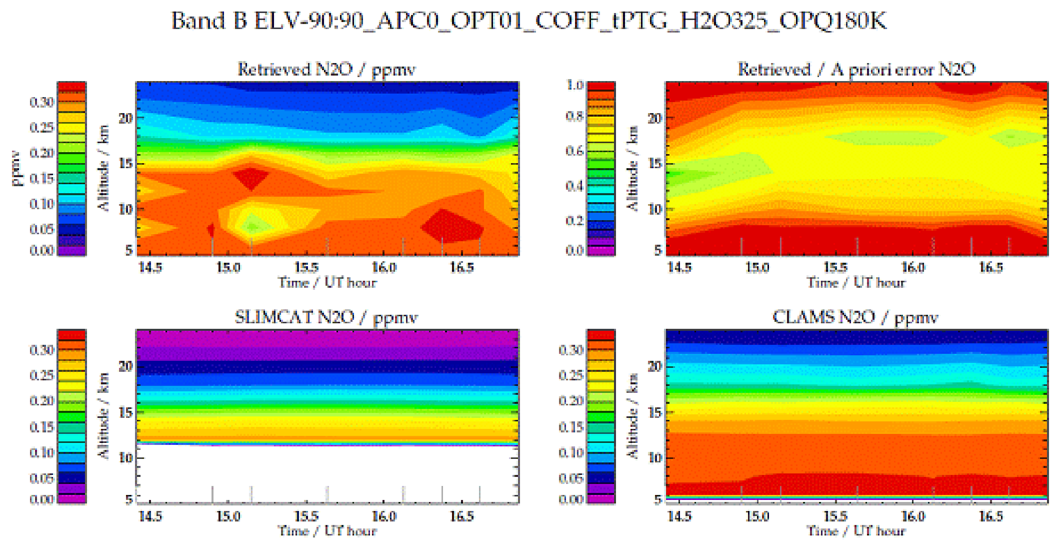

Figure 3.18.: Band B nitrous oxide from Flight 2.

3.4. Inter-comparison with the GLORIA chemistry mode measurements

GLORIA provides us with a high-resolution profile of O_3 and HNO_3 during a 20 minutes chemistry mode measurement at the start of the flight of 16th December (Flight 2). We can use this for a direct inter comparison between GLORIA and MARSCHALS. Primarily this is important because GLORIA have observed a thin filament structure in both gases of sub-km thickness. It is therefore interesting to see whether MARSCHALS is able to reproduce this feature. In order to do so we have to increase the vertical resolution of our retrieval setup. The changes we've introduced to our retrieval algorithm are described in the following section.

3.4.1. Simulation study of the detectability of thin filaments by MARSCHALS

First of all we have done a simulation to determine if MARSCHALS is physically able to detect such a thin trace gas layer as observed by GLORIA. For this we have run forward model simulations of atmospheric spectra based on the mixing ration profiles measured by GLORIA, first of all including the filament at 14km altitude, and then again with modified profiles in which we have removed the filaments. We have then computed the residual spectra and compared them to the spectral measurement errors. This will tell us if the spectral feature due to these filaments is physically detectable by MARSCHALS based on its spectral performance. The results of this analysis are shown in Figures 3.19 to 3.21.

The conclusion of this study is that we should be able to detect a filament as measured by GLORIA at 14km altitude in O_3, but that the same filament in HNO_3 is elusive to MARSCHALS because of the dismissive magnitude of the feature in the HNO_3 spectral line at this frequency. A direct comparison with GLORIA is therefore useful, and we can reasonably expect to detect the filament structure in our own O_3 data by increasing the vertical resolution of the retrieval. The following section presents the updated retrieval settings used in the MARSCHALS-GLORIA inter comparison. The scans that were used in the comparison are given in the following Table. Scan 1 of Band B and scan 1 of Band C are also compatible with the GLORIA observation, but their exploitation is hampered by a bad scan range in Band B (roll-angle update) and some bad channels in Band C (possibly related to thermal instability during the initial phase of the flight).

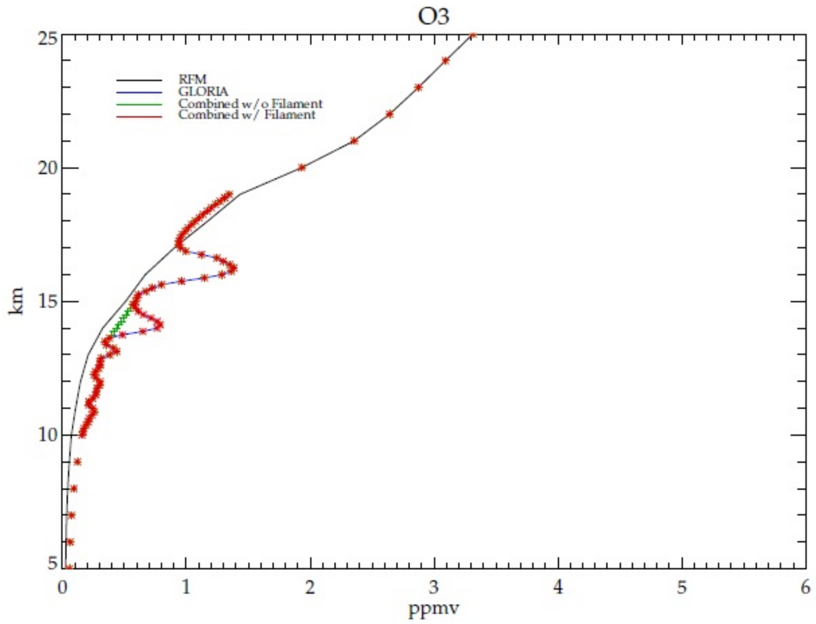

Figure 3.19.: Mixing ratio profiles of O_3 used in the simulation study to determine the spectral impact and detectability of a thin filament structure as measured by GLORIA in Flight 2.

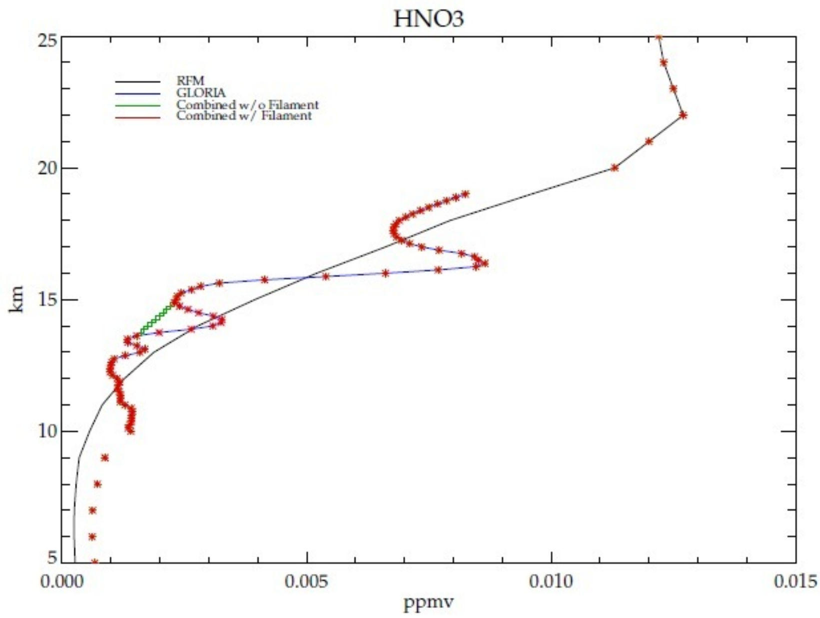

Figure 3.20.: Mixing ratio profiles of HNO_3 used in the simulation study to determine the spectral impact and detectability of a thin filament structure as measured by GLORIA in Flight 2.

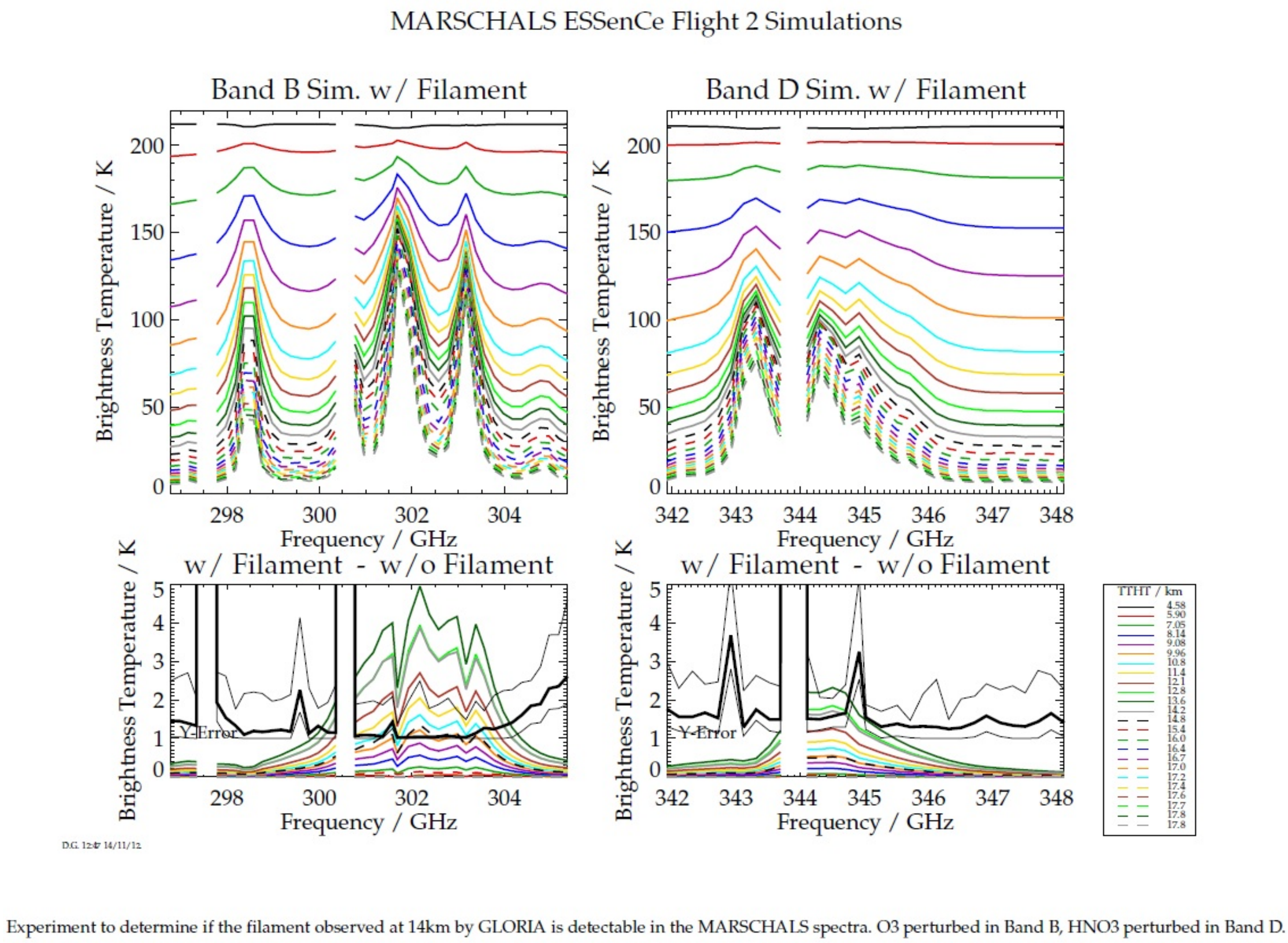

Figure 3.21.: Results of the simulation study to determine the detectability of a thin filament structure as observed by GLORIA in Flight 2. Simulated spectra have been calculated with and without the filament and the residuals are compared to the spectral noise performance of MARSCHALS. In Band B the O_3 profile was perturbed, and in Band D accordingly the HNO_3 profiles pas perturbed. The residuals show that the filament signature for O_3 is above the detection threshold, wheres for HNO_3 the signature is comparable to the noise threshold and therefore not guaranteed to be detectable.

3.5. Updated Retrieval Settings for ESSenCe

The previous retrieval settings were based on a conservative retrieval grid spacing of a minimal step-width of 2 km. In turn we have allowed the vertical correlation length to be zero and used tight a priori constraint. This setup happened to work well with the PremierEx Data. In order to be able to resolve structures of less than or up to 1km we have to move to a more finely spaced retrieval grid. We have done many different test runs of retrievals with either a fixed altitude grid of 1km at its narrowest, and also with a non-equidistant retrieval spacing where a retrieval grid point is placed at each tangent point where a measurement has been acquired.

Nominally the measurements should be spaced at roughly 1km intervals as well (calculated for a nominal scan and platform altitude), but in practise this can be more or less. This was especially true for ESSenCe, where as a result of the erroneous roll-angle updates at times of non-horizontal aircraft attitude (discussed above) a scan can be offset to its nominal tangent point range. In the case of the retrieval grid that follows the measurement spacing we would remove any given grid-point that is closer to its nearest neighbour than 500 metres. The reason for this is that, even though a narrow grid spacing is good for vertical resolution, too closely spaced retrieval levels can lead to problems with oscillations in the results.

We have found that the slight benefit in vertical resolution that a retrieval on the measurement grid allows, results in a better representation of the very thin filament that GLORIA was observing. For the scan that is directly comparable in time, we see the filament represented at two retrieval altitudes on the finer grid, whereas if we run the same retrieval on a retrieval grid fixed at absolute 1km steps the layer is just covered by a single retrieval level. The results we're showing for the inter comparison between MARSCHALS and GLORIA are based on the retrieval grid that matches the measurements altitudes. If we were to look at the whole flight (i.e. comparing several scans at once), then the uniform 1km retrieval grid would be more stable and better suited for visualisation, at the cost of losing some details in the vertical structure.

Additionally, we have introduced a 1km vertical correlation length in order to stabilise the retrieval despite the very narrow grid spacing. This still returns the filament structures of the same magnitude. As a test, we have tried a 2km vertical correlation length. This performed as expected by further smoothing the retrieved profiles, but making any sub-km features invisible. These results are much the same as the old retrieval setup with a 2km retrieval grid and no vertical correlation.

A detailed account of the retrieval settings for the improved ESSenCe retrievals is given in Tables 3.1 to 3.5.

Table 3.1.: Updated Retrieval Settings for ESSenCe (as used in the inter-comparison with GLORIA results from Flight2)

Parameter	Value
Retrieval Algorithm	Optimal Estimation, Single spectral band
Retrieved products Band B	O_3, N_2O, Continuum absorption coefficients
Retrieved products Band C	H_2O, O_3, N_2O, HNO_3, CH_3Cl, Continuum absorption coefficients
Retrieved products Band D	O_3, CO, HNO_3, CH_3Cl, BrO, ClO, Continuum absorption coefficients
Spectral line shapes	VVW/Voigt where Doppler width significant
Continuum Function	Continuum fitted to two independently retrieved continuum absorption coefficients at either band edge
Spectral line data Band B	Modified HITRAN (902 dominant transitions from 0.741691 wn to 33.203354 wn. Non-HITRAN species from JPL or GEISA)
Spectral line data Band C	Modified HITRAN (928 dominant transitions from 0.741691 wn to 33.203354 wn. Non-HITRAN species from JPL or GEISA)
Spectral line data Band D	Modified HITRAN (891 dominant transitions from 0.741691 wn to 33.203354 wn. Non-HITRAN species from JPL or GEISA)

Table 3.2.: Frequency and Altitude Grids (Updated Retrieval Settings for ESSenCe)

Parameter	Value
Radiative transfer code	FM2D (RAL in-house code)
Frequency grid Band B	Optimised frequency grid (627 spectral points from 296.50000 to 305.50000 GHz)
Frequency grid Band C	Optimised frequency grid (600 spectral points from 316.60000 GHz to 326.69900 GHz
Frequency grid Band D	Optimised frequency grid (621 spectral points from 341.50000 GHz to 348.50000 GHz
Forward model levels	219 levels from 0 km to 60 km at minimal spacing of 125m (+ constant offset levels of 50m, 100m, 150m, 200m, 300m, 350m, 400m and 450m below each calculated pencil beam)
Retrieval code	RET2D (RAL in-house code)
Retrieval levels H_2O, O_3, HNO_3, Abs.Coeff.	0km, 2km, 4km, 6km, 8km, 10km, 11km, 12km, 13km, 14km, 15km, 16km, 17km, 18km, 23km, 30km, 40km
Retrieval levels N_2O, CH_3Cl, BrO, ClO	0km, 2km, 4km, 6km, 8km, 10km, 12km, 14km, 16km, 18km, 23km, 30km, 40km
Retrieval levels CO	4km, 8km, 12km, 16km, 23km
Vertical correlation length	1km (optionally 2km)

Table 3.3.: Instrument Parameters (Updated Retrieval Settings for ESSenCe)

Parameter	Value
FoV function Band B	Measured at QMUL (Final Regridded QMUL Co-Pol Raster Data from: 8J8a40.P, Regridded QMUL X-Pol data from: 8J7p46.P)
FoV function Band C	Measured at QMUL (Final Regridded QMUL Co-Pol Raster Data from: 27I3p19.P, Regridded QMUL X-Pol data from: 28I8a40.P)
FoV function Band D	Measured at QMUL (Final Regridded QMUL Co-Pol Raster Data from: 5J1209.P, Regridded QMUL X-Pol data from: 6J7a46R.P)
Spectral Response Function Band B	Measured at RAL (File: FILTER_FILE_MARSCHALS_2010_B_20100215-2b-0212-1a-0221-2a.essence.44chns)
Spectral Response Function Band C	Measured at RAL (File: FILTER_FILE_MARSCHALS_2010_C_20100215-2b-0212-1a-0221-2a.essence.39chns)
Spectral Response Function Band D	Measured at RAL (File: FILTER_FILE_MARSCHALS_2010_D_20100215-2b-0212-1a-0221-2a.essence.32chns)

Table 3.4.: A Priori Values (Updated Retrieval Settings for ESSenCe)

Parameter	Value
Temp (profile)	ECMWF operational gridded 1.125
Pres (profile)	ECMWF operational gridded 1.125
H_2O (profile)	ECMWF operational gridded 1.125
O_3 (profile)	ECMWF operational assimilated ERA40
All other trace gases	RFM climatology (polar winter)
continuum absorption coefficients (profile)	Modelled on Liebe-93 continuum model
Pointing bias	0 deg
Frequency calibration offset	-12.5 MHz
Cold load temperature bias	0 K
Radiometric gain	1
Radiometric offset	0

Table 3.5.: A Priori Errors (Updated Retrieval Settings for ESSenCe)

Parameter	Value
H_2O	100% + 1E-0 ppmv
O_3	100% + 1E-1 ppmv
CO	100% + 1E-1 ppmv
N_2O	100% + 1E-1 ppmv
HNO_3	100% + 1E-3 ppmv
CH_3Cl	100% + 1E-6 ppmv
BrO	100% + 1E-11 ppmv
ClO	100% + 1E-4 ppmv
Temp	2% + 1 K
continuum absorption coefficients	200% + 1E-6
pointing bias	0.3 deg
frequency calibration offset	0.5 MHz
cold load temperature bias	2 K
radiometric gain	1
radiometric offset	0.5 K

3.6. Retrieval Results for ESSenCe (Updated Settings)

The following sections show results of the analysis of three MARSCHALS scans:

MARSCHALS Band D Scan 1	2011-12-16 14:41-14:46 UTC
MARSCHALS Band C Scan 2	2011-12-16 14:46-14:51 UTC
MARSCHALS Band B Scan 2	2011-12-16 14:51-14:56 UTC
GLORIA Chemistry Mode Measurements	2011-12-16 14:30-14:49 UTC

As predicted in the simulation study, the filament structure is not observed in HNO_3, however the O_3 results in all three bands consistently show a filament structure around 14km, just as it was seen by GLORIA. The best match we find in Band B, which is an expected results because we have 3 strong O_3 lines in Band B so we expect the O_3 retrieval to perform best in this band. Band C and D only feature a single O_3 line each, and at a lower strength. It can be argued that there are hints of a layer structure in Band C HNO_3 profile, but they are only marginally conclusive.

There are slight differences in the altitude of the retrieved layer between the three spectral bands. Band C shows the biggest discrepancy in peak altitude compared to GLORIA, whereas the other bands compare very well to the GLORIA profile. There are four potential reasons for this.

1) The bands have been measured at different times and places due to the aircraft movement. There is also a slight mismatch between the GLORIA and MARSCHALS measurements so we can't expect a perfect match.

2) The retrieval grid is tied to the measurement altitudes, which in reality vary slightly between different scans. The sampling pattern will have an impact on how a given feature is displayed in the results (i.e. the peak of the curve will be at one of the retrieval grid points, but these are not identical between the three results presented).

3) The retrieval quality is dependant of the signal strength in the measurements, which are different for each band. Band B will give the best O_3 retrievals, Band C slightly less so because there is only a single line (and atmospheric transmittance is lower at higher frequencies) and Band D should be even worse (because the Band D O_3 line is weaker and atmospheric transmittance even lower than in Band C).

4) There could be discernible pointing bias between the three spectral bands. We write more about this in the following section on Pointing Bias. Pointing Bias is something we retrieve as an instrument parameter. In contradiction to past studies there is no evidence of a significant pointing bias found in the improved ESSenCe results. I.e. from a previous analysis of O_2 pointing retrievals in Band B we found indications of a possible 0.5deg pointing bias. This however doesn't hold true because in the higher resolution retrievals we have matching altitudes of the filament layer under the assumption of no pointing bias. It is however worth

noting that in the retrievals of instrument parameters, the Band C results indicate twice the pointing bias of the other two bands (i.e. 0.14 deg compared to 0.07-0.11 deg) so there is a distinct difference in pointing results that sets Band C apart. This could maybe go towards explaining the difference in filament altitude match. There is more about the pointing bias in the corresponding section.

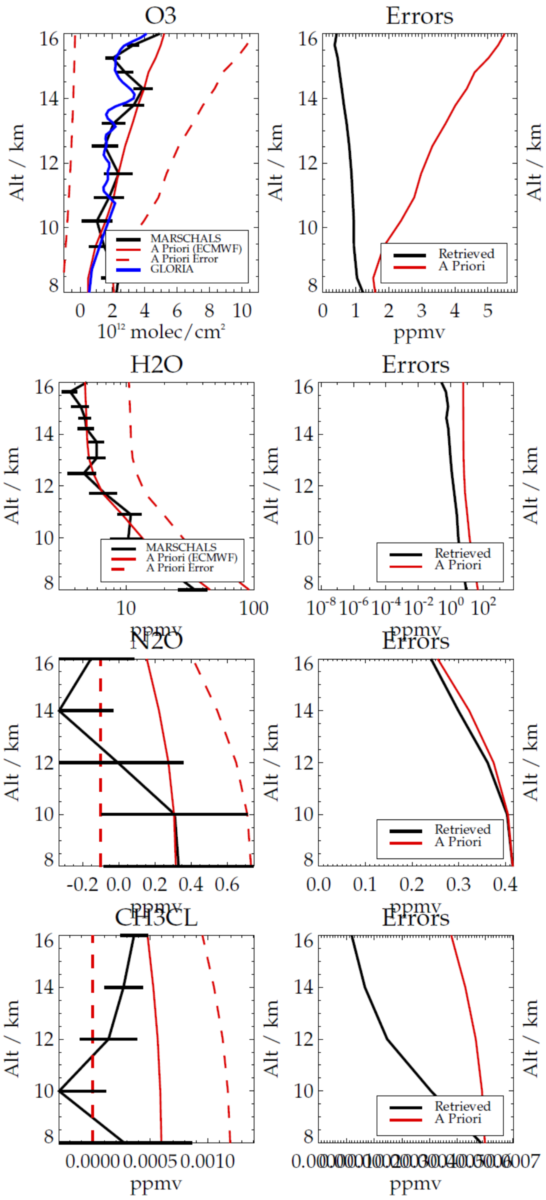

Figure 3.22.: Retrieved volume mixing ratio and error profiles for the species in Band B and C (Scan 2).

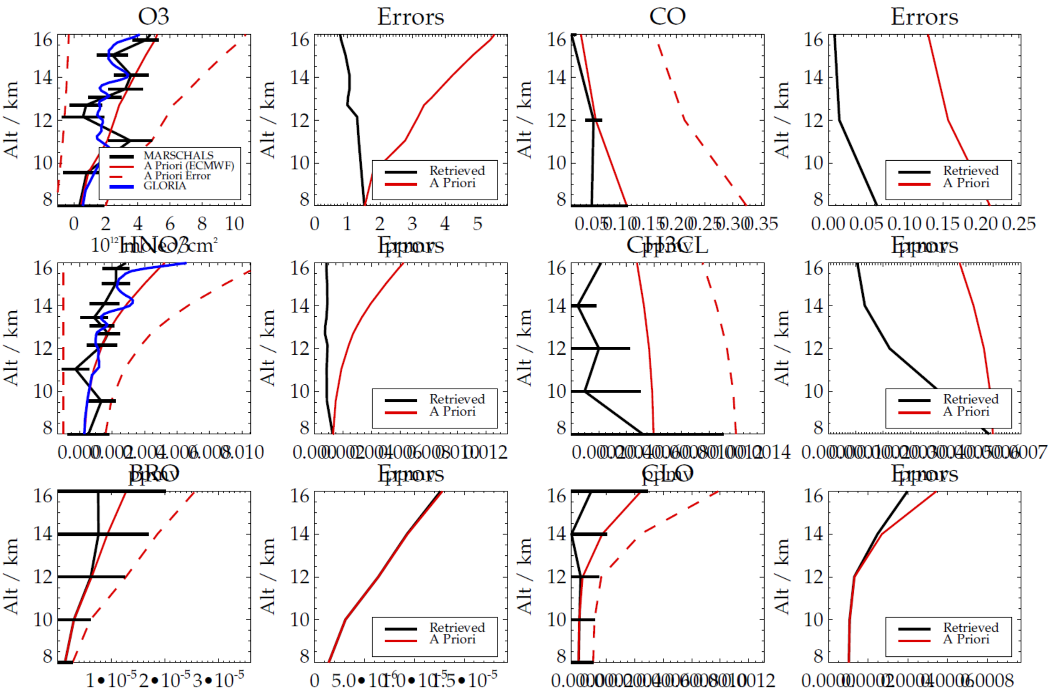

Figure 3.23.: Retrieved vmr and error profiles for the species in Band D (Scan 1).

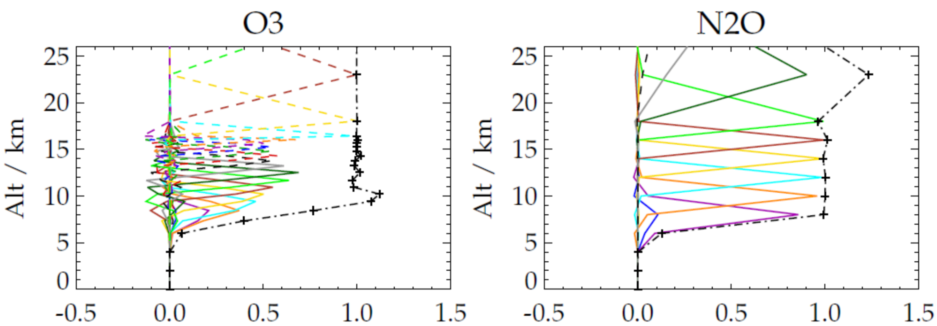

Figure 3.24.: Averaging kernels for the retrieved species in Band B (Scan 2).

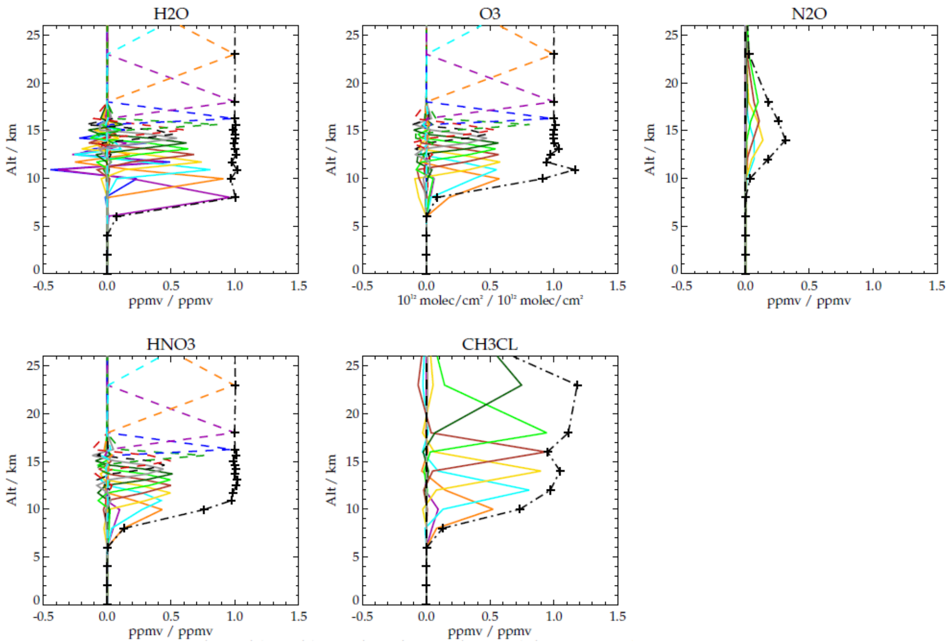

Figure 3.25.: Averaging kernels for the retrieved species in Band C (Scan 2).

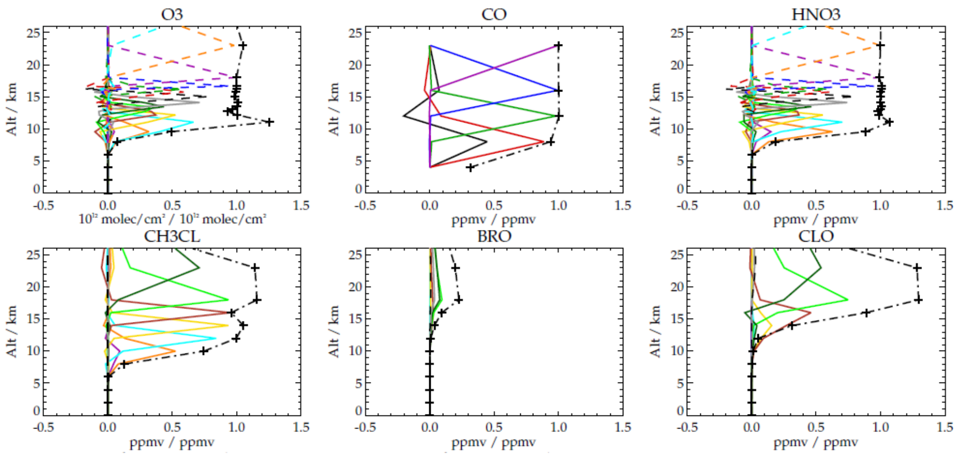

Figure 3.26.: Averaging kernels for the retrieved species in Band D (Scan 1).

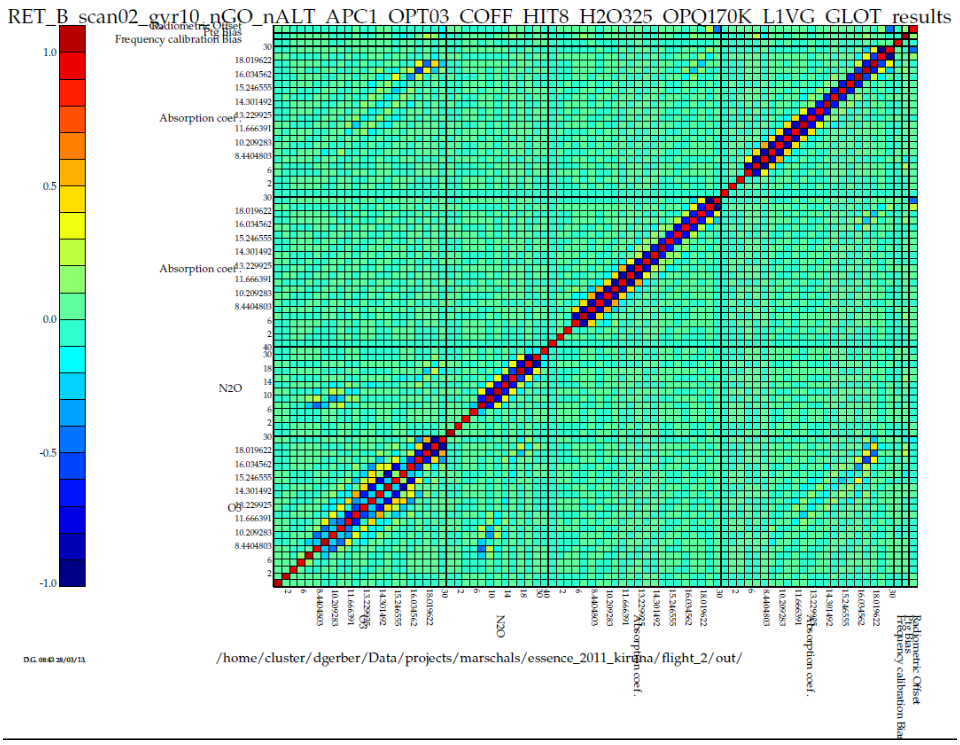

Figure 3.27.: Cross-correlation matrix for the retrieved species in Band B (Scan 2).

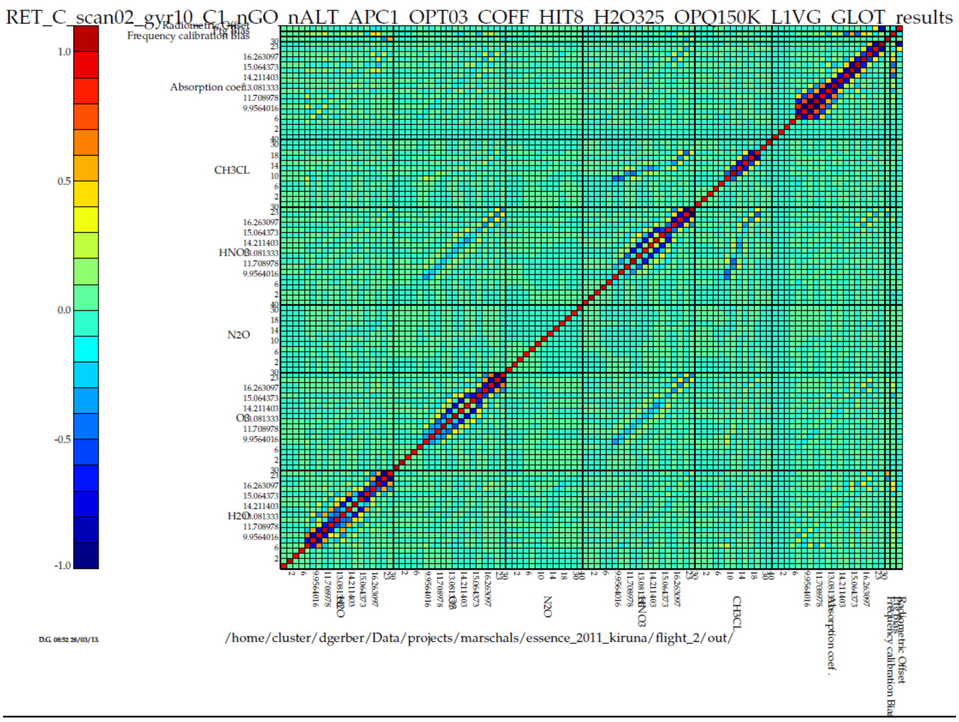

Figure 3.28.: Cross-correlation matrix for the retrieved species in Band C (Scan 2).

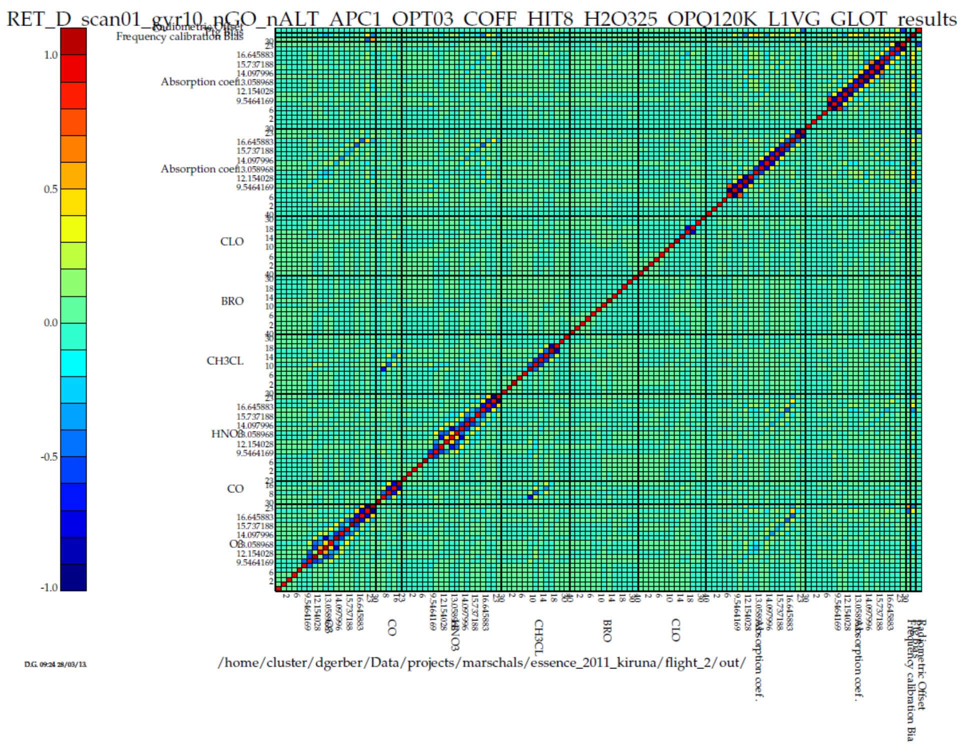

Figure 3.29.: Cross-correlation matrix for the retrieved species in Band D (Scan 1).

Frequency calibration Bias / GHz:
Ret: -0.01099 +/- 1.686E-05
Apr: -0.01250 +/- 5.000E-04
Tru: -0.01250

Ptg Bias / km/deg:
Ret: -0.01072 +/- 0.006237
Apr: 0 +/- 0.3000
Tru: 0

Radiometric Offset /

K:
Ret: 1.604 +/- 0.2014
Apr: 0 +/- 2.000
Tru: 0

Figure 3.30.: Retrieved instrument parameters for Band B (Scan 2). The term labelled Radiometric Offset is a correction term for the cold target radiance only.

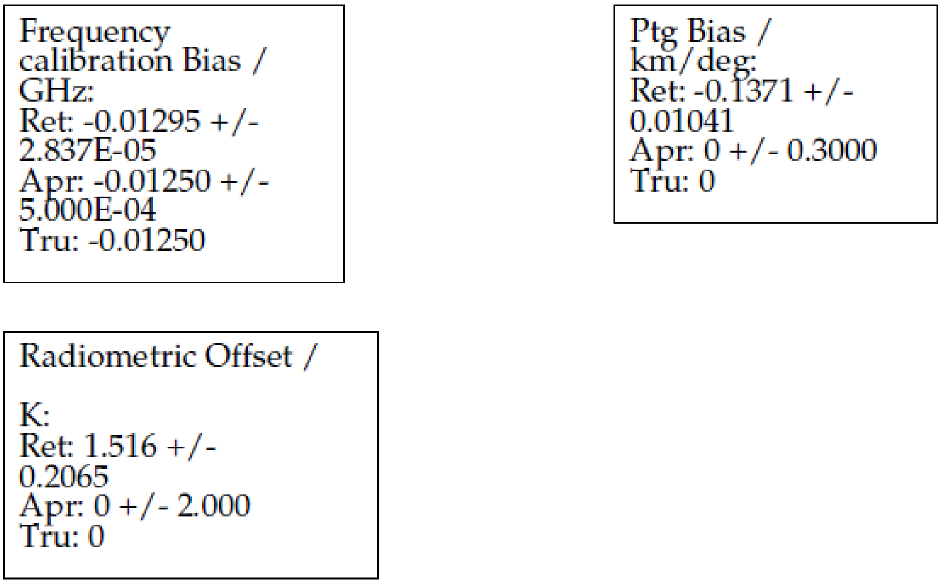

Figure 3.31.: Retrieved instrument parameters for Band C (Scan 2). The term labelled Radiometric Offset is a correction term for the cold target radiance only.

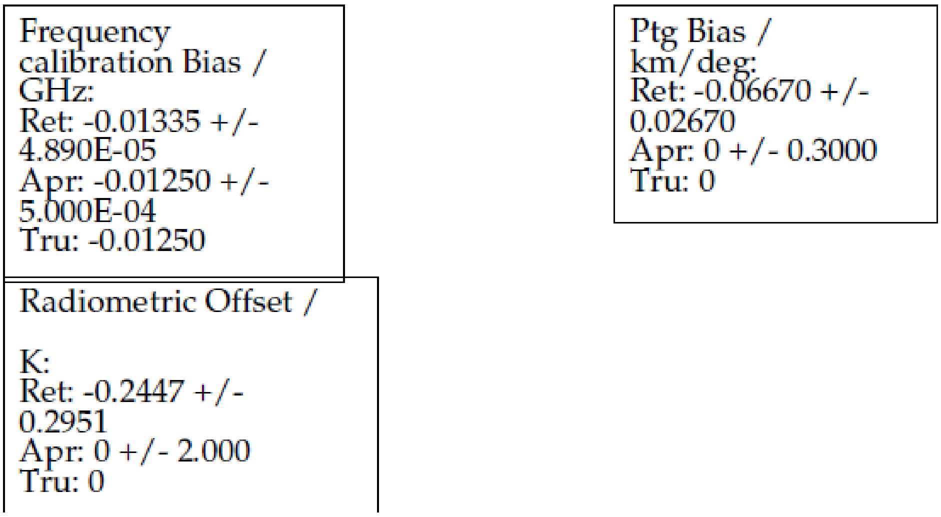

Figure 3.32.: Retrieved instrument parameters for Band D (Scan 1). The term labelled Radiometric Offset is a correction term for the cold target radiance only.

3.6.1. Pointing Bias Retrievals

In PREMIER-Ex we retrieved a single pointing bias per scan which returned a non-zero result but which was strongly correlated to continuum emission and the continuum-like water vapour product. We then resorted to retrieve pointing bias individually from a micro window containing only the 298.5 GHz oxygen line in Band B, as well as from all views above the continuum regime (>13 km) for the other bands where no oxygen is present or the lines are too weak. This was then used as a fixed value in the subsequent retrieval of trace gases.

Pointing retrievals from oxygen line should be more reliable than for other species. Oxygen is well mixed in the atmosphere (constant mixing ratio) and its line shape is therefore uniquely dependent on atmospheric pressure, i.e. altitude. The oxygen feature at 298.5 GHz is strong and should theoretically yield sufficient pointing information. There is another oxygen line in Band D at 345 GHz, which means it's located exactly between the stronger HNO_3 and the weaker CO lines in this band. Both these lines are in fact from the oxygen isotope O-18O. The Band D line on the other hand is very weak, and what makes it worse is falling on a channel with comparatively high measurement error, so it can't likely be used for pointing retrievals.

When we run all our different retrieval scenarios (i.e. gyro correction time steps, a priori errors, various opacity thresholds and some binary keywords) we always retrieved a fairly consistent, positive pointing bias. When on the other hand we tried to retrieve pointing in the same manner we apply to the other bands, i.e. using views above the continuum regime only but for the full frequency band, then we only found a small pointing bias, if at all. This initially raised the question, whether the latter is a valid method to retrieve pointing after all.

However we then notice a systematic spectral residual for the oxygen line in the full-band retrievals which weren't obvious in the oxygen only retrievals. This could mean that for the full band retrieval not all of the line-shape information of the oxygen line has gone in the pointing retrieval. On the other hand it could also mean that we got the spectroscopy wrong and that the oxygen only retrievals return misleading pointing results because they use pointing to compensate for an error in the spectroscopy.

A search for updated versions of spectral line data for the oxygen isotopes returned a couple of new results, which had been collectively added in an addendum to the HITRAN 2008 catalogue published in September 2009:

'*Update for O_2 (Oxygen): The band of oxygen at 1.27 um has been updated using new intensities calculated by Prof. A. Orr-Ewing and new line-shape parameters that are explained in Washenfelder et al, 'Carbon dioxide column abundances at the Wisconsin Tall Tower site,' J.Geophys.Res. 111, D22305 (2006). We thank G.C. Toon of JPL for providing this line list. Two lines (at 7883.626 and 7885.778 cm-1) of the 16O18O isotopologue that were missing from previous editions of HITRAN and from the this latter list have now been added. In addition, the intensities of the 1(v=0) -3S(v=1) band were scaled based on the recent results reported in Kassi et al, 'Very high sensitivity CW-cavity ring down spectroscopy: Application* *to the a1g(0) - X3Sg-(1) O_2 band near 1.58 um,' Chem.Phys.Lett. 409, 281-287 (2005). Finally, the intensity of the line at 7.803602 cm-1 in the pure rotational band of the isotopologue 16O18O was found to be erroneous by about a factor of 4 (we thank S. Paine of SAO for finding this error). The intensity of this line is now corrected adapting the value from the JPL catalogue.'*

We have updated our spectral line data catalogue with these new results and repeated our retrievals. The updated line data for our selected transitions is given in the table below. The result was a better spectral fit and a reduction in the retrieved pointing bias, but in both cases the features had not disappeared altogether.

```
UPDATED O2 SPECTRAL DATA RECORDS IN OUR BAND B RETRIEVALS:
----------------------------------------------------------
72    9.955987 1.618E-28 5.797E-09.05000.049    0.00000.71
73   10.158857 2.019E-30 3.864E-10.06000.059    0.01260.71
73   10.159165 2.825E-30 5.407E-10.06000.059    0.01260.71
73   10.159687 1.882E-30 3.603E-10.06000.059    0.01260.71
73   10.164425 1.214E-30 2.325E-10.06000.059    0.00730.71
73   10.164947 3.695E-30 7.077E-10.06000.059    0.00730.71
73   10.165692 5.188E-30 9.937E-10.06000.059    0.00730.71
73   10.172247 4.826E-31 9.249E-11.06000.059    0.00000.71
73   10.172993 2.892E-30 5.543E-10.06000.059    0.00000.71
73   10.173979 1.010E-29 1.936E-09.06000.059    0.00000.71
----------------------------------------------------------

UPDATED O2 SPECTRAL DATA RECORDS IN OUR BAND C RETRIEVALS:
----------------------------------------------------------
72    9.955987 1.618E-28 5.797E-09.05000.049    0.00000.71
73   10.158857 2.019E-30 3.864E-10.06000.059    0.01260.71
73   10.159165 2.825E-30 5.407E-10.06000.059    0.01260.71
73   10.159687 1.882E-30 3.603E-10.06000.059    0.01260.71
73   10.164425 1.214E-30 2.325E-10.06000.059    0.00730.71
73   10.164947 3.695E-30 7.077E-10.06000.059    0.00730.71
73   10.165692 5.188E-30 9.937E-10.06000.059    0.00730.71
73   10.172247 4.826E-31 9.249E-11.06000.059    0.00000.71
73   10.172993 2.892E-30 5.543E-10.06000.059    0.00000.71
73   10.173979 1.010E-29 1.936E-09.06000.059    0.00000.71
72   11.508552 4.113E-29 1.748E-09.04800.047    4.52470.71
----------------------------------------------------------

UPDATED O2 SPECTRAL DATA RECORDS IN OUR BAND D RETRIEVALS:
----------------------------------------------------------
72    9.955987 1.618E-28 5.797E-09.05000.049    0.00000.71
73   10.173979 1.010E-29 1.936E-09.06000.059    0.00000.71
72   11.508552 4.113E-29 1.748E-09.04800.047    4.52470.71
71   12.130018 1.148E-29 1.896E-09.04800.047 1560.32490.71
71   12.291783 2.213E-26 1.920E-09.04800.047    3.96110.71
----------------------------------------------------------
```

DIFFERENCE IN SPECTRAL DATA RECORDS FROM PREVIOUS VERSION:

	Hitran04		Hitran08 +2009 Corrections	
ID	WaveNum.(*)	LineStr.	WaveNum.	LineStr.(**)
72	9.955993	1.649E-28	9.955987	1.618E-28
73	--		10.158857	2.019E-30
73	--		10.159165	2.825E-30
73	--		10.159687	1.882E-30
73	--		10.164425	1.214E-30
73	10.165240	3.749E-30	10.164947	3.695E-30
73	10.165980	5.268E-30	10.165692	5.188E-30
73	--		10.172247	4.826E-31
73	--		10.172993	2.892E-30
73	10.173390	1.030E-29	10.173979	1.010E-29
72	11.508559	4.191E-29	11.508552	4.113E-29
71	12.132482	1.135E-29	12.130018	1.148E-29
71	--		12.291783	2.213E-26

(*) Some lines previously left out for processing speed.
(**) Only lines stronger than 1*E-31 inside the spectral bands and some particularly strong lines outside of the spectral bands are selected (selection threshold increases with distance outside of band definition).

It is quite striking that the updated O_2 spectral data dramatically change the results for the retrieved pointing bias, basically more than halving it from previously 0.5 deg to 0.2 deg. This value is also in better agreement with alternative attempts to retrieve pointing from other bands (although because of the lack of spectral lines with good pointing information the latter are just approximations). Because we are dealing with isotopologues, in addition to the spectral line parameters we also have to consider the fractionation ratio of the isotope in the atmosphere and the natural variability thereof. The line strengths in the spectral data catalogues are computed for a default isotope mixing, but any inaccuracies in this would also have an impact on the line strength at least. Correcting for that would probably again change the picture.

So the availability of new spectral data seems to imply that pointing bias can not be reliably retrieved from the Band B O_2 line alone. With the availability of the GLORIA results there is now however a redundant method to gauge our pointing bias. With both instruments observing the sharp filament feature at 14 km, we can run our retrieval with various different assumptions of pointing biases and then verify, which of them are in best agreement with the GLORIA results.

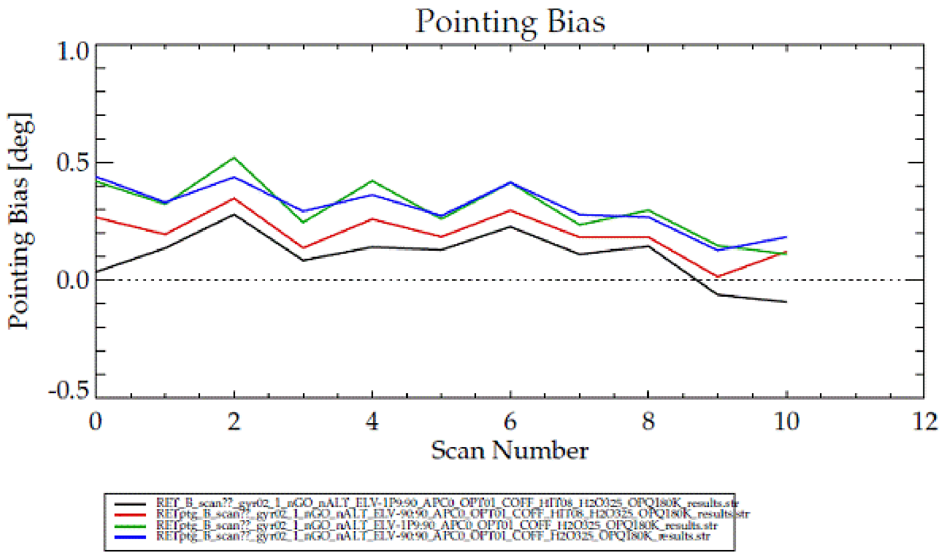

Figure 3.33.: Several pointing bias test retrievals for Flight 2. BLUE: O_2 only, GREEN: O_2 only but high views only, RED: O_2 only but new spectroscopic data, BLACK: Full Band B high views only.

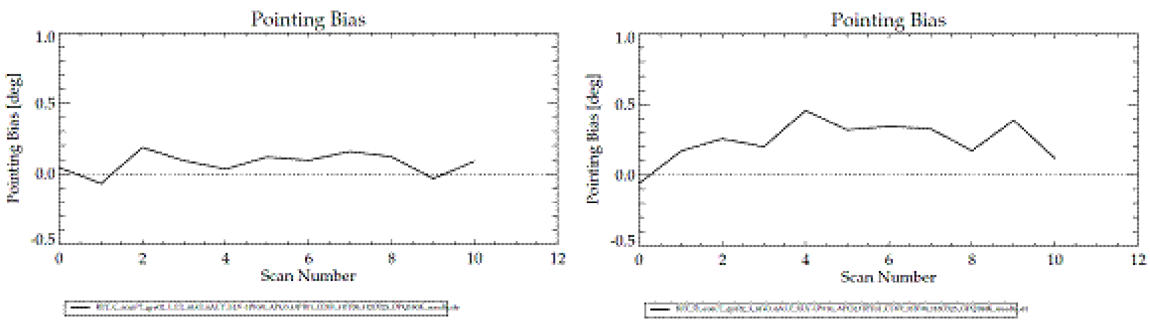

Figure 3.34.: Equivalent pointing bias retrievals for Band C (left) and Band D (right). These are taken from full band retrievals of high views only and should per definition yield less reliable pointing information than Band B oxygen.

We have done this for the three different scenarios:

1. Zero deg a priori pointing bias and default a priori errors
2. Zero deg a priori pointing bias and 1E-6 a priori errors (fixing retrieval to a priori)
3. "O_2 derived" a priori pointing bias and default a priori errors
4. "O_2 derived" a priori pointing bias and 1E-6 a priori errors (fixing retrieval to a priori)

A sample result of such retrieval runs is shown in Figure 3.35. The conclusion from this is that if we force the retrieval to use the pointing bias we have originally found in the analysis of the O_2 line only, then the resulting profile (blue curve in Figure 3.35) is the odd one out and presents the worst match with GLORIA. We are therefore led to believe that the original indications of significant pointing biases based on O_2 data are misleading. As a consequence we have adopted in our updated retrieval settings a Zero degree a priori pointing bias, with an error of 0.3 deg. Pointing bias retrievals according to the new settings are well within this error.

A further illustration of this behaviour is shown in Figure 3.36 where the three scenarios Zero pointing bias and retrieved, Zero pointing bias and fixed, as well as O_2-derived pointing bias and fixed are set against each other. This again shows that - especially in comparison with the GLORIA reference profile, the suggestion of a large pointing bias is not tenable.

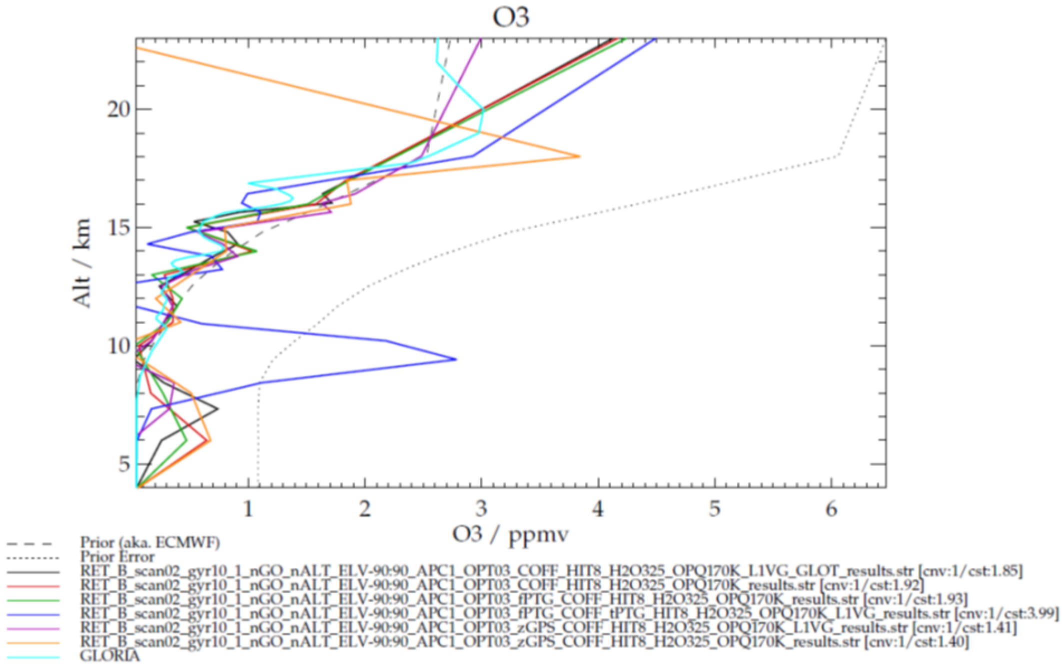

Figure 3.35.: Comparison of retrievals for the same Band and Scan with different retrieval settings. The parameters which vary - identified by the file name - are: Level 1b retrieval grid (LIVG) or not, GLORIA temperature profile (GLOT) or ECMWF, GPS platform altitude (zGPS) or not, ”true” pointing bias (tPTG) a priori as opposed to zero pointing bias a priori and fixed pointing bias retrieval (fPTG) as opposed to free running pointing bias retrieval. The one point we want to make here is that when we fix the pointing bias to the ”true” value we have found in the O_2 pointing retrievals (blue curve), then there is a flagrant mismatch in the retrieved filament altitude, as well as a generally worse retrieval behaviour at other altitudes. We take this as a strong hint that the original pointing bias figures are flawed, and in fact not ”true”.

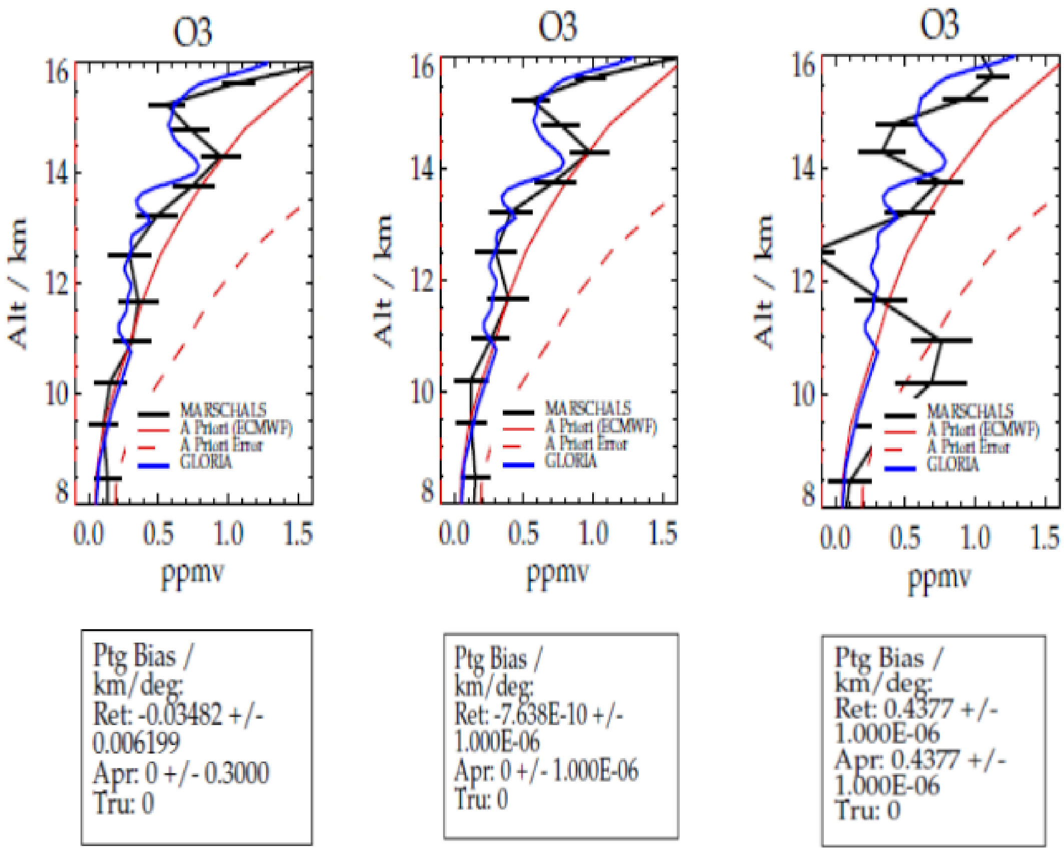

Figure 3.36.: Comparison of retrievals for the same Band and Scan with different retrieval settings. The panel to the left assumes Zero pointing bias but tries to retrieve it as well. The middle panel assumes Zero pointing bias and fixes it. The panel to the right assumes 0.5 deg pointing bias (which was the original finding for Band B from the O_2 pointing analysis and fixes it at that value. Of the three, case using the large pointing bias is clearly the worst.

3.6.2. Frequency Calibration Offset

Analogous to PREMIER-Ex we retrieve a frequency calibration offset over the full frequency window. We have performed various scenarios in which instrument parameters were retrieved, including/excluding trace gases and also with different first guesses for instrument parameters. The result of this has always been a consistent -12 MHz frequency offset, which is very close to the number we had found in PREMIER-Ex. We can therefore conclude that this is a well established property. The value is also constant in each band (which are retrieved independently).

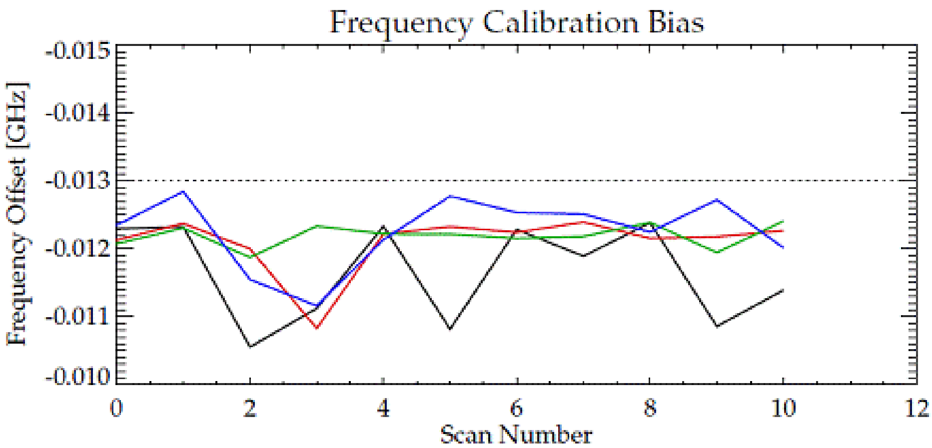

Figure 3.37.: Frequency calibration offset for four different retrieval scenarios. The results are very consistent and close to the -13 MHz we obtained on average for PREMIER-Ex.

3.6.3. Cold Load Radiative Offset

Before the upgrade of the cold calibration target blackbody it was necessary to retrieve a radiative offset for the cold calibration target. Standing waves which increased for cold limb views had identified that the blackbody calibration target in this load wasn't as 'black' as it was supposed to be. This resulted in a calibration error predominantly for cold limb spectra (i.e. the space view) which meant that these could occasionally become negative. We don't observe this feature anymore in the ESSenCe spectra. For the time being we're still including the retrieval of a calibration offset, but test are ongoing for both scenarios and based on the outcome of this we might eventually decide to drop it.

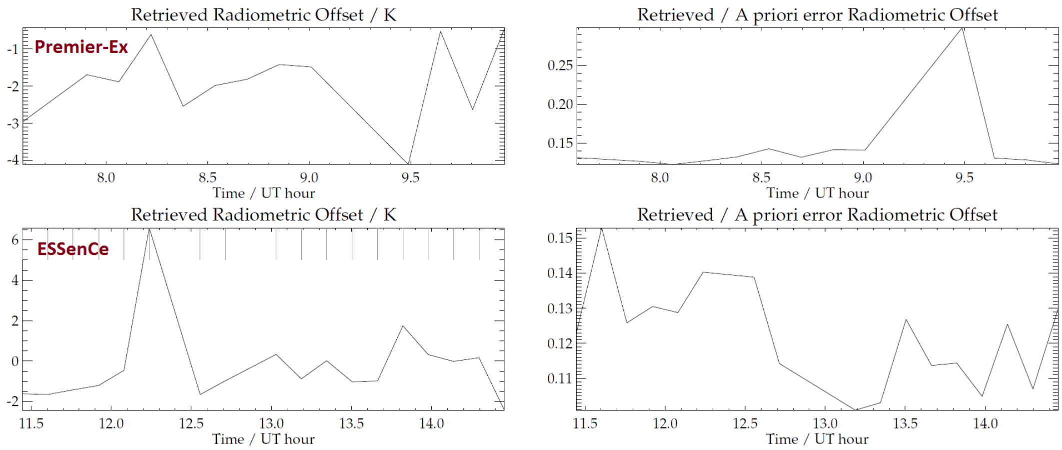

Figure 3.38.: Cold load radiative offset retrieval for Premier-Ex (top row) and ESSenCe (bottom row) for Band C. With the old calibration target load the retrieval compensated the blackbody mismatch with a negative radiative offset value. In ESSenCe the mean radiative offset is close to zero (with the notable exception of one outlier scan.)

3.7. Potential to Observe CO

The model prediction for CO during ESSenCe indicate mixing ratios consistently below the minimal detection threshold which from simulation we believe to be at around 120 ppbv. A CLaMS plot of the CO distribution across the flight track for the 11th December 2011 is shown in Figure 3.39 (courtesy of Baerbel Vogel and Jens-Uwe Groos of FZ Juelich). The threshold is based on the 200 MHz resolution of the MARSCHALS channelisers, which make the narrow CO spectral line particularly hard to detect (note that this will be addressed by the upcoming upgrade for the Band D channel with a SHIRM receiver and a higher-resolution spectrometer).

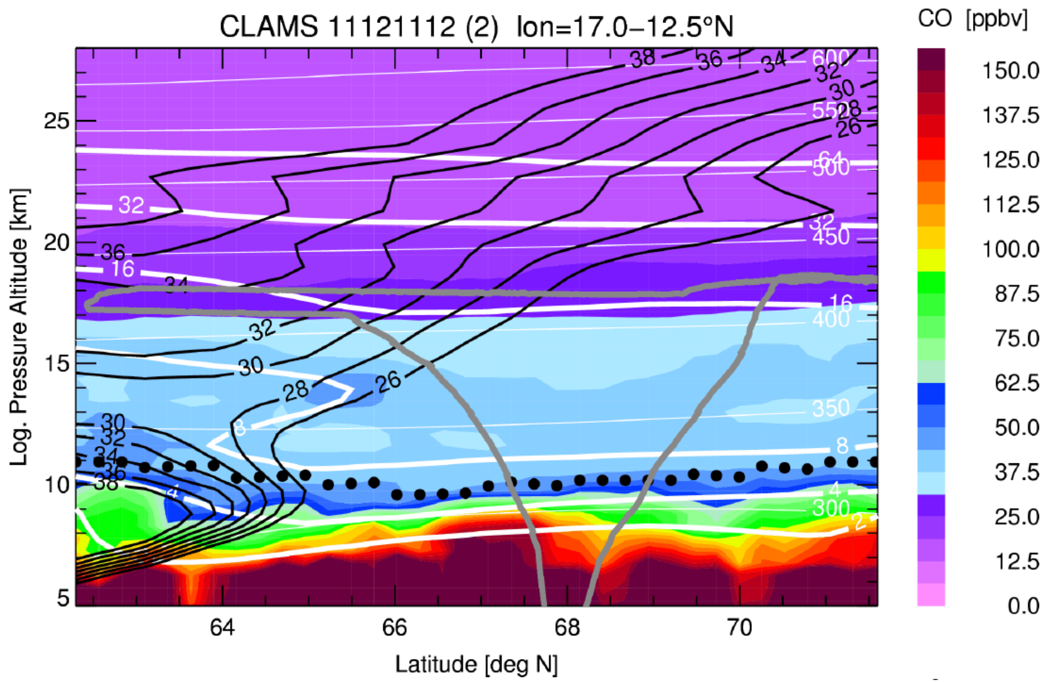

Figure 3.39.: This plot - courtesy of B. Vogel and J.-U. Groos of FZ Juelich - shows the CO distribution across the flight track of Flight 1 in ESSenCe. Values are below the theoretical detection threshold of 120 ppbv at all altitudes that can reasonably be measured.

In Figure 3.40 we show retrieved CO profiles for all scans of Flight 2. This includes some bad scans acquired during aircraft turns as well, but it's obvious that all results indicate very low CO concentrations in the atmosphere. The retrieval grid for CO is unchanged for ESSenCe as there is little potential for this weak emitter to increase the vertical resolution. Typical Averaging kernels for the CO retrieval have already been shown in Figure 3.26. Four layers are resolved in the atmosphere, with no information below 8 km. This is consistent with the cut-off altitude for opaque measurements of 120K, i.e. measurements below 120K wing-temperature are considered opaque and are removed from the scan prior to retrieval so there can be no information below 8 km.

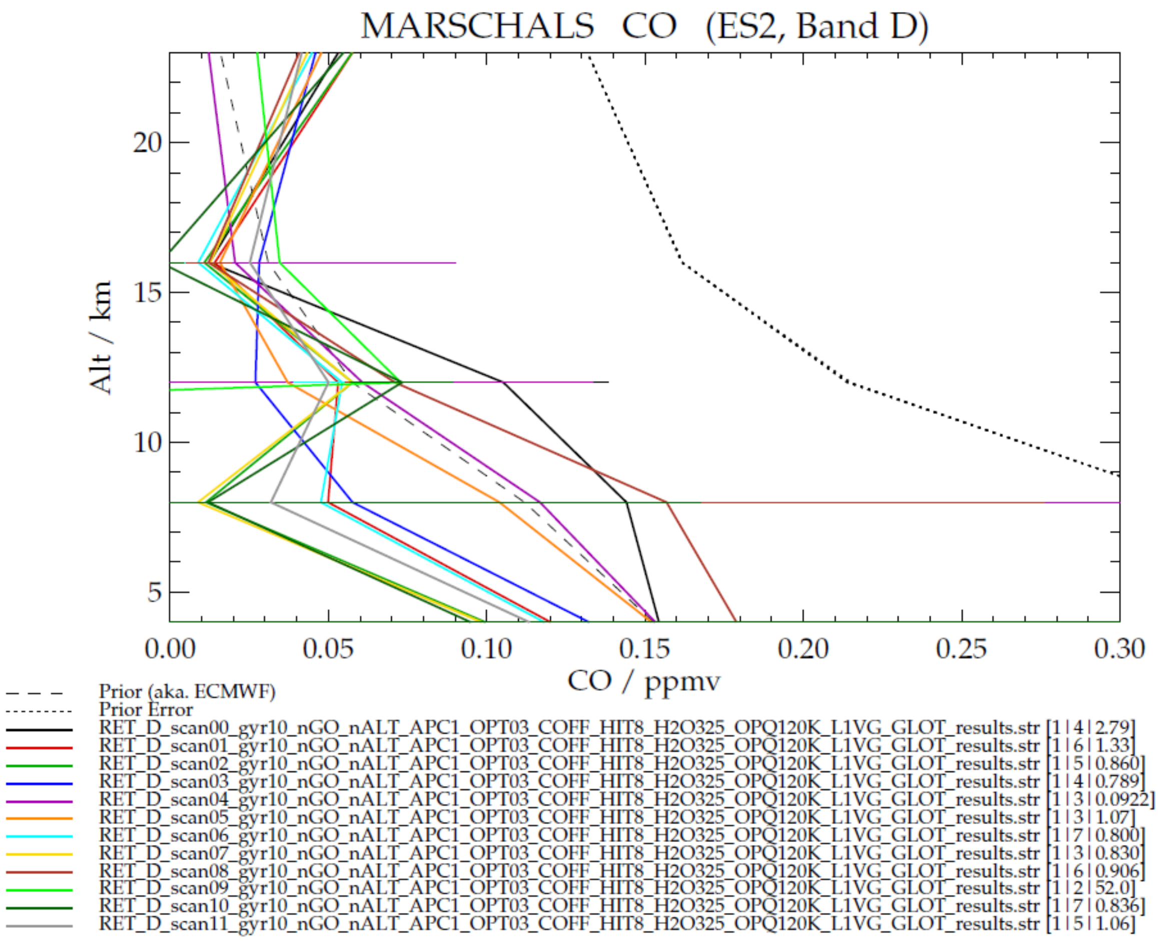

Figure 3.40.: Retrieved CO profiles for the whole of Flight 2. The retrieval results are below the a priori value in all cases, confirming the fact that there was very little CO in the atmosphere during ESSenCe, as the models had predicted.

In a nutshell, we wouldn't expect to be able to retrieve CO based on the very low abundance during ESSenCe, but nevertheless the retrievals return a very consistent picture of a CO distribution of less than half the a priori abundance at 8 km altitude (i.e. 10-60 ppbv vs. 120 ppbv of the a priori). The deviation from the a priori is just about significant within the error bars, so we believe we are at the threshold where we do actually get some information on CO from the measurements. However, due to the size of the error bars, the small scale variations in the CO profiles in Figure 3.40 certainly have to be viewed with caution.

3.8. Conclusions

Millimetre-wave spectra have been acquired in all three MARSCHALS bands for the full duration of both ESSenCe Flights. The recent instrument improvements performed under the UAMS upgrade have resulted in the following improvements in the data:

The revised receivers with lower system noise temperatures increase the spectral performance of the instrument, which results in lower measurement errors compared to previous campaigns. This is especially noticeable in Band B.

The new calibration target in the cold calibration load is showing a much improved blackbody performance, which improves the radiometric calibration and gets rid of the standing wave which was noticeable in the Band B spectra of PREMIER-Ex. It also mitigates a minor radiometric calibration error on the space view spectra noted in PREMIER-Ex, therefore possibly eliminating the need to retrieve this parameter.

The software modifications to the ICU controller and the more frequent, commandable roll-angle updates have increased the system reliability and no scans (with the obvious exemption of turns) have been completely lost due to bad pointing.

On the downside we have discovered an error in the pointing update code which manifests only when a pointing update is performed while the platform is at uneven flight attitude. Unfortunately for Flight 1 this has been the case almost continuously (for yet undisclosed reasons) so for this flight we observe a negative offset of the full atmospheric scan range towards low view angles.

A workaround solution to this has been devised for Flight 2 in the shape of an extended and oversampled scan pattern, which results in better vertical coverage at the cost of reduced horizontal sampling.

The source of the problem has been identified and will be addressed before the next deployment.

The retrieval code has been adapted to the ESSenCe campaign. Using the high-resolution GLORIA profile as a reference, we have managed to reduce the retrieval grid spacing from a 2km fixed grid to a 1km fixed grid, and even to a sub-1km grid spaced at the measurement tangent points. Thus we have managed to reproduce the GLORIA observations of a thin filament structure at 14 km in O_3 mixing ratio of Flight 2. We don't see the filament in the HNO_3 data, but simulations have confirmed that this is not possible within the spectral performance of Band D.

From the filament retrieval study we have also gained insight in the pointing behaviour of MARSCHALS and have therefore concluded some open questions on pointing bias.

The successful validation of MARSCHALS with GLORIA was documented in the PREMIER Delta Report (addendum to the Report for Mission Selection, Figure 3.41).

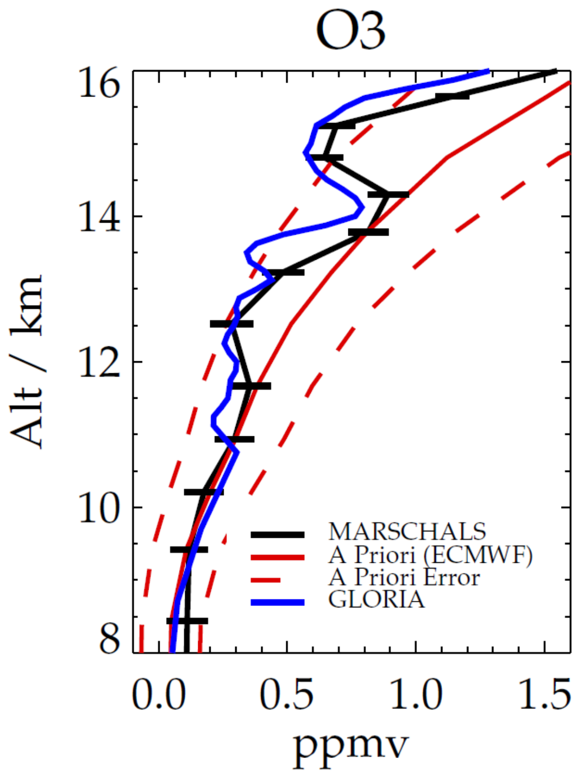

Figure 3.41.: Figure illustrating the joint performance of GLORIA and MARSCHALS in the PREMIER Delta Report.

4. Supporting Measurements

4.1. MIPAS-STR

In this section we briefly describe the sampling characteristics and results from the MIPAS-STR instrument (Piesch et al., 1996) during ESSenCe Flight 2 on December 16th 2011. The MIPAS-STR measurements are utilized for comparisons with the GLORIA and MARSCHALS measurements of the discussed flight and share approximately the same viewing geometry. Instrument characteristics, data processing and retrieval details related to MIPAS-STR are described in Woiwode et al. (2012).

Since for the ESSenCe Flight 2 exceptional low cloud indices (i.e. high levels of continuum probably due to aerosols and PSCs) were found at stratospheric altitudes, the retrieval was adapted for fitting also spectra with low cloud indices but still allowing moderate vertical resolutions of the retrieval results. Slight modifications in the Level-1 processing will not be discussed here. We point out that all results shown here have preliminary character.

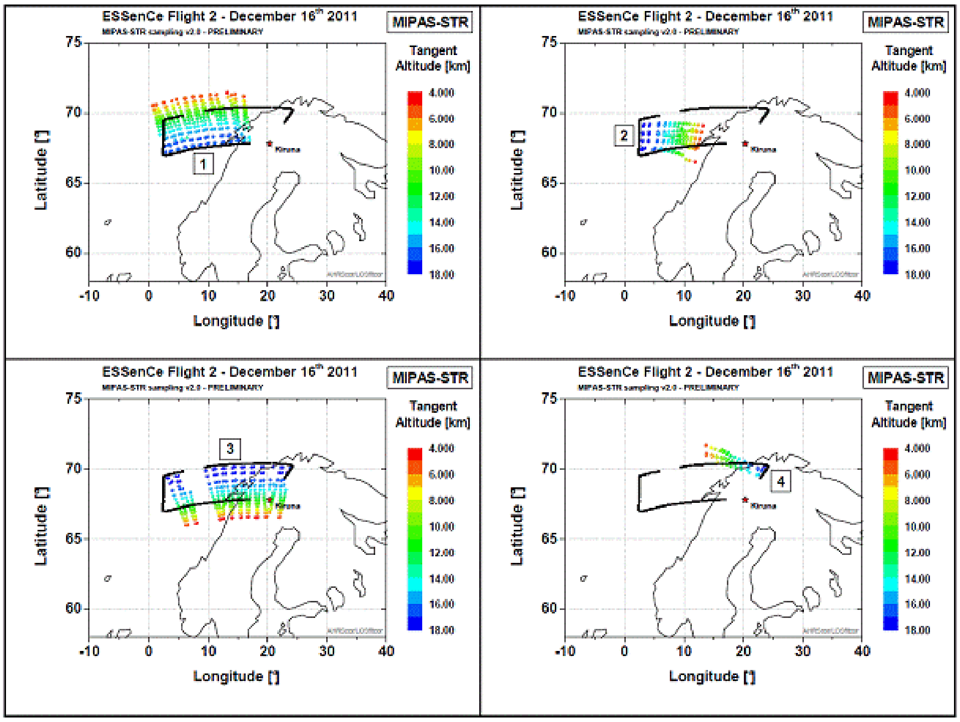

Figure 4.1.: Horizontal distribution of MIPAS-STR tangent points during ESSenCe Flight 2.

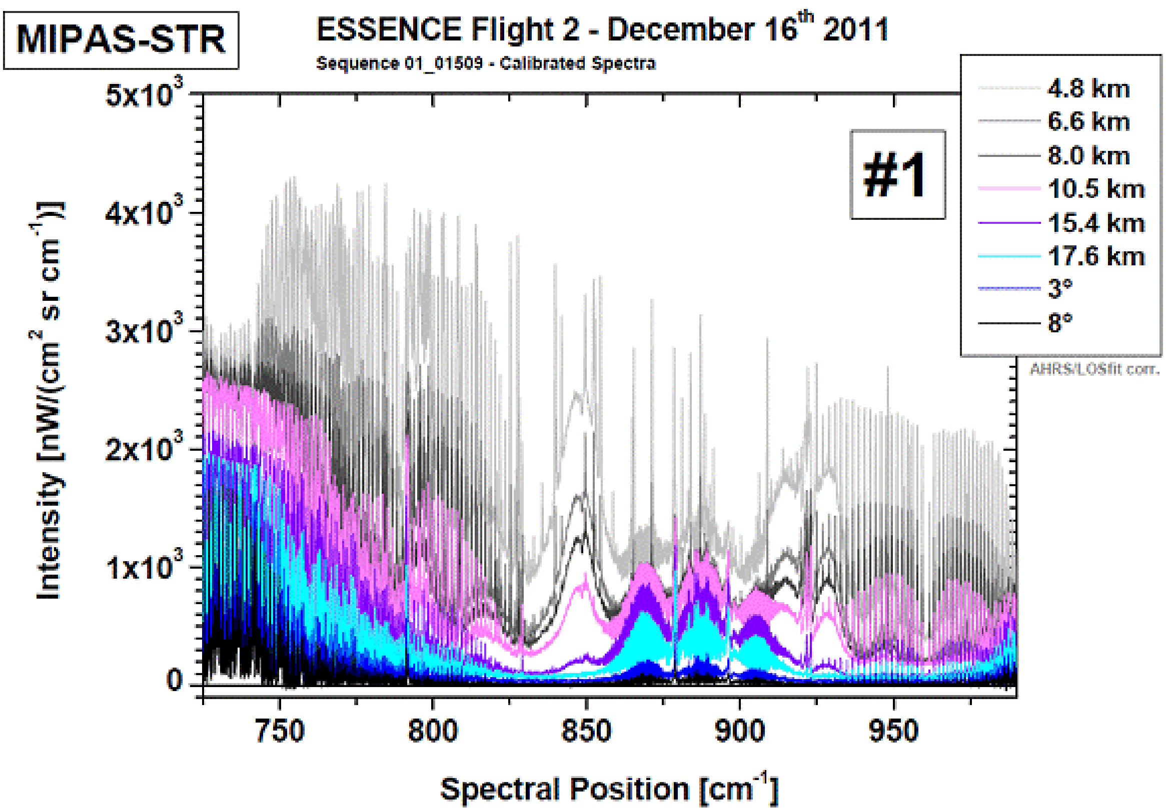

Figure 4.2.: Subset of calibrated MIPAS-STR measurements with weak cloud/aerosol effects at tropospheric altitudes. Box: Associated tangent altitudes or elevation angles, respectively (0° corresponding to horizontal view)

4.1.1. MIPAS-STR sampling during ESSenCe Flight 2

During the ESSenCe Flight 2, a modified measurement scenario with increased vertical sampling down to tangent altitudes below 5km was performed by MIPAS-STR. Scientifically valuable measurements have been obtained during all flight legs.

Electromagnetic disturbances due to the installation of a SATCOM antenna associated to GLORIA on top of the MIPAS-STR electronics module resulted in additional significant spikes and interferences in the interferograms during the entire flight. Efforts during the campaign for improving the electromagnetic shielding of the instrument significantly improved the quality of the measurements, but could not fully remove the disturbances. Consequently, the noise filtering of the MIPAS-STR measurements was performed less strictly, whereas however no major impact on the subsequent data processing was observed. The horizontal distribution of the MIPAS-STR tangent points associated to the flight legs 1 to 4 is shown in Figure 4.1 Comprehensive sampling was obtained during the entire flight, allowing for extensive comparisons with GLORIA and MARSCHALS. The sampling gap during flight leg 3 is associated to a phase dedicated to calibration measurements for the determination of the detector non-linearity.

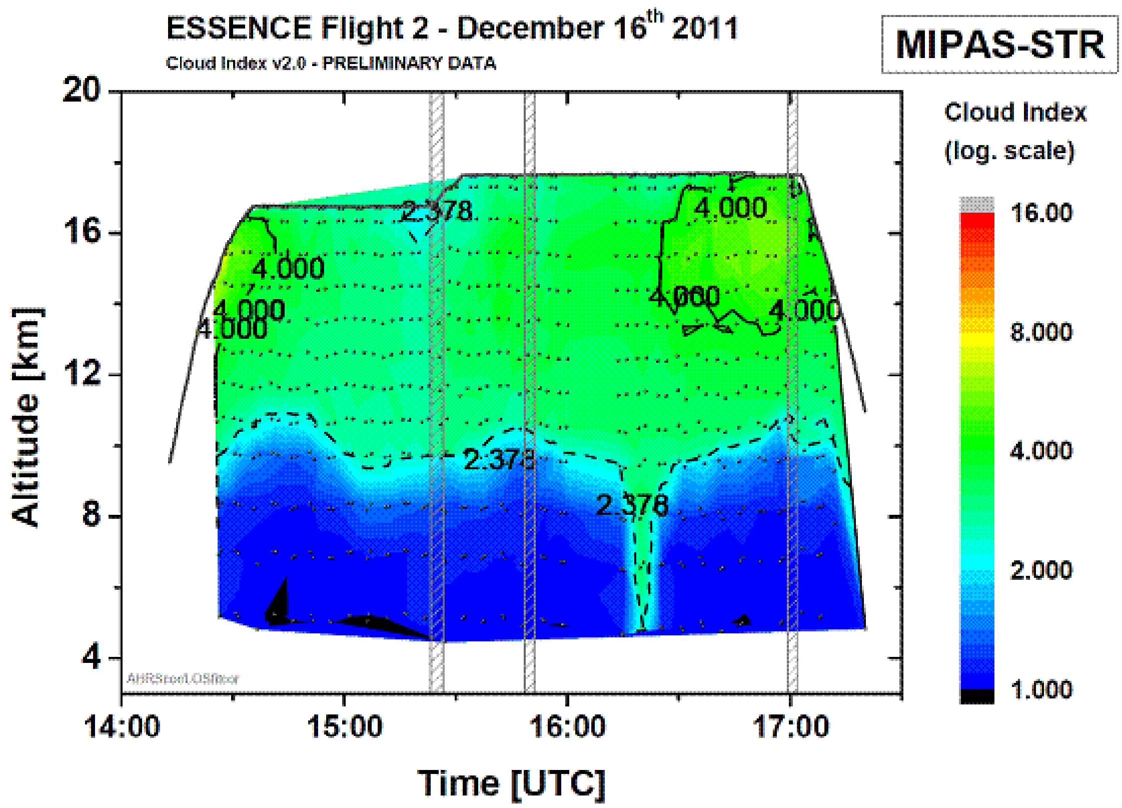

Figure 4.3.: MIPAS-STR vertical sampling (upward viewing geometries not indicated) and cloud index.

A subset of calibrated MIPAS-STR Channel 1 measurements associated to a limb scan located around 16:18 UTC with comparably low cloud/aerosol influences at tropospheric altitudes is shown in Figure 4.2. The measurements exhibit clearly separable non-saturated trace gas emission signatures even down to a tangent altitude of 4.8 km (after postflight-correction), indicating that IR limb emission spectra from the arctic UTLS region under such conditions are retrievable down to low tropospheric altitudes. We mention that the spectrum associated to a tangent altitude of 17.6 km shows already a weak continuum-like offset (compare regions with low density of spectral signatures, i.e. CO_2 laser-band region centred at 961 cm^{-1}), hinting at the presence of stratospheric aerosol or PSCs.

In Fig 4.3, the vertical distribution of the tangent points along flight track is shown together with the interpolated cloud index (Spang et al., 2004). By convention, cloud-free spectra are assigned by cloud indices higher than 4, while clearly cloud-affected spectra are indicated by cloud indices close to 1. Cloud index values between 1 and 4 indicate spectra slightly/partly affected by aerosol, whereas the threshold between cloud-free and cloud-affected is diffuse and also depends on the instrument type. For the ESSenCe Flight 2, low cloud index values are observed during the entire flight and at all altitudes. Assuming a threshold of 2.4 between strongly cloud-affected and only slightly cloud-affected spectra as a proxy, a variable cloud top altitude between about 9 and 11 km can be indentified in the troposphere. Only a narrow zone with higher cloud index values in the troposphere down to the lowest tangent altitudes is visible around 16:25 UTC. In this region, also the lowest viewing geometries are included in the retrieval. Spectra with cloud index values higher than 4 are only found for the ascent phase and during the last part of the flight. Low cloud index values between 2 and 3 close to the flight altitude indicate stratospheric aerosol, probably due to the occurrence of early winter polar stratospheric clouds (PSCs).

4.1.2. MIPAS-STR retrieval results

As a consequence of overall low cloud index values observed for spectra at all altitudes, the threshold for cloud filtering for the retrieval was set to 2 (for conservative cloud filtering a threshold of 4 is applied usually). Due to the observed high variability in aerosol background, logarithmic inversion was performed for wavenumber-independent background continuum (this parameter is retrieved simultaneously with the target parameter for each retrieval and microwindow). Regarding the line-of-sight offset retrieval, slight drifts in the order of arc minutes attributed to thermal misalignment were visible in the individually retrieved line-of-sight offset parameters along the flight. For an improved correction of these line-of-sight variations, here a polynomial line-of-sight correction was applied instead of considering the average line-of-sight offset value of all scans (as done previously). The sizes of the retrieval microwindows for the line-of-sight and temperature retrievals were slightly reduced to minimize spectral interference with spectral lines of H_2O at lower tropospheric altitudes. Furthermore, the climatological CO_2 profile used for forward modelling was updated for the arctic winter 2011 conditions.

In Figure 4.4-Figure 4.7, the retrieved vertical cross-sections of the different target parameters are shown together with the flight altitude of the Geophysica. For interpolation of the cross-sections, results at retrieval grid points with vertical resolution of better than 5 km are used (the only exception is background continuum, where points with vertical resolutions better than 10 km are used to better visualize the trend above the flight path). White spots in the interpolated cross-sections correspond to grid points with lower vertical resolution not used for interpolation. Typical vertical resolutions of the retrieval results are in the order of 1.5 km for HNO_3, CFC-11, H_2O and background-continuum, 1.8 km for temperature, O_3 and CFC-12, and 2.7 km for $ClONO_2$. In fact, the vertical resolution for an individual parameter varies with altitude,.e.g. for HNO_3 and CFC-11 vertical resolutions better than 1.5 km are obtained between flight altitude and several kilometres below.

The vertical cross-section of temperature (upper panel of Figure 4.4) shows relatively low values in the region of TNAT (existence temperature for nitric acid trihydrate, TNAT 195 K and depends on local atmospheric conditions) around flight altitude. Temperatures at lower altitudes appear relatively homogeneous, while increased variability is observed at tropospheric altitudes. Also shown in the lower panel of Figure 4.4 is the retrieved vertical cross-section of the wavenumber-independent background continuum for the 956.0–958.2 cm^{-1} microwindow associated to the temperature retrieval. The result shows a complementary pattern to the cloud-index: regions with low cloud indices are characterised by increased levels of background continuum, which qualitatively indicates increased aerosol loading. Further substructures with moderately increased background continuum are visible at stratospheric altitudes, such as several maxima at flight altitude and along flight track. Taking into account the low temperatures around flight altitude, PSC particles composed of NAT might be a reasonable explanation for the low cloud index values and increased background continuum levels observed around flight altitude between 14:30 and 16:40 UTC.

The cross-sections of HNO_3 and O_3 (Figure 4.5) indicate relatively homogeneous distributions of these constituents in the stratosphere. Around the first turning point (15:25 UTC), the cross-section of HNO_3 exhibits a region of decreased HNO_3 around flight altitude, which is less pronounced in the O_3-distribution. A complementary structure is found in the cross-sections of CFC-11 and CFC-12 in Figure 4.6, characterised by increased mixing ratios and probably hinting on a dynamical structure. The cross-sections of the CFCs show variable mixing ratios above 15 km, whereas the distributions appear patchy especially during the first flight leg. The distributions of the CFCs in this altitude region indicate that considerably inhomogeneous stratospheric airmasses were sampled during this flight. The observed variability of the CFCs at altitudes below 15 km is attributed to the horizontally extended viewing geometries associated to the lower tangent views, whereas spectral information is accumulated along hundreds of kilometres along the line-of-sight. Here, horizontal dynamical structures sounded at different horizontal positions by different viewing geometries associated to the same limb scan might also affect the retrieval result below (i.e. at tropospheric altitudes), at least by intrinsic smoothing associated to the retrieval. This might be an explanation for the observed variability at tropospheric altitudes. Furthermore, retrieval errors might contribute to the observed pattern at lower altitudes, which by trend increase towards lower observation geometries.

The vertical cross-section of $ClONO_2$ (Figure 4.7) with comparably low vertical resolution (arising from the very low $ClONO_2$ abundance and the rather large continuum values) shows relatively low mixing ratios during the entire flight, which is plausible at this early stage of the arctic winter. Slightly increased mixing ratios are observed in the second half of flight leg 3 and during leg 4.

The vertical cross-section of H_2O (also Figure 4.7) shows relatively homogenous concentrations in the stratosphere above 11 km with local maxima above (around 12 km) and quickly increasing mixing ratios towards tropospheric altitudes.

In summary, the MIPAS-STR results indicate that inhomogeneous airmasses with significant aerosol-loading associated to the early polar vortex were sampled during ESSenCe Flight 2 close to the flight level. This is supported by (i) low and variable cloud-index values at stratospheric altitudes and associated strong variability observed in the retrieved background continuum hinting at the presence of aerosol and or PSCs, as well as (ii) low and variable concentrations of CFC-11 and CFC-12 (which can be regarded as dynamical tracers) along flight track and around flight altitude. Low temperatures around flight altitude around TNAT might indicate the presence of NAT PSC particles. On the other hand, the HNO_3 and tracer cross sections do not indicate any significant filaments as observed in some of the RECONCILE flights

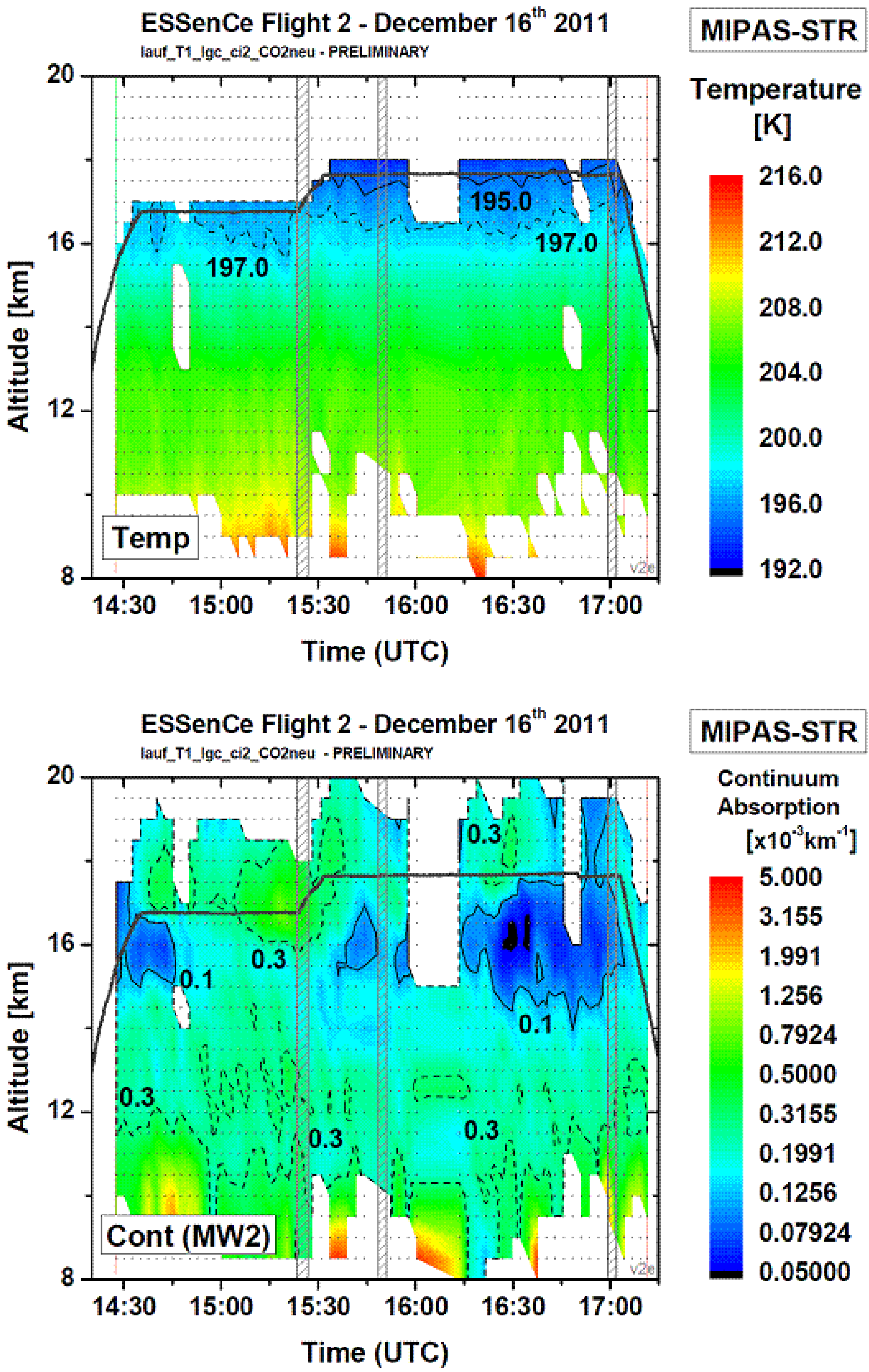

Figure 4.4.: Vertical cross-sections of temperature and wavenumber-independent background continuum.

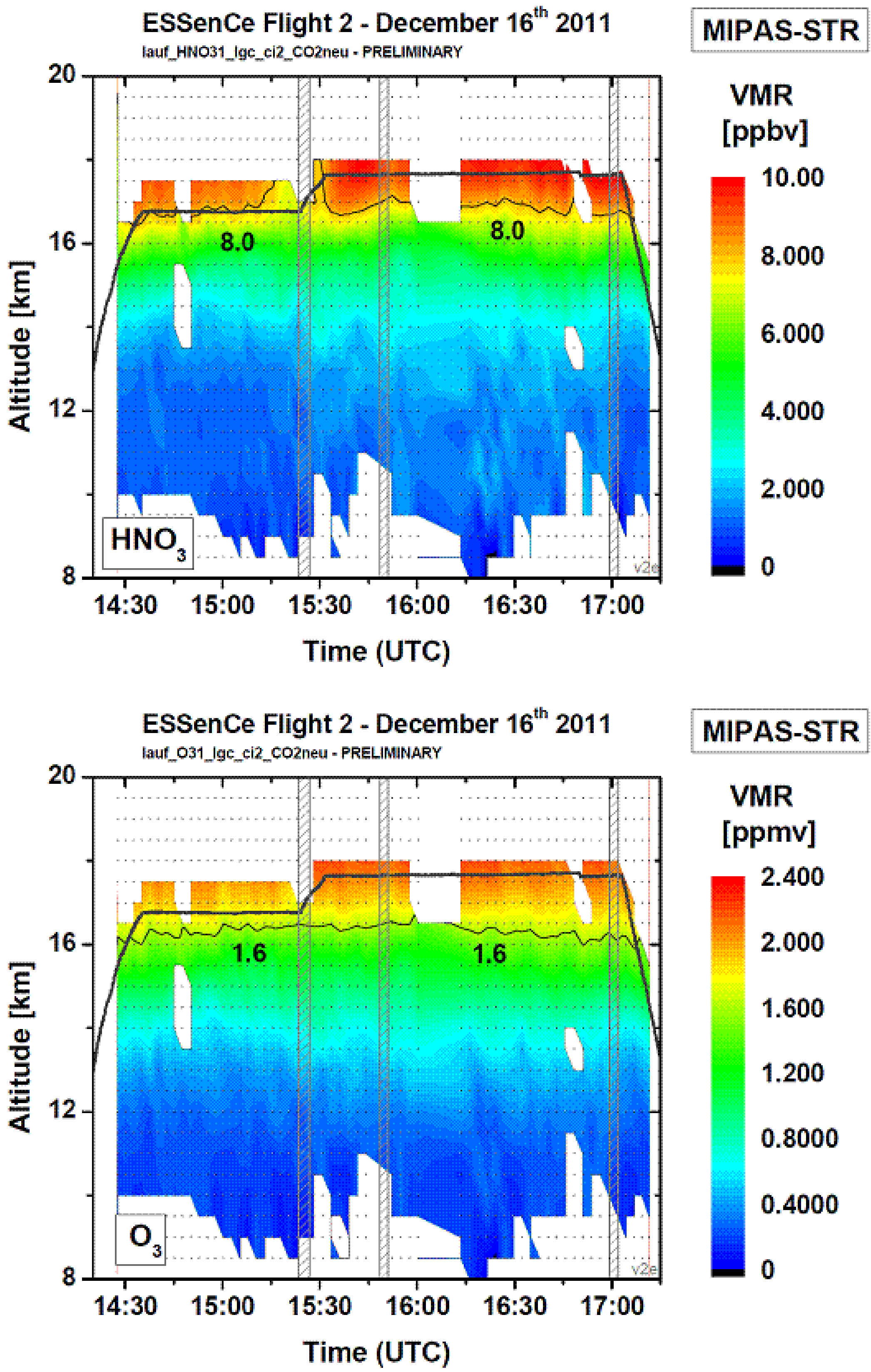

Figure 4.5.: Vertical cross-sections of HNO_3 and O_3.

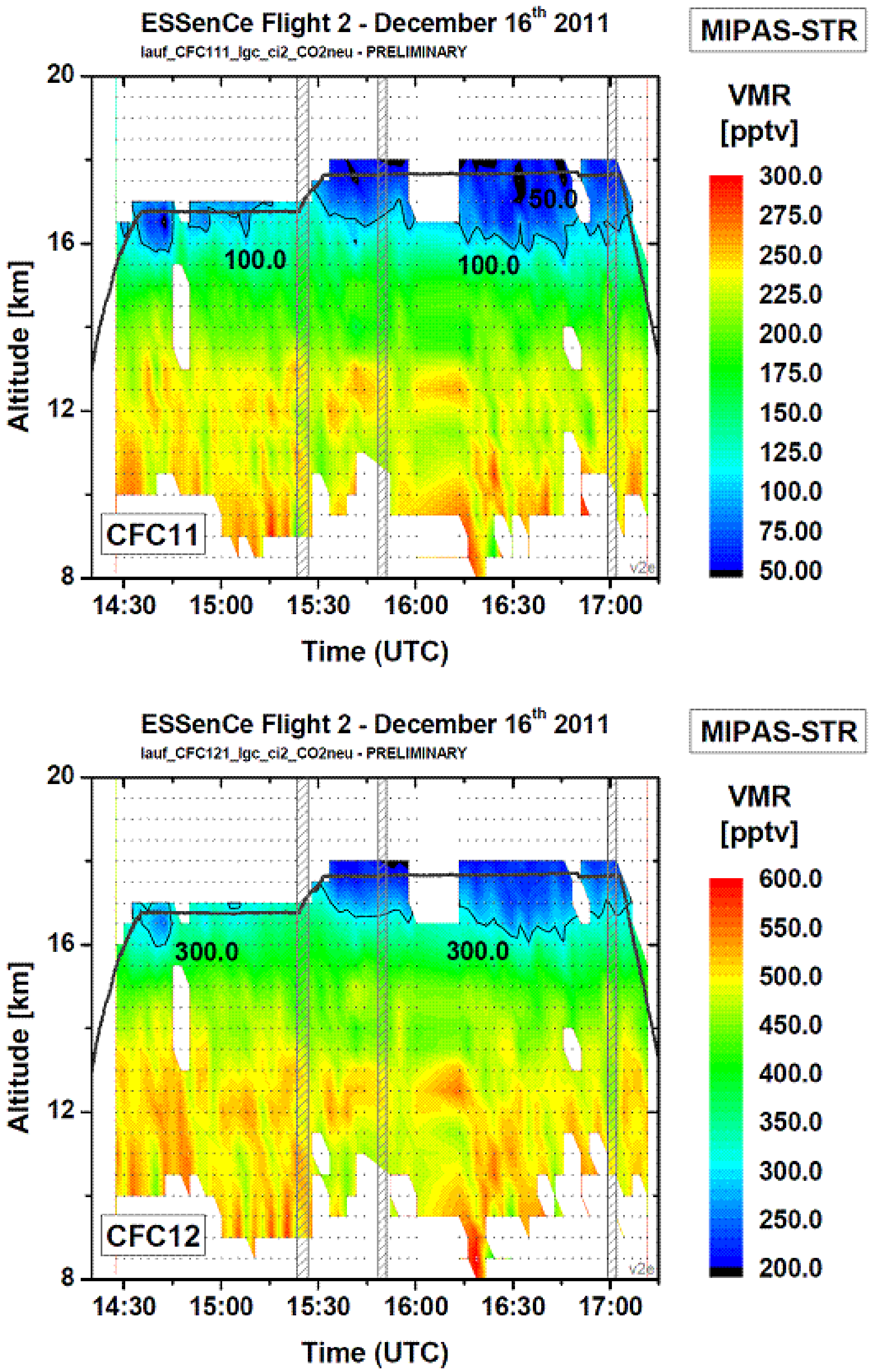

Figure 4.6.: Vertical cross-sections of CFC-11 and CFC-12.

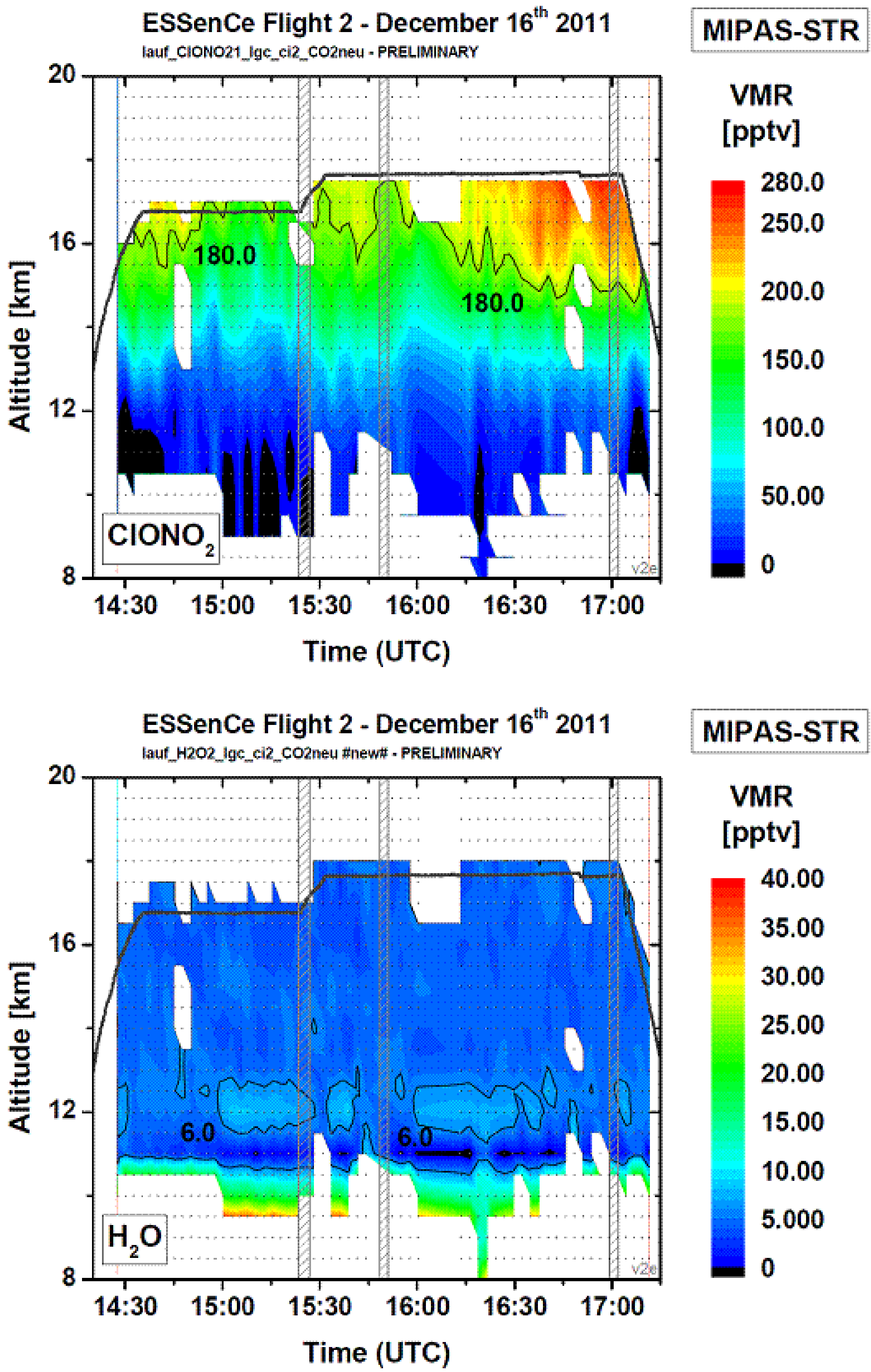

Figure 4.7.: Vertical cross-sections of $ClONO_2$ and H_2O.

5. Conclusions

5.1. Technical Achievements

5.1.1. GLORIA

During the first part of the ESSenCe campaign, IRLS-prototype instrument GLORIA was characterized in a thermal vacuum chamber, including calibration and pointing of the instrument and comparisons with modeled data. The technical performance of GLORIA was confirmed.

During ESSenCe field campaign, GLORIA was deployed on the high-flying Russian research aircraft Geophysica for the first time. The instrument was integrated into the Geophysica high-flying research aircraft and two test flights to assess the performance of GLORIA were conducted. The GLORIA instrument performance was to a large extent within the specification, with a very good line of sight stabilization of some tens of meters, a negligible interferometer shear and a nominal data acquisition. A few critical components have been identified, such as the the mounting of the fixed cube corner within the interferometer, the thermal adjustment of the cold calibration blackbody, or the functionality of the gimbaled frame after 1–2 h of flight time (c.f. ESSenCe Compact Data Acquisition Report). These components have been replaced or modified meanwhile to avoid similar problems in the future.

Although Flights 3 and 4 (so called scientific flights) were cancelled for different reasons, GLORIA demonstrated its ability to observe small scale structures in the vicinity of polar stratospheric clouds, which was not sensed by collocated conventional limb sounder MIPAS-STR.

5.1.2. MARSCHALS

Marschals acquired data in all three bands for the full duration of both ESSenCe Flights. The recent instrument improvements performed under the UAMS upgrade have resulted in significant improvement of the data, such as lower measurement errors compared to previous campaigns, or an improved blackbody performance and radiometric calibration.

5.2. Infrared-Microwave Synergies

Infrared and microwave limb sounding in the UTLS region complement each other with respect to altitude coverage and number of atmospheric species to be observed. For PREMIER, both spectral intervals have been selected to exploit optimally the complementary and synergistic attributes of the IR and millimeter-wave regions.

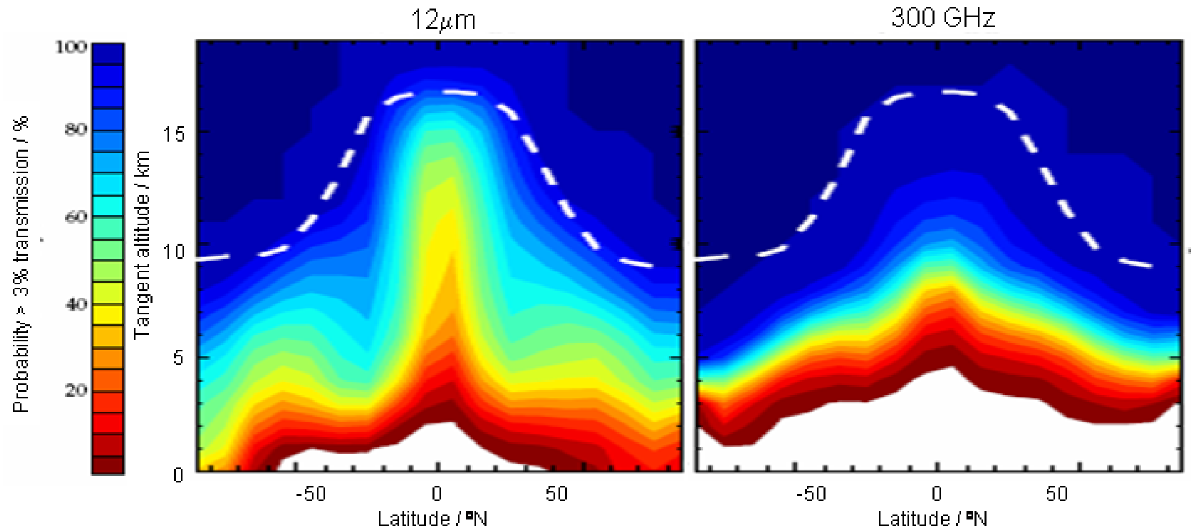

Figure 5.1.: Comparison of limb path transparencies at IR (12μm) and millimeter (300GHz 1mm) wavelengths. Annual mean percentage probabilities of transmittance ¿ 0.03 calculated from ECMWF analyzes of temperature, humidity and cloud are shown as functions of latitude and tangent-height. (R. Siddans).

One important aspect is that trace gas emissions at millimeter-wavelengths are not attenuated significantly by aerosols (or PSCs) and are attenuated much less by cirrus clouds than emissions at infra-red wavelengths. Only cirrus clouds containing relatively large particles (>100 μm) can significantly attenuate/scatter limb-emission at millimeter-wavelengths, which means that trace gases can still be retrieved in the presence of most cirrus clouds. By contrast, cirrus clouds with predominantly smaller size components (and aerosol and PSCs) can be observed by infrared limb-sounding, as also required to meet PREMIER mission objectives.

Limb path transparency at IR and mm-wave wavelengths to be exploited by PREMIER is illustrated in Figure 5.1. The figure shows annual mean probabilities of transmittance >3% at the two wavelengths as a function of latitude and height as calculated from ECMWF analyses of temperature, humidity and clouds. At millimeter-wavelengths, penetration is controlled by water vapor attenuation. Retrievals (of adequate precision and accuracy for all gases) are generally confined to water vapor mixing ratios <1,000 ppmv, and effectively therefore to the upper half of the troposphere. In infrared windows, tropospheric penetration is limited principally by clouds. In the absence of cloud, IR limb-sounding extends down to the lower troposphere at high and mid-latitudes and down to about 10 km in the tropics.

5.2.1. Observations during ESSenCe

During ESSenCe, we could verify some of the synergies suggested by Figure 5.1 in practice. This is shown in Figure 5.2 for ozone results obtained from MARSCHALS, MIPAS-STR and GLORIA (chemistry mode) retrievals, respectively. The lower limit of the GLORIA retrieval is determined by a conservative cloud top determination. In the measurement sequence shown in Figure 2 it is around 11 km. Obviously, MARSCHALS ozone retrievals penetrate

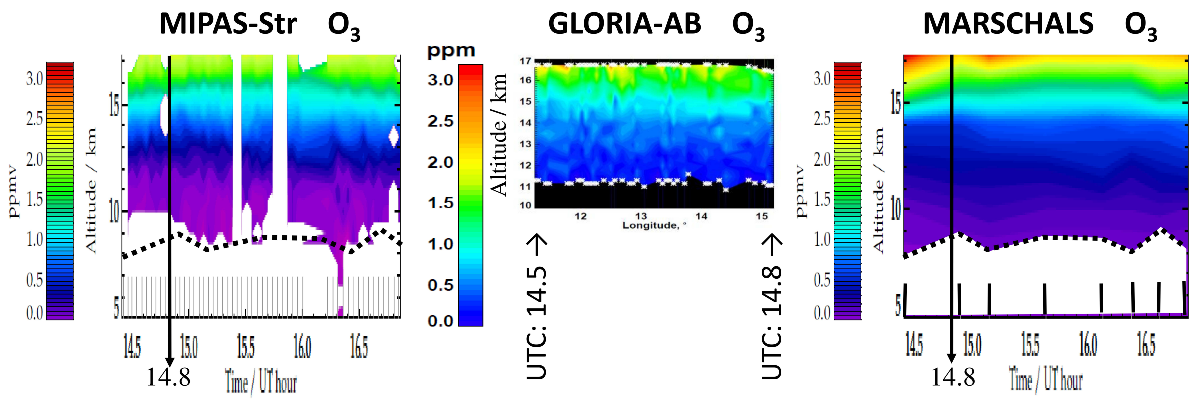

Figure 5.2.: Lower altitude limits of ozone retrieval for MIPAS-STR (left), GLORIA (middle), and MARSCHALS (right) for a measurement sequence obtained during the 2nd ESSenCe flight. The lower limit for GLORIA is determined by the presence of clouds and a rather conservative cloud filter, indicated by the horizontal dashed line.

about 2 km deeper into the troposphere (down to 9 km) for this situation. MARSCHALS retrievals of water vapor even penetrate down to 5 to 7 km, i.e. 4 to 6 km below the lower altitude limit of GLORIA.

The second ESSenCe flight provided, in addition, the opportunity to study the capability of IR remote sensing to penetrate deeper into the troposphere at high- and mid latitudes in the absence of clouds (or low cloud influence). Figure 4.3 shows cloud indices derived from MIPAS-STR spectra for a relatively long time sequence of the 2nd ESSenCe flight on December 16, 2011. The data shows a small area of relatively high cloud indices down to 5 km. Analyses of IMK indicate that several trace gases such as CFC-11, CFC-12, H2O etc. can be retrieved in this window, i.e. there are clear trace gas signatures in the spectra (see Section 2.2.3).

In summary, the ESSenCe observations demonstrate some of the synergies of IR and mm-wave remote sensing that have been expected from Figure 5.1. In particular, the penetration of suitable retrievals into the troposphere is enhanced by a few kilometers for ozone and water vapor during the ESSenCe flights.

Bibliography

Dee, D. P., Uppala, S. M., Simmons, A. J., Berrisford, P., Poli, P., Kobayashi, S., Andrae, U., Balmaseda, M. A., Balsamo, G., Bauer, P., Bechtold, P., Beljaars, A. C. M., van de Berg, L., Bidlot, J., Bormann, N., Delsol, C., Dragani, R., Fuentes, M., Geer, A. J., Haimberger, L., Healy, S. B., Hersbach, H., Hólm, E. V., Isaksen, L., Kållberg, P., Köhler, M., Matricardi, M., McNally, A. P., Monge-Sanz, B. M., Morcrette, J.-J., Park, B.-K., Peubey, C., de Rosnay, P., Tavolato, C., Thépaut, J.-N., and Vitart, F. (2011). The ERA-Interim reanalysis: configuration and performance of the data assimilation system. *Quarterly Journal of the Royal Meteorological Society*, 137(656):553–597.

Froidevaux, L., Jiang, Y. B., Lambert, A., Livesey, N. J., Read, W. G., Waters, J. W., Browell, E. V., Hair, J. W., Avery, M. A., Mcgee, T. J., Twigg, L. W., Sumnicht, G. K., Jucks, K. W., Margitan, J. J., Sen, B., Stachnik, R. A., Toon, G. C., Bernath, P. F., Boone, C. D., Walker, K. A., Filipiak, M. J., Harwood, R. S., Fuller, R. A., Manney, G. L., Schwartz, M. J., Daffer, W. H., Drouin, B. J., Cofield, R. E., Cuddy, D. T., Jarnot, R. F., Knosp, B. W., Perun, V. S., Snyder, W. V., Stek, P. C., Thurstans, R. P., and Wagner, P. A. (2008). Validation of Aura Microwave Limb Sounder stratospheric ozone measurements. *Journal of Geophysical Research - Atmospheres*, 113(D15).

Garcia, R. R., Marsh, D. R., Kinnison, D. E., Boville, B. A., and Sassi, F. (2007). Simulation of secular trends in the middle atmosphere, 1950–2003. *Journal of Geophysical Research*, 112.

Grooß, J.-U., Günther, G., Müller, R., Konopka, P., Bausch, S., Schlager, H., Voigt, C., Volk, C., and Toon, G. C. (2005). Simulation of denitrification and ozone loss for the arctic winter 2002/2003. *Atmospheric Chemistry and Physics*, 5(6):1437–1448.

Kleinert, A. and Glatthor, N. (2011). Cloud detection for onboard irls co-addition. *Technical Note, PREMIER – Consolidation of Requirements and Synergistic Retrieval Algorithms, Task 6.2 – WP 6220, Version 6*.

Piesch, C., Gulde, T., Sartorius, C., Friedl-Vallon, F., Seefeldner, M., Wulfel, M., Blom, C. E., and Fischer, H. (1996). Design of a MIPAS instrument for high-altitude aircraft. *Proc. of the 2nd Internat. Airborne Remote Sensing Conference and Exhibition, ERIM, Ann Arbor, MI, Vol. II*, pages 199–208.

Remedios, J. J., Leigh, R. J., Waterfall, A. M., Moore, D. P., Sembhi, H., Parkes, I., Greenhough, J., Chipperfield, M., and Hauglustaine, D. (2007). MIPAS reference atmospheres and comparisons to v4.61/v4.62 MIPAS level 2 geophysical data sets. *Atmospheric Chemistry and Physics Discussions*, 7(4):9973–10017.

Rodgers, C. D. (2000). *Inverse Methods for Atmospheric Sounding: Theory and Practice*, volume 2 of *Series on Atmospheric, Oceanic and Planetary Physics, F. W. Taylor, ed.* World Scientific.

Rothman, L., Gordon, I., Barbe, A., Benner, D., Bernath, P., Birk, M., Boudon, V., Brown, L., Campargue, A., Champion, J.-P., Chance, K., Coudert, L., Dana, V., Devi, V., Fally, S., Flaud, J.-M., Gamache, R., Goldman, A., Jacquemart, D., Kleiner, I., Lacome, N., Lafferty, W., Mandin, J.-Y., Massie, S., Mikhailenko, S., Miller, C., Moazzen-Ahmadi, N., Naumenko, O., Nikitin, A., Orphal, J., Perevalov, V., Perrin, A., Predoi-Cross, A., Rinsland, C., Rotger, M., Šimečková, M., Smith, M., Sung, K., Tashkun, S., Tennyson, J., Toth, R., Vandaele, A., and Auwera, J. V. (2009). The hitran 2008 molecular spectroscopic database. *Journal of Quantitative Spectroscopy and Radiative Transfer*, 110(9–10):533 – 572.

Spang, R., Remedios, J., and Barkley, M. (2004). Colour indices for the detection and differentiation of cloud types in infra-red limb emission spectra. *Advances in Space Research*, 33(7):1041–1047.

Stiller, G. P., editor (2000). *The Karlsruhe Optimized and Precise Radiative Transfer Algorithm (KOPRA)*, volume FZKA 6487 of *Wissenschaftliche Berichte*. Forschungszentrum Karlsruhe.

Tikhonov, A. (1963). On the solution of incorrectly stated problems and method of regularization. *Dokl. Akad. Nauk. SSSR*, 151(3):501–504.

Ungermann, J., Blank, J., Lotz, J., Leppkes, K., Hoffmann, L., Guggenmoser, T., Kaufmann, M., Preusse, P., Naumann, U., and Riese, M. (2011). A 3-D tomographic retrieval approach with advection compensation for the air-borne limb-imager GLORIA. *Atmospheric Measurement Techniques*, 4(11):2509–2529.

Volk, C. M., Riediger, O., Strunk, M., Schmidt, U., Ravegnani, F., Ulanovsky, A., and Rudakovand, V. (2000). In situ tracer measurements in the tropical tropopause region during apetheseo. *Eur. Comm. Air Pollut. Res. Report*, 73:661 – 664.

von Clarmann, T., Glatthor, N., Grabowski, U., Höpfner, M., Kellmann, S., Kiefer, M., Linden, A., Mengistu Tsidu, G., Milz, M., Steck, T., Stiller, G. P., Wang, D. Y., Fischer, H., Funke, B., Gil-López, S., and López-Puertas, M. (2003). Retrieval of temperature and tangent altitude pointing from limb emission spectra recorded from space by the Michelson Interferometer for Passive Atmospheric Sounding (MIPAS). *J. Geophys. Res.*, 108(D23).

von Clarmann, T., Höpfner, M., Kellmann, S., Linden, A., Chauhan, S., Funke, B., Grabowski, U., Glatthor, N., Kiefer, M., Schieferdecker, T., Stiller, G. P., and Versick, S. (2009). Retrieval of temperature, H_2O, O_3, HNO_3, CH_4, N_2O, $ClONO_2$ and ClO from MIPAS reduced resolution nominal mode limb emission measurements. *Atmospheric Measurement Techniques*, 2(1):159–175.

Woiwode, W., Oelhaf, H., Gulde, T., Piesch, C., Maucher, G., Ebersoldt, A., Keim, C., Höpfner, M., Khaykin, S., Ravegnani, F., Ulanovsky, A. E., Volk, C. M., Hösen, E., Dörnbrack, A., Ungermann, J., Kalicinsky, C., and Orphal, J. (2012). MIPAS-STR measurements in the Arctic UTLS in winter/spring 2010: instrument characterization, retrieval and validation. *Atmos. Meas. Tech.*, 5(6):1205–1228.

Zöger, M., Afchine, A., Eicke, N., Gerhards, M.-T., Klein, E., McKenna, D. S., Mörschel, U., Schmidt, U., Tan, V., Tuitjer, F., Woyke, T., and Schiller, C. C. (1999). Fast in situ stratospheric hygrometers: A new family of balloon-borne and airborne lyman photofragment fluorescence hygrometers. *J. Geophys. Res.*, 104:1807–1816.

Appendices

A. Data Inventory

The data inventory of the ESSenCe campaign covers level 2 data of the GLORIA instrument for the test flight of 16 December and of the MARSCHALS instrument for 11 December and 16 December as well as MIPAS-STR level 1 data for the test flight of 16 December. Potential users of this data are encouraged to contact the instrument principal investigators for the latest data version, because these datasets are still under investigation. Instrument PIs are:

GLORIA P. Preusse (p.preusse@fz-juelich.de) and H. Oelhaf (hermann.oelhaf@kit.edu)

MARSCHALS B. Kerridge (brian.kerridge@stfc.ac.uk)

MIPAS-STR H. Oelhaf (hermann.oelhaf@kit.edu)

A.1. GLORIA Dynamics Mode Data

GLORIA dynamics mode data was recorded during ESSenCe Flight 2 from 14:58 to 15:10 at 16 December 2011. The total sequence consists of 121 individual images. Retrieval targets are temperature, Ozone, HNO_3, and CFC-12. In addition, three aerosol profiles according to Table 2.5 were obtained, which represent the aerosol load as well as non-resolved forward model and instrumental effects. The vertical resolution (full width at half maximum of the averaging kernel) is also given. Finally, the viewing direction of each pixel is listed as well. Data format is netCDF4 (http://www.unidata.ucar.edu/software/netcdf/). A description of the dimensions of the variables is given in Table A.2, and individual variables are explained in Table A.1. Filename is *essence_gloria_dynamics_mode_data.nc*

Name	Dimensions	Units	Description
profile_lon, profile_lat, profile_time	nr_profiles		Carrier position and time of measurement per profile
atm_z, atm_lon, atm_lat	nr_profiles, nr_atm_pts		Geolocation of the atmospheric grid point
atm_*_final_val	nr_profiles, nr_atm_pts	Kelvin, ppv and cm^2	Retrieved atmospheric state of entities (Temperature, O_3, HNO_3, CFC-12 and Aerosols)
atm_*_final_res_fwhm_z	nr_profiles, nr_atm_pts	km	Vertical resolution. Full width at half maximum of the averaging kernel.
pixel_offset	nr_profiles, nr_pixel	$W/(cm^2 cm^{-1} sr)$	Radiometric offset for each pixel after retrieval
tp_z, tp_lon, tp_lat	nr_profiles, nr_pixel		Geolocation of tangent points
pixel_elevation, pixel_azimuth	nr_profiles, nr_pixel		Viewing direction of pixels

Table A.1.: GLORIA dynamics mode variable names

Dimension	Description
nr_profiles	Number of measurements (images, profiles) taken
nr_atm_pts	Number of points in the retrieval atmosphere
nr_pixel	Number of pixel on the GLORIA detector

Table A.2.: GLORIA dynamics mode dimension names

A.2. GLORIA Chemistry Mode Data

The results of the ESSenCE chemistry mode data retrieval are included in netCDF files (20111216_GLORIA_CM_x.nc, where x denotes a target parameter) created with Interactive Data Language (IDL) 8.1.

Each of the netCDF files includes global part with the target name, spectral range and contact data. The data structure is characterized by three **dimensions**:

- **altgrid**: altitude profile grid consisting of 92 altitudes between 0 and 100 km
- **time**: measurement time in Julian seconds after the 1st January 2000, depending on the number of successfully retrieved images (profiles) the axis includes between 39 and 42 values
- **length_id**: dimension for the image identifiers characters (char).

The result and supplementary information are grouped in 21 data arrays:

- **time**: UTC time array in the Julian seconds after the 1st January 2000, double-precision floating-point format
- **id_name**: image (profile) identifiers providing measurement time information, alphanumeric strings
- **latitude**: image latitudes in degrees N, floating-point format
- **longitude**: image longitudes in degrees E, floating-point format
- **dof**: profile degrees of freedom, floating-point format
- **n_tang**: values providing the number of tangent altitudes of single profiles, integer format
- **rms_real**: image root-mean-square values of residual in nW/cm^2 sr cm^{-1} , floating-point format
- **htang_eng_low**: profile minimal tangent angles in radians, floating-point format
- **htang_eng_high**: profile maximal tangent angles in radian, floating-point format
- **htang_km_low**: profile minimal tangent altitudes in km, floating-point format, representative data only above the altitudes, floating-point format
- **htang_km_high**: profile maximal tangent altitudes in km, floating-point format, representative data only below the altitudes, floating-point format
- **altitude**: 92 levels over the sea level in km, floating-point format
- **ak_diag**: averaging kernel diagonal elements, floating-point format
- **result**: retrieval results for a target (temperature in K, O_3 and H_2O in ppm, $ClONO_2$ and HNO_3 in ppb, CFC-12 in ppt), floating-point format
- **initial_guess**: initial guess array, floating-point format
- **target_noise_error**: noise error array
- **vres**: vertical resolution array in km
- **los10perc_error**: array including differences in retrieval result resulting from 10% line-of-sight correction change, floating-point format
- **gain2perc_error**: array including differences in retrieval result resulting from 2% gain change, floating-point format
- **pressure_ini**: initial pressure array in hPa, floating-point format
- **temperature_ini**: initial temperature array in K, floating-point format

A.3. MARSCHALS Data

```
The archive marschals_essence_l2data.zip containst the following 2 files:

- marschals_essence_20111211.nc : MARSCHALS L2 data of ESSenCe Flight 1
- marschals_essence_20111211.nc : MARSCHALS L2 data of ESSenCe Flight 2

The binary data format is netCDF. The data is structured (and validated)
according to CF-Convention v1.0 (Climate and Forecast Metadata Covention)
and is therefore considered to be self-explanatory.

/****************************************************************/
/*                                                              */
/* IMPORTANT! Please check the README_FIRST attribute in the   */
/*            data structures for important information on     */
/*            known issues with this version of the data!      */
/*                                                              */
/****************************************************************/

2012-11-30   daniel.gerber@stfc.ac.uk

dimensions:
        band_b_o3_alt = 13 ;
        band_b_n2o_alt = 13 ;
        band_b_scans = 21 ;
        band_c_o3_alt = 13 ;
        nd_c_h2o_alt = 13 ;
        band_c_scans = 20 ;
        band_d_o3_alt = 13 ;
        band_d_hno3_alt = 13 ;
        band_d_co_alt = 5 ;
        band_d_scans = 20 ;

variables:
        float band_b_o3_alt(band_b_o3_alt) ;
                band_b_o3_alt:long_name = "Retrieval Grid Altitude Levels" ;
                band_b_o3_alt:units = "km" ;
        float band_b_o3_vmr(band_b_o3_alt, band_b_scans) ;
                band_b_o3_vmr:long_name = "O3 Volume Mixing Ratio Profile" ;
                band_b_o3_vmr:units = "1e-6" ;
        float band_b_n2o_alt(band_b_n2o_alt) ;
                band_b_n2o_alt:long_name = "Retrieval Grid Altitude Levels" ;
                band_b_n2o_alt:units = "km" ;
        float band_b_n2o_vmr(band_b_n2o_alt, band_b_scans) ;
                band_b_n2o_vmr:long_name = "N2O Volume Mixing Ratio Profile" ;
                band_b_n2o_vmr:units = "1e-6" ;
        float band_c_o3_alt(band_c_o3_alt) ;
                band_c_o3_alt:long_name = "Retrieval Grid Altitude Levels" ;
                band_c_o3_alt:units = "km" ;
        float band_c_o3_vmr(band_c_o3_alt, band_c_scans) ;
                band_c_o3_vmr:long_name = "O3 Volume Mixing Ratio Profile" ;
                band_c_o3_vmr:units = "1e-6" ;
        float band_c_h2o_alt(nd_c_h2o_alt) ;
                band_c_h2o_alt:long_name = "Retrieval Grid Altitude Levels" ;
                band_c_h2o_alt:units = "km" ;
        float band_c_h2o_vmr(nd_c_h2o_alt, band_c_scans) ;
                band_c_h2o_vmr:long_name = "H2O Volume Mixing Ratio Profile" ;
                band_c_h2o_vmr:units = "1e-6" ;
        float band_d_o3_alt(band_d_o3_alt) ;
                band_d_o3_alt:long_name = "Retrieval Grid Altitude Levels" ;
                band_d_o3_alt:units = "km" ;
        float band_d_o3_vmr(band_d_o3_alt, band_d_scans) ;
                band_d_o3_vmr:long_name = "O3 Volume Mixing Ratio Profile" ;
                band_d_o3_vmr:units = "1e-6" ;
        float band_d_hno3_alt(band_d_hno3_alt) ;
                band_d_hno3_alt:long_name = "Retrieval Grid Altitude Levels" ;
                band_d_hno3_alt:units = "km" ;
        float band_d_hno3_vmr(band_d_hno3_alt, band_d_scans) ;
                band_d_hno3_vmr:long_name = "HNO3 Volume Mixing Ratio Profile" ;
                band_d_hno3_vmr:units = "1e-6" ;
        float band_d_co_alt(band_d_co_alt) ;
                band_d_co_alt:long_name = "Retrieval Grid Altitude Levels" ;
                band_d_co_alt:units = "km" ;
        float band_d_co_vmr(band_d_co_alt, band_d_scans) ;
                band_d_co_vmr:long_name = "CO Volume Mixing Ratio Profile" ;
                band_d_co_vmr:units = "1e-6" ;
        short band_b_scans(band_b_scans) ;
                band_b_scans:long_name = "Band B Scan Index" ;
        short band_c_scans(band_c_scans) ;
                band_c_scans:long_name = "Band C Scan Index" ;
        short band_d_scans(band_d_scans) ;
                band_d_scans:long_name = "Band D Scan Index" ;
```

A.4. MIPAS-STR Data

Instrument Information:

- **Instrument name**: MIPAS-STR (**M**ichelson **I**nterferometer for **P**assive **A**tmospheric **S**ounding – **STR**atospheric Aircraft)
- **Measuring technique**: Fourier Transform Infrared Limb Emission Sounder
- **Technique references:**
    - Woiwode, W., Oelhaf, H., Gulde, T., Piesch, C., Maucher, G., Ebersoldt, A., Keim, C., Höpfner, M., Khaykin, S., Ravegnani, F., Ulanovsky, A. E., Volk, C. M., Hösen, E., Dörnbrack, A., Ungermann, J., Kalicinsky, C., and Orphal, J.: MIPAS-STR measurements in the Arctic UTLS in winter/spring 2010: instrument characterization, retrieval and validation, *Atmos. Meas. Tech.*, 5, 1205-1228, doi:10.5194/amt-5-1205-2012, 2012.
- **Data products**:
    - ***L1B product*** - Calibrated spectra and sampling information (including characterization data and cloud index)
    - ***L2 product*** - Vertical profiles along flight track of temperature (K) and trace gas volume mixing ratios of HNO_3 (ppbv), O_3 (ppmv), $ClONO_2$ (pptv), CFC-11 (pptv), CFC-12 (pptv), H_2O (ppmv) and continuum absorption (km^{-1})
- **Measuring range**: typically from 5 km to flight altitude and upward viewing
- **Data Resolution**: typically 1 profile in ~3 min
- **PI**: Karlsruhe Institute of Technology
  Institute for Meteorology and Climate Research -
  Atmospheric Trace Gases and Remote Sensing (IMK-ASF)
  Hermann Oelhaf
  76344 Leopoldshafen
  Germany

  hermann.oelhaf@kit.edu

Data Information:

- **Campaign name**: ***ESSenCe***
  Location: Kiruna, Sweden
- **File names**:
    - **111216a_MIPASSTR_geos_v2e_ESA.nas** (*sampling information and cloud index*)
    - **_MIPASSTR_results_5thGen_v2e_ESA.nas** (*retrieved temperature/trace gas vmr/continuum absorption*)
    - **111216a_MIPASSTR_characterisation.dat** (*additional characterization of L1B data:* noise equivalent spectral radiance (NESR), radiometric accuracy, vertical field of view (FOV) weighting function, pointing accuracy)
    - **atm_xx_yyy(y)_ch1_cal.kop** (*calibrated spectra* with xx = number of system reboot (pre) and yyy(y) = number of scan (scn))

- **Processed flight:** 16.12.2011 (Kiruna-Kiruna)
- **Data format (*nas):** Nasa Ames (http://badc.nerc.ac.uk/help/formats/NASA-Ames/)

  - Columns in **111216a_MIPASSTR_geos_ve2_ESA.nas**:

GMTs	- Elapsed UT seconds from 0 hours on the day given by DATE	
t_lon	- tangent point longitude	(°)
t_lat	- tangent point latitude	(°)
t_alt	- tangent point altitude	(km)
ci	- cloud index	(unitless)
M55_lon	- Geophyisca longitude	(°)
M55_lat	- Geophyisca latitude	(°)
M55_alt	- Geophysica altitude (GPS)	(°)
t_alt(-0.3deg)	- as t _alt, uppermost view only	(°)
pre	- reboot number	(unitless)
seq	- sequence number	(unitless)
scn	- scan number	(unitless)
elev	- line-of-sight elevation angle	(°)

  - Columns in **111216a_MIPASSTR_results_5thGen_v2e_ESA.nas**:

GMTs	- Elapsed UT seconds from 0 hours on the day given by DATE (mean time of profiles)	
alt	- GEOMETRIC ALTITUDE	(km)
T_fit	- T	(K)
T_err	- T ERROR 1-sd	(K)
T_vert	- T VERTICAL RESOLUTION	(km)
HNO3_fit	- HNO_3 MIXING RATIO	(ppbv)
HNO3_err	- HNO_3 ERROR 1-sd	(ppbv)
HNO3_vert	- HNO_3 VERTICAL RESOLUTION	(km)
O3_fit	- O_3 MIXING RATIO	(ppmv)
O3_err	- O_3 ERROR 1-sd	(ppmv)
O3_vert	- O_3 VERTICAL RESOLUTION	(km)
ClONO2_fit	- $ClONO_2$ MIXING RATIO	(pptv)
ClONO2_err	- $ClONO_2$ ERROR 1-sd	(pptv)
ClONO2_vert	- $ClONO_2$ VERTICAL RESOLUTION	(km)
CFC-11_fit	- CFC-11 MIXING RATIO	(pptv)
CFC-11_err	- CFC-11 ERROR 1-sd	(pptv)
CFC-11_vert	- CFC-11 VERTICAL RESOLUTION	(km)
CFC-12_fit	- CFC-12 MIXING RATIO	(pptv)
CFC-12_err	- CFC-12 ERROR 1-sd	(pptv)
CFC-12_vert	- CFC-12 VERTICAL RESOLUTION	(km)
H2O_fit	- H_2O MIXING RATIO	(ppmv)
H2O_err	- H_2O ERROR 1-sd	(ppmv)

H2O_vert	- H_2O VERTICAL RESOLUTION	(km)
CON2_fit	- CONTINUUM ABSORPTION	(km^{-1})
CON2_err	- not included -	
CON2_vert	- CONT. ABS. VERTICAL RES.	(km)
H2O#new#_fit	- H_2O MIXING RATIO	(ppmv)*
H2O#new#_err	- H_2O ERROR 1-sd	(ppmv)*
H2O#new#_vert	- H_2O VERTICAL RES.	(km)*
pre	- REBOOT NUMBER	(unitless)
seq	- SEQUENCE NUMBER	(unitless)

*alternative H_2O retrieval, improved vertical resolution

- scale_factor: see file headers, line 11
- fill_value: see file headers, line 12

Data format (111216a_MIPASSTR_characterisation.dat): ASCII (text)

- see file text -

Data format (atm_xx_yyy(y)_ch1_cal.kop): ASCII

column 1	- spectral position	(cm^{-1})
column 2	- radiance	($nW/(cm^2\ sr\ cm^{-1})$)

- **Measurand:**
  - Level1: Calibrated spectra and sampling information
  - Level2: cloud index (ci), temperature/trace gas volume mixing ratio (x_fit, with x=T, HNO_3, O_3, $ClONO_2$, CFC-11, CFC-12, H_2O, continuum absorption) inclusive 1-sigma error (x_err) and vertical resolution (x_ver
- **Uncertainty/Characterisation (L1B product):** see 11216a_MIPASSTR_characterisation.dat
- **Uncertainty (L2 product):**
  - Error: combined total 1-sigma error (x_err)
  - Vertical resolution: @ retrieval grid altitude (x_vert)
- **Data status**:
  - Quality checked data
  - **Important:** Combined total 1-sigma error valid in context of vertical resolution. Additional uncertainties possible especially at tropospheric altitudes (i.e. spectral interference with not specified trace gases/aerosol, smoothing effects of the retrieval and horizontal gradients of atmospheric parameters)

- **Calibration:**
  - Radiometric calibration (radiometric gain, radiometric offset and detector-nonlinearity) of Level1 data using in-flight calibration measurements
  - Line-of-sight calibration step included in Level2 processing (polynomial)
  - For details see reference
- **Problems**:
  - EMC problems through interference with SATCOM antenna; enhanced abundance of spikes in interferograms → less conservative data quality filtering; enhanced noise / systematic errors in calibrated spectra possible
- **Comments:**
  - Please inform the PI when you like to use the data and for what purpose.